STRATIGRAPHIC-FORWARD AND REACTIVE-TRANSPORT MODELING OF DEPOSITIONAL AND DIAGENETIC PROCESSES IN SILICICLASTIC SANDSTONES

Mohammad R. Khadhrawi

Submitted to the faculty of the University Graduate School
in partial fulfillment of the requirements
for the degree
Doctor of Philosophy
in the Department of Geological Sciences
Indiana University
June 2011

Accepted by the Graduate Faculty, Indiana University, in partial fulfillment of the requirements for the degree of Doctor of Philosophy.

Prof. Lisa Pratt (Chair), Ph.D.

Mary Parke, Ph.D.

Prof. Simon Brassell (Minor Advisor), Ph.D.

Assc. Prof. Greg Olyphant, Ph.D.

Todd Thompson, Ph.D.

June 2011

Copyright © 2011
Mohammad R. Khadhrawi
ALL RIGHTS RESERVED

to my late father Sayed Radhi, my late mother Alawia,
and my late brother Sayed Ghalib.
may God rest their souls in eternal peace

Acknowledgements

I thank God Almighty for blessing me with the patience and perseverance and persist through difficult times during the years it took to reach the destination of my educational journey. I would like to start by thanking my parents for instilling in me the desire to succeed and the motivation to work harder when adversity arises. I would also like to my family: my wife, my daughters, my son, my brothers and sisters for their support and patience. I would like to thank my Chairperson, Professor Lisa Pratt for her enormous support and invaluable encouragement. I owe a debt of gratitude to my committee members. Ms. Mary Iverson, of the Geological Sciences Department at Indiana University, Bloomington (IUB), deserves a special "thank you" for all her efforts that guided me through the processes and procedures of Indiana University. Sincere thanks go to the high performance computing group at the IUB Computing Center. I would like to also acknowledge my employer, Aramco, for giving me the full scholarship that enabled me to pursue this degree. Mr. N. Danner is thanked for creating the IU Dissertation document class for use with LaTeX and granting permission for others to use it. Lastly, I would like to thank Dr. Chris Dyt of the Commonwealth Scientific and Industrial Research Organization (CSIRO) of Australia. This graduate degree took a lot longer than originally planned because of unforeseen reasons that are not within the control of any single individual. During this additional period, I lost both my beloved parents and my dear younger brother Ghalib. I regret that they passed away before we all had the opportunity to share the joy of fulfilling this dream of mine. May God bless them.

Mohammad R. Khadhrawi

Stratigraphic-Forward and Reactive-Transport Modeling of Depositional and Diagenetic Processes in Siliciclastic Sandstones

Modeling natural processes is one of the most effective ways to test the plausibility of multiple hypotheses. Numerical experiments can be set to assess different scenarios that may be responsible for development of a certain phenomenon. Reaction-Transport Modeling (RTM) is a numerical approach that permits tracking multiple species simultaneously. This can be done as a system evolves spatially and temporally. RTM was applied to understanding the mechanism under which calcite mega-concretions form. The studied geological formation was the Sierra Ladrones in the Rio Grande Rift, Albuquerque Basin near Socorro, New Mexico. Initial results of the mega-concretion study were not insightful concerning cementation mechanisms despite numerical representations of the reactions based on measured groundwater characteristics, so this project was not pursued further.

Stratigraphic-Forward Modeling (SFM) is a technique that allows for testing how stratal architecture evolves through time and space. A series of numerical experiments were set up to assess the effects of distance to sediment source and seasonally varying discharge on fluvial processes in a tropical paleoclimate. Post-depositional processes, such as the influence of burial depth on location and amount of preserved sediment also were considered. Input into SFM is based on parameters that control the physical processes through erosion, transportation, and, deposition of sediment. Cores and outcrop samples were used to constrain the range and proportion of grain size.

Experiments described above were applied on a regional scale for an area of 70 km (E-W) by 40 km (N-S). The center of this area of interest is the Mumford Hills petroleum field located in southwestern Indiana. The target of the modeling simulations is the Late Mississippian Mount Pleasant member of the Clore Formation. Available data from the literature were used to estimate the total time for accumulation of the Clore Formation at 2 Ma. Numerical values for sedimentological parameters such flow velocity, sediment concentration, and sediment flux were derived from fluvial characteristics of the Mekong River delta which was inferred to be a useful modern analogue. The selection of an analogue was based on similarity to the studied paleodepositional system in aspects such as latitude, distance to highlands, and seasonal climatic conditions. Results show that relative proportions of different grain sizes in the range of fine-grained sand to silt affect not only the amount of preserved sediment under burial, but also the location where sediment is preserved.

Contents

List of Figures

Part I

Reaction-Transport Modeling: Sierra Ladrones Formation, Socorro, New Mexico

CHAPTER 1

Literature Review

1. Introduction

Cementation is probably the most important diagenetic process controlling reservoir permeability. Cementation commences almost immediately after deposition and continues over a wide range of burial depths and salinity values (Longman, 1980; Beckner, 1996). Composition of cements as well as mode of formation vary. Manifestation of cements range from alteration of petrophysical properties of host rock to building mega-concretions (Figure 1). Longman (1980) suggested four principal environments in which calcite

FIGURE 1. Photograph of mega-concretions and cementation pattern along the Loma Blanca Fault, Socorro Basin, New Mexico.

cementation takes place. These diagenetic environments are distinguished on the basis of the chemical composition of the pore fluids and their distribution in the pore spaces. These four environments are:

(1) **Vadose Zone:** This diagenetic environment lies in the zone that is above the water table and below the surface of the land. The pores in this zone are occupied by air and meteoric water. Diagenetic processes in this zone may either cause solution or precipitation of cements in carbonate sediments. Soil P_{CO_2}, vertical temperature gradients, weathering reactions, and evaporation are important factors that interact to control cementation in the vadose zone (Longman, 1980).

(2) **Phreatic Zone:** Below the water table, calcite cementation can occur in three main diagenetic sections: solution, active, and stagnant. Meteoric water, unsaturated with respect to $CaCO_3$, can dissolve carbonates and develop moldic porosity and vugs in some instances. If aragonite is present, it can be leached and replaced by calcite. Many types of cements may develop in this zone due to a variety of factors including topography, climate, distribution of porosity and permeability, and rate of fluid movement. Cements types that are characteristic of this sub-environment include: equant calcite and isopachous blade calcite (Longman, 1980).

(3) **Mixing Zone:** This zone is characterized by mixing of salt water and fresh water. Cementation in this zone is uncommon. Mixing of freshwater and marine water may results in water that is undersaturated with respect to $CaCO_3$ (Longman, 1980; Sanford and Konikow, 1989a). The degree of saturation depends on the composition and proportion of each end member. Examples of the cements that develop closer to the freshwater end member include micrite and bladed calcite cements.

(4) **Marine Environments:** Sea water is saturated with respect to calcite in marine environments. Tides, waves, and currents induce fluid circulation through pore spaces (Longman, 1980). Most of the cementation processes take place in the close proximity of the sediment/water interface in reefs or surf areas. At the marine water end member of the mixing continuum, Mg-calcite isopachous cements have been

found (Moore, 1977; Longman, 1980). When water movement provides sufficient enough amounts of Mg^{2+}, dolomitization takes place in this zone.

2. Isotopic Signatures in Calcite Cements

Some studies show that cements exhibit identifiable patterns, which are referred to as "cement stratigraphy" (Frykman, 1986; Frank et al., 1982; Tucker and Wright, 1990, p. 355-357). Cements which exhibit similar appearances may be produced in different environments. Therefore, reliance on geochemical analyses (e.g., trace elements, fluid inclusions, stable isotopes) to understand development of cements is becoming increasingly important (Harris et al., 1985).

Isotopic data may be used to identify the zone in which cements precipitated. Additionally, isotopic data may also be used to infer the isotopic signature of the water from which the cements precipitated. For example, Beckner (1996) noted that $\delta^{13}\mathrm{C}$ and $\delta^{18}\mathrm{O}$ exhibit opposite behaviors to one another within vadose and phreatic environments. The vadose zone typically exhibits $\delta^{13}\mathrm{C}$ values that are heavier than those for the phreatic zone. The $\delta^{18}\mathrm{O}$ trend is opposite with values for the vadose zone lighter than those of the phreatic zone.

Clastic sediments can host diverse forms of carbonate cements. Examples of the most common types of these carbonate cements are calcite ($CaCO_3$), dolomite ($CaMg(CO_3)_2$), ankerite ($Ca(\mathrm{Fe, Mg, Mn})(CO_3)_2$), and siderite ($FeCO_3$). A number of factors determine the prevalent type of cement in a particular sandstone. Such factors include: composition of pore fluids, pH, and temperature (Schwartz and Longstaffe, 1988).

Carbonate cements hosted within sandstone rocks may form concretions. In some cases, these concretions may be composed —in their entirety— of calcite. Alternatively, the calcite can form the outer shell of the concretions. The latter type of concretions develop when pore-filling calcite cements precipitate in high permeability zones of sandstone bodies

creating incipient concretions. Calcite cementation continues, after the pores have been filled, forming the outer shells. (Bramlette, 1941; Wilkinson and Dampier, 1990; Cibin et al., 1993; Mozley and Davis, 1996). To date, quantitative models accounting for calcite cementation and concretion formation are rare.

3. Geochemical Mechanisms of Calcite Cementation

Most quantitative geochemical studies of carbonate diagenesis have focused on calcite dissolution rather than precipitation. Suggested mechanisms for calcite dissolution/precipitation include:

(1) **Acid-Induced Dissolution:** King and Liu (1933) conducted their study on marble in acids of dilute concentrations at temperatures ranging between $15\,^{\circ}\mathrm{C}$ and $35\,^{\circ}\mathrm{C}$. They reported that the rate of dissolution is directly proportional to acid concentration and temperature and inversely proportional to viscosity. The latter proportionality indicates that rate is highly dependent on transport. Berner and Morse (1974) showed that at pH < 4, diffusion —H^+ to the surface and Ca^{2+}, HCO_3^-, CO_3^{2-} out of the surface— plays the controlling role. They also showed that in these highly acidic solutions, the dissolution rate is not affected by $\mathrm{P}_{\mathrm{CO}_2}$. Highly basic solutions would result in calcite precipitation.

(2) $\mathrm{P}_{\mathrm{CO}_2}$ **Levels:** The amount of CO_2 dissolved in formation water depends on $\mathrm{P}_{\mathrm{CO}_2}$ as well as on CO_2 produced in soil and/or underlying strata. Higher levels of $\mathrm{P}_{\mathrm{CO}_2}$ lower the pH of water, thus, increasing the rate of dissolution of calcite. A higher rate of CO_2 transport to the mineral-water interface increases the reaction rate too.

(3) **Effects of Impurities:** Impurities can either accelerate or decelerate the rates of calcite precipitation. For example, consider the following reaction:

$$CaCO_3 \quad \underset{b}{\overset{f}{\rightleftharpoons}} \quad Ca^{2+} + \quad CO_3^{2-} \tag{1}$$

where f = forward reaction and b = backward reaction.

The introduction of an impurity, such as PO_4^{3-} will increase the rate of dissolution. This increase is due to the fact that PO_4^{3-} removes Ca^{2+} cations from solution by precipitating $Ca_3(PO_4)_2$. As a result, the reaction is driven to the right. The reverse effect would take place if calcite precipitation were to be considered. (Plummber et al., 1979; Morse, 1983). Growth of calcite ($CaCO_3$) requires that the solution from which it precipitates be supersaturated with respect to $CaCO_3$. Growth is represented by reaction (1) in the backward direction. Formation of the first calcite crystal requires a higher degree of supersaturation to produce a nucleation seed on which the rest of the calcite body would grow. Growth nucleus may also be a foreign seed. (Plummber et al., 1979; Cibin et al., 1993).

(4) **Physical Mechanisms:** Temperature has a two-fold effect on calcite precipitation/dissolution. Higher temperatures cause CO_2 degassing, increasing pH and leading to higher rates of $CaCO_3$ precipitation. Higher temperatures also decrease the solubility product of $CaCO_3$, therefore increasing the rate of precipitation. Increasing fluid pressure has the opposite effect of temperature. Higher pressures produce an increase in the amounts of dissolved CO_2 which in turn decreases the pH value and causes dissolution. (Boggs, 2001).

(5) **Transport Mechanisms:** Mixing of fluids of different chemical compositions and spatial variations in the velocity of ground water flow produce fluids with a variety of saturation states. Sanford and Konikow (1989b) have found that groundwater flux has an important effect on the rate of calcite dissolution. Higher groundwater flux, near discharge zones, gives rise to higher rates of dissolution. Calcite precipitation can be diffusion or advection controlled. Diffusion plays the major role as long as the ions needed for the precipitation reaction are available at the vicinity of the precipitation surface to keep up with the reaction rate. When the reaction starts to

consume the ions faster, advection becomes the major control.

4. Concretions

As calcite cements grow around nucleation points, they sometimes produce hard cemented bodies known as concretions. Calcite concretions are found in the sandstones of the Sierra Ladrones Formation (Pliocene-Pleistocene) in New Mexico and the Northern Apennines (Eocene-Pliocene), Italy (Wilkinson and Dampier, 1990; Cibin et al., 1993; Beckner, 1996; Mozley and Davis, 1996). The shape of these calcite concretions is generally subspherical–ellipsoidal. (Cibin et al., 1993; Beckner, 1996; Mozley and Goodwin, 1995; Mozley and Davis, 1996). These elongated calcite concretions range in size from a few centimeters to meters along the major axis of elongation (Mozley and Goodwin, 1995; Mozley and Davis, 1996). It was suggested in previous studies (Mozley and Davis, 1996; Johnson, 1989; Mcbride et al., 1994; Theakstone, 1981) that the elongated shape of the calcite concretions is related to the direction of the flow of the fluid from which these concretions precipitated.

The inferred relationship from these studies is that the long axis of the concretion is parallel to the direction of the groundwater paleoflow (Mcbride et al., 1994; Mozley and Davis, 1996). This suggests that advection plays an important role in concretion formation. In diagenetic studies, the following question is frequently asked: is the rate of cementation ultimately controlled by transport of species by the moving fluid or by the reaction rate? Determining the controls upon which the rate of cement precipitation depends is one of the most difficult tasks involved in understanding calcite cementation and is one of the focus points of this study.

Diffusion has been suggested as the transport mechanism responsible for the formation of spherical concretions (Wilkinson and Dampier, 1990). Diffusion is a very slow and inefficient transport process. This is mainly due to small diffusion coefficients $(10^{-10} - 10^{-11}\ m^2/s)$.

Upward flow of deep, warm fluids through permeable faults can cause degassing of these fluids. Wood and Boles (1991) hypothesized that calcite cementation could occur under these conditions.

To date, no studies attempt to quantify the geochemical and hydrologic controls of calcite cements and concretions.

5. Purpose of the Study

The present study intends to assess the geochemical and hydrologic mechanisms responsible for the formation of calcite concretions in sandstone formations. We hypothesize that the elongate concretions and fault zone cements form as a result of focused flow into regions of high permeability. We further hypothesize that precipitation within high permeability zones is facilitated by nucleation kinetics. Several specific questions will be addressed in this study including:

- What is the relative importance of chemical diffusion, advection, and nucleation kinetic in forming concretions?
- How do permeability heterogeneities influence calcite concretion? Do high permeability sands and gravels favor formation of calcite concretions?
- What is the precipitation mechanism responsible for cementation along fault zones?
- How long does it take to form concretions?
- Are mechanisms responsible for cement formation in fault zone cements similar to those responsible for concretion genesis?

We will address these questions using a reactive-transport model of carbonate diagenesis. We will construct a series of idealized and site-specific numerical experiments in which geochemical and hydrologic parameters are varied over their known range of uncertainty. The model will be constrained by field observation of calcite cementation within the Sierra Ladrones Formation, New Mexico.

The model will investigate effects of advection, diffusion, temperature, pressure, and nucleation kinetics on calcite precipitation in shallow sandstone aquifers. The geochemistry of the system will be discussed in detail in a subsequent section in this dissertation. This will be followed by a description of the reactive-transport and geochemical speciation model used to represent formation and growth of calcite concretions. We also present a detailed discussion of calcite cementations within the Sierra Ladrones Formation, NM.

6. Reaction-Transport

Reaction-transport modeling is applicable to several fields. For example, ecological and environmental studies (Parkhurst et al., 2003), hydrocarbon reservoir studies in both exploration and production phases (Rocha et al., 2001), and management and remediation of natural water resources (Sracek et al., 2004). Geological problems, usually, have more than one plausible solution. Modeling studies help in testing the plausibility of various scenarios. Predicting the geological outcome of each possible scenario is one of the areas of strength for reaction-transport studies.

Several studies employed the technique of reaction-transport in the study of diagenetic processes. Numerical modeling presents a powerful technique in such studies. This technique permits simultaneous tracking of several species. This approach allows for the accounting of chemical changes along flow paths. Geochemical reactions have the ability to enhance geologic petrophysical properties features, such as porosity via the creation of more pore space through dissolution. Conversely, the same type of reactions may degrade porosity through precipitation which in effect reduces the total pore volume in the rock. (Lasaga, 1984; Steefel and Lasaga, 1992; Lee, 1997)

Lee (1997) and Bethke et al. (2002) illustrate the use of the reaction-transport method in a study that investigates the diagenetic changes that are induced by the flow of groundwater in a hypothetical sedimentary basin (Figure 2). They show that the temperature gradient drives

the fluid movement within the system. This behavior is due to the influence of temperature on fluid density that in turn drives water to flow from zones of lower temperature (higher density) to those of higher temperatures (lower density). (Lee, 1997; Lee and Bethke, 1994; Bethke et al., 2002)

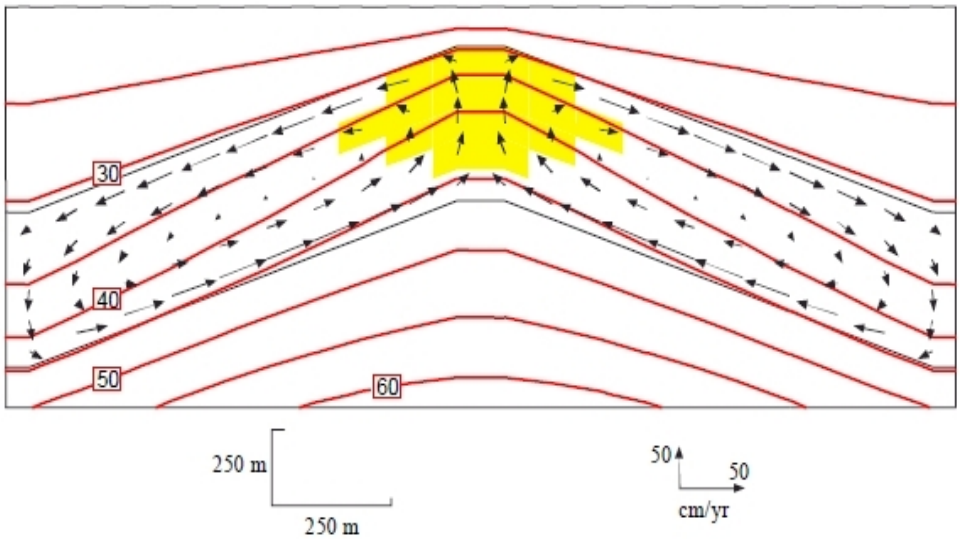

FIGURE 2. Schematic diagram showing predicted patterns of quartz cementation in a hypothetical sloping aquifer. Cementation occurs predominantly within the zone highlighted in yellow. (after Bethke et al., 2002).

7. General Literature Review

7.1. Historical Review of:

7.1.1. Study Area: The study formation and area is the Sierra Ladrones Formation of the Rio Grande Rift in the Albuquerque Basin of central New Mexico (Figure 3). This basin formed as a result of extensional tectonics about 30 Ma. This formation is the uppermost unit (Pliocene-Pleistocene) of the upper Santa Fe Group. The Sierra Ladrones is an important aquifer for urban and rural communities in the area (Davis et al., 1993; Mozley and Davis, 1996; Connell et al., 1998).

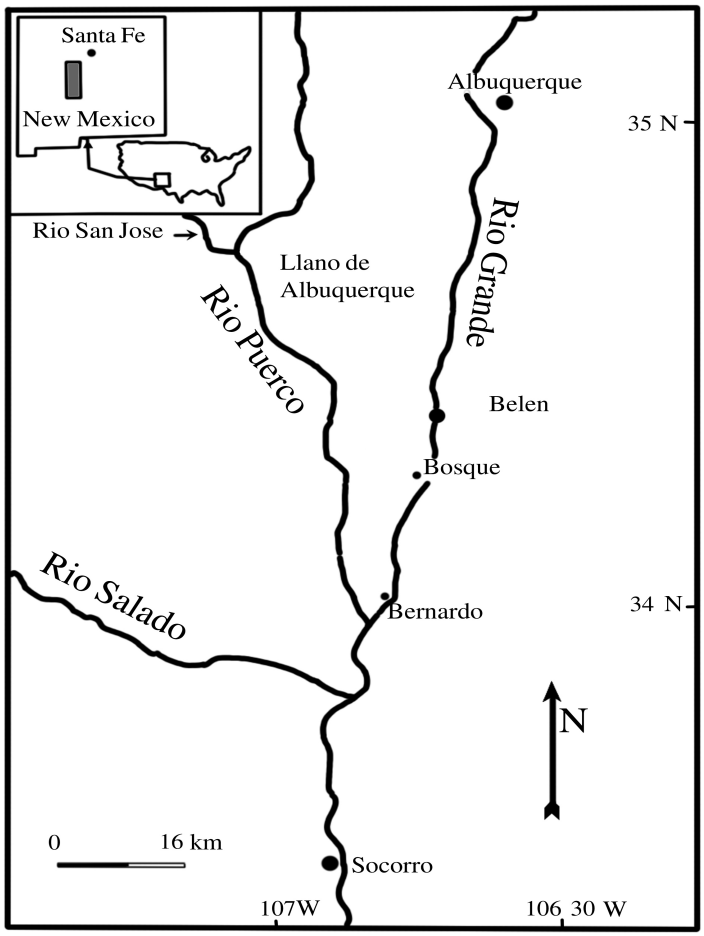

FIGURE 3. General location map of the Rio Grande Rift in New Mexico (after Davis et al., 1993).

The thickness of the Sierra Ladrones Formation is about 460 m in the deepest parts of the basin. It is made up of fluvial deposits developed by the ancestral Rio Grande. This formation is underlain by the closed basin facies of the Zia Formation of the lower Santa Fe Group (McAda and Barroll, 2002).

The Sierra Ladrones Formation sediments are made of two main types of deposits: alluvial-fan and fluvial. Four major elements of depositional architecture were recognized by Davis et al. (1993), (Figure: 4):

- High-energy channel facies: coarse sand and gravel with a thickness of 1–3 m that

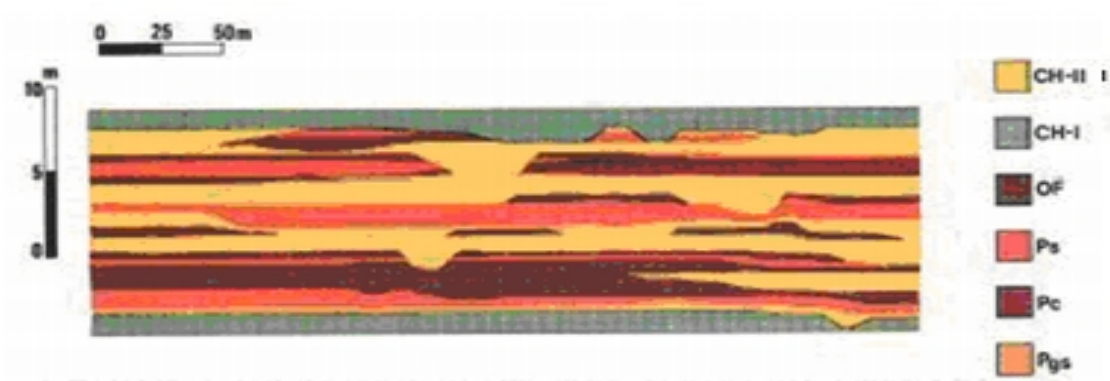

FIGURE 4. Cross-section of the different depositional architectural-elements in the Sierra Ladrones Formation, Albuquerque Basin, New Mexico. CH-II: sand dominated channel deposits; CH-I: gravel and coarse-sand channel deposits; OF: overbank fines; Ps, Pgs, and Pc: paleosoles with varying grain sizes (after Davis et al., 1993).

abruptly pinch-out at the margins of the channel.

- Low-energy channel facies: very fine to medium sand interlaminated with clay drapes; very fine sand; laminated clay and silt near the top; 0.5–5 m thickness.
- Overbank facies: dark brown clay interbedded with tan silt and paleosol (thin immature sand & clay); 1–4 m thickness.
- Paleosol facies: mature sand and clay; thin beds of silty sand and clay are interbedded within the mature sands and clays.

7.1.2. The Loma Blanca Fault: A number of faults are recognized along the Rio Grande Rift. One of these faults is the Loma Blanca Fault (LBF). This is a roughly north-south trending normal fault dipping towards the east that is located at the base of the eastern slopes of the Ladron Mountains (Figure 5). (Machette et al., 1998; Connell, 2001)

This fault is responsible for offsetting both of the Sierra Ladrones Formation (Pliocene-Pliestocene) and the middle to upper alluvium (Pleistocene). The magnitude of this offset has a range of 0.5–10 m (Figure 6). (Machette, 1978; Machette et al., 1998)

The LBF exhibits a feature that is important to the present study. This characteristic is

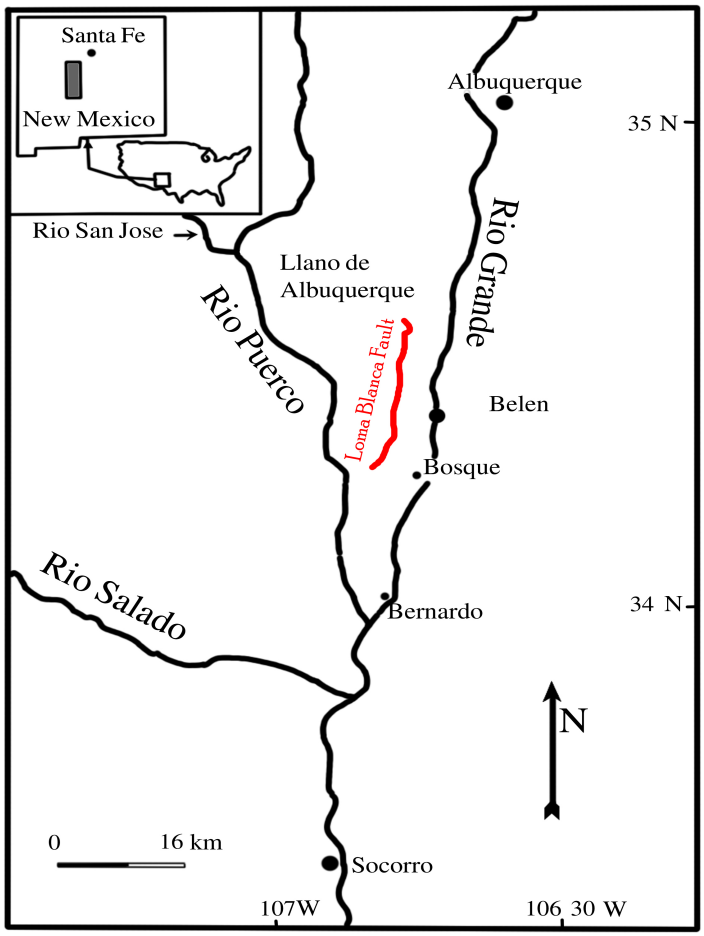

FIGURE 5. Map showing the Loma Blanca Fault, the Rio Grande Rift, New Mexico (modified from Davis et al. (1993) based on Machette, 1978).

manifested in a clastic dike cemented with calcium carbonate and manganese. The width of dike has a range of 2–5 m. This is a clastic dike that is cemented mostly with calcium carbonate and manganese. It is located between Arroyo Canthe and the Rio Salado, New Mexico. (Machette et al., 1998)

This fault has not been extensively studied and Machette and McGimsey (1983) used data collected from scarp morphology as evidence to interpret that latest paleoseismic event involving this fault took place during the late Quaternary ($<$ 130 ka).

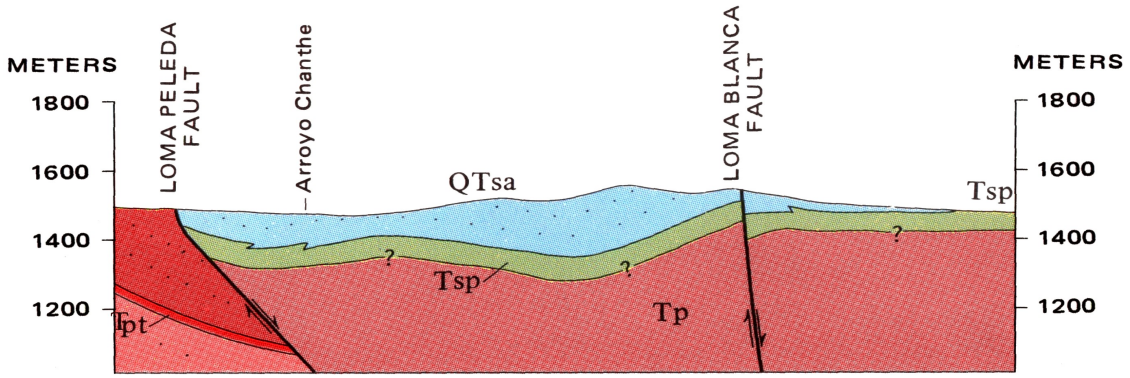

FIGURE 6. Cross-section of the stratigraphy around the Loma Blanca Fault, the Rio Grande Rift, New Mexico. Tpt: Miocene transitional beds; Tp: Miocene Popotosa Formation; Tsp: Upper ? to Lower Pliocene Piedmont slope and alluvial flat deposits; QTsa: Middle Pleistocene-middle? Pliocene axial stream deposits. (modified from Machette, 1978).

8. Patterns of Cementation in the Study Area

Calcite cements within the Sierra Ladrones Formation have two forms: tabular cement beds of great lateral span (over 200 m in some localities) and concretions of various sizes and shapes. The coarser grained sediments within the Sierra Ladrones Formation appear to be preferentially cemented (Figure 7). This suggests that grain size is an important factor on permeability (Mozley and Goodwin, 1995; Mozley and Davis, 1996). The major constituents of the calcite cements are micrite, microspar, and sparite with detrital carbonates as a minor component.

One important feature of the calcite concretions in the Sierra Ladrones Formation is their elongated shape (Figure 8). These concretions are, for the most part, all aligned with each other and are believed to be indicators of groundwater flow directions in the Sierra Ladrones Formation. Groundwater paleoflow direction is south–southeast (Mozley and Davis, 1996). Some of these concretions also have a nodular interior (Figure 9).

Mozley and Davis (1996) employed statistical calculations on the calcite concretions and channel orientations to record the orientation of both features. They show that there is a

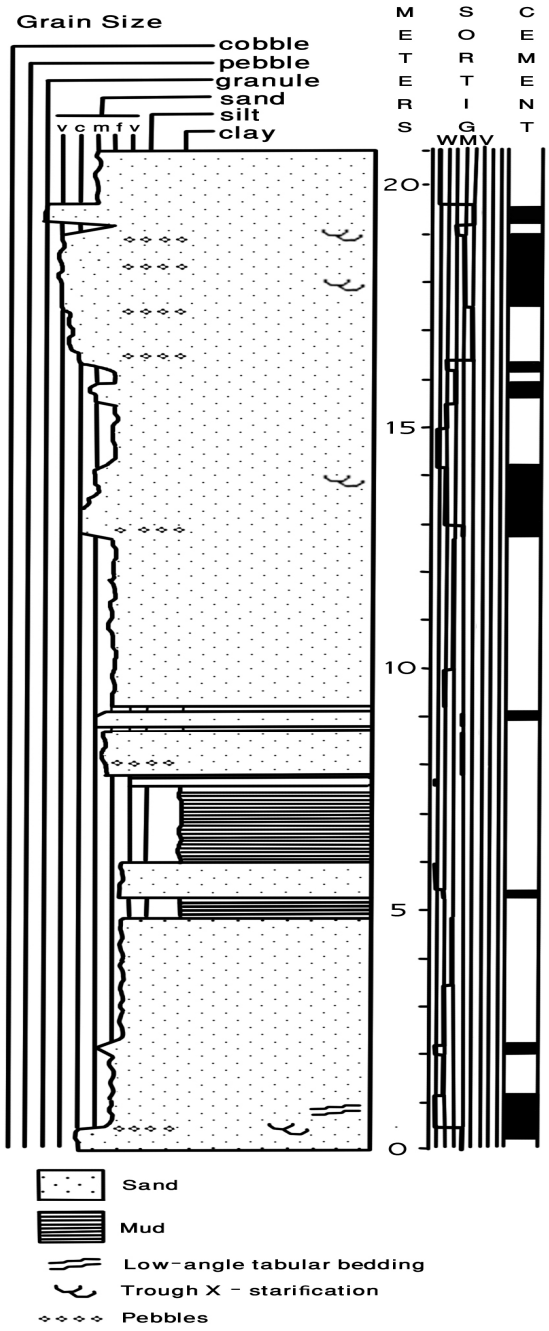

FIGURE 7. Stratigraphic column showing the correlation between cementation and coarse grain zones (modified from Mozley and Davis, 1996).

FIGURE 8. Photographs of elongated concretions from the Sierra Ladrones formation, Socorro Basin, New Mexico.

FIGURE 9. Photograph of nodular concretion from the Sierra Ladrones formation, Socorro Basin, New Mexico.

strong correlation between the direction of groundwater paleoflow of the channels and the axes of elongation of the calcite concretions found in the Sierra Ladrones Formation. The conclusion they drew from the above observation is that in alluvial deposits, the direction of

groundwater paleoflows (major axis of permeability within the system) exerts great influence on the primary structure of the calcite concretions in terms of the major axis of elongated concretions. These findings are in agreement with previous studies e.g., Johnson (1989).

Some faults within the Albuquerque Basin are cemented. There is a great deal of similarity between the cements within the Sierra Ladrones Formation and the cements in the Loma Blanca Fault.

The cements of the LBF are predominantly on the western wall of the fault. This pattern aligns with the general direction of the paleoflow in this area (Figure 1). (Mozley and Davis, 1996)

9. Chemical Composition of the Calcite Cements in the Study Area

Analysis of the chemical composition of the calcite cements shows that there are few impurities (Figure 10) (Mozley and Davis, 1996). One minor impurity in these cements is Mg, but it is present only in very low concentrations. At the present, calcite saturation levels vary spatially in the Rio Grande. Formation waters of the Sierra Ladrones Formation near the Rio Grande River are typically undersaturated whereas those away from the Rio Grande are supersaturated (Mozley et al., 1995). This is most likely due to dissolution of plagioclase and volcanic glass. Aquifers close to the Rio Grande have saturation indices close to the threshold value of saturation of 0.1 (Figure 11). The value of this index increases to 0.5 furthest from the river. These variations may be due to dilution effects caused by mixing of the undersaturated/saturated waters from the river.

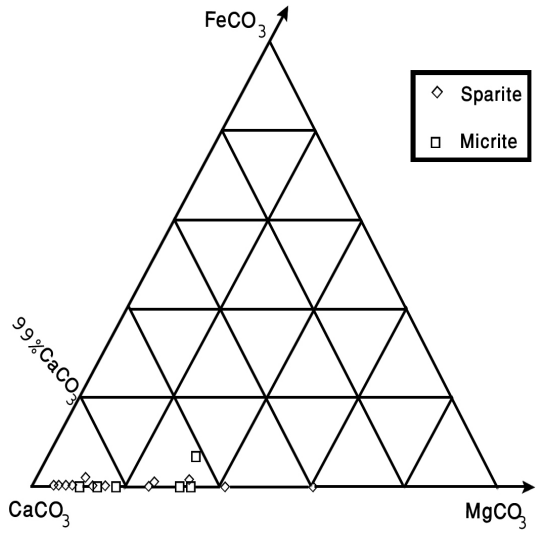

FIGURE 10. Ternary diagram showing the chemical composition of calcite cements from ancestral Sierra Ladrones formation. The scale of the plot is 95 % $CaCO_3$ (mol %) (after Mozley and Davis, 1996).

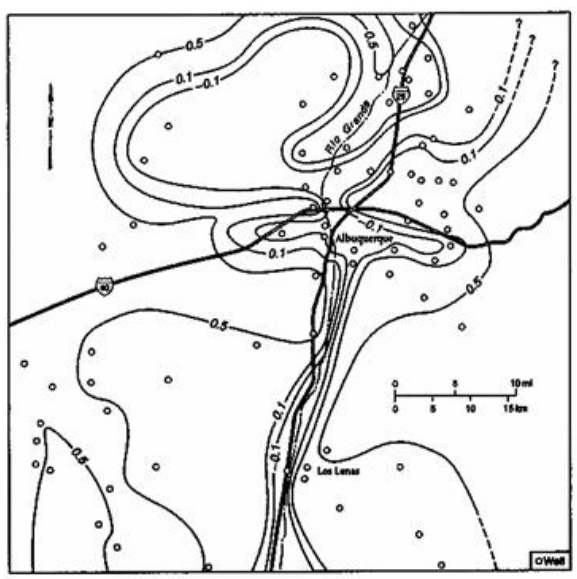

FIGURE 11. Map of calcite saturation levels of groundwater around the Rio Grande river in the central Albuquerque Basin. Supersaturation is indicated by saturation indices greater than 0.1. Waters with indices between -0.1 and 0.1 are saturated. Values below -0.1 indicate undersaturation (after Mozley et al., 1995).

CHAPTER 2

Methods and Results

Section 6 (Reaction-Transport; page 9) of chapter 1 discusses reaction-transport modeling and areas of its application. Modeling studies help in testing the plausibility of various scenarios. In this study, numerical modeling is used to test a number of hypotheses. Each hypothesis represents a mechanism that has been proposed as a controlling factor on development of calcite cements and concretions in the Sierra Ladrones Formation and the Loma Blanca Fault.

1. Basic Governing Equations

1.1. Transport.

(1) **<u>Fluid Flow:</u>**

In order to quantify cementation, geologically constrained flow rates must be determined. The governing flow equation for steady-state, variable density groundwater flow is given by:

$$\left\{ \begin{array}{l} \dfrac{\partial}{\partial x}\left[K_{xx}\,\mu_r\,\dfrac{\partial h}{\partial x} + K_{xy}\,\mu_r\left(\dfrac{\partial h}{\partial y} + \rho_r\right) + K_{xz}\,\mu_r\left(\dfrac{\partial h}{\partial z} + \rho_r\right)\right] \\ + \dfrac{\partial}{\partial y}\left[K_{yx}\,\mu_r\,\dfrac{\partial h}{\partial x} + K_{yy}\,\mu_r\left(\dfrac{\partial h}{\partial y} + \rho_r\right) + K_{yz}\,\mu_r\left(\dfrac{\partial h}{\partial z} + \rho_r\right)\right] \\ + \dfrac{\partial}{\partial z}\left[K_{zx}\,\mu_r\,\dfrac{\partial h}{\partial x} + K_{zy}\,\mu_r\left(\dfrac{\partial h}{\partial y} + \rho_r\right) + K_{zz}\,\mu_r\left(\dfrac{\partial h}{\partial z} + \rho_r\right)\right] \end{array} \right\} = 0 \qquad (2)$$

where:

$K_{xx}, K_{xy}, K_{xz}, K_{yx}, K_{yy}, K_{yz}, K_{zx}, K_{zy}, K_{zz}$ — components of the hydraulic conductivity tensor $[K = k\rho g/\mu]$;

μ_r — relative viscosity $[\mu_r = \mu_o/\mu_f]$;

ρ_r — relative density $[\rho_r = (\rho_f - \rho_o)/\rho_o]$;

x, y, z — spatial coordinates.

The above equation (2) can represent flow induced by fluid density gradients as well as imposed water table gradients along the top boundary. The equation is steady-state. This implies that changes in thermal and hydraulic boundary conditions change slowly on geological time scale over which cementation is thought to occur. Hydraulic head (h) in equation (2), originally derived by Hubbert (1940), is given by:

$$h = \left(\frac{P}{\rho_o\, g}\right) + z \tag{3}$$

where P is fluid pressure, g is gravitational acceleration and z is elevation above some datum. The fluid flux can be related to the gradient in hydraulic head through Darcy's law. A variable density form of Darcy's law that is written in terms of head (see Garven and Freeze, 1984) is used, namely:

$$\begin{aligned}
q_x &= K_{xx}\, \mu_r\, \rho_f\, \frac{\partial h}{\partial x} + K_{xy}\, \mu_r\, \rho_f\, \frac{\partial h}{\partial y} + K_{xz}\, \mu_r\, \rho_f\, \frac{\partial h}{\partial z} \\
q_y &= K_{yx}\, \mu_r\, \rho_f\, \frac{\partial h}{\partial x} + K_{yy}\, \mu_r\, \rho_f\, \frac{\partial h}{\partial y} + K_{yz}\, \mu_r\, \rho_f\, \frac{\partial h}{\partial z} \\
q_z &= K_{zx}\, \mu_r\, \rho_f\, \frac{\partial h}{\partial x} + K_{zy}\, \mu_r\, \rho_f\, \frac{\partial h}{\partial y} + K_{zz}\, \mu_r\, \rho_f\, \frac{\partial h}{\partial z} + K_{zz}\, \mu_r\, \rho_f\, \rho_r
\end{aligned} \tag{4}$$

The principal components of the hydraulic conductivity tensor K are assumed to align with and normal to sedimentary layering. These principal components of the tensor, K_{xx}, K_{yy}, and K_{zz} are thus calculated using the dip of the sedimentary layering as follows:

$$\begin{aligned}
K_{xx} &= K_{max}\, \cos(\theta) + K_{min}\, \sin(\theta) \\
K_{zz} &= K_{max}\, \sin(\theta) + K_{min}\, \cos(\theta) \\
K_{yy} &= K_{max}\, \cos(\theta) + K_{min}\, \sin(\theta)
\end{aligned} \tag{5}$$

where K_{max} is the maximum hydraulic conductivity, K_{min} is the minimum hydraulic conductivity, and dip (θ) is measured relative to horizontal. The maximum conductivity is usually assumed to be in the direction of bedding (or the fault plane in fault zones). The minimum conductivity is typically assumed to be perpendicular to bedding. For faults, K_{max} is oriented parallel to the fault plane. Hydraulic conductivity, in turn, depends on the properties of both the medium and the fluids as:

$$K = \frac{\rho_f \, g \, k}{\mu_f} \tag{6}$$

where k is the medium permeability, which is also a tensor quantity. For each lithologic unit, we will either specify constant a k value or a log-linear relation between k and porosity. Thermodynamic equations of state are required to compute the density and viscosity of ground water at elevated temperature, pressure, and salinity conditions. We will use fitted polynomial expressions presented by Kestin et al., 1981, which are given by:

$$\frac{1}{\rho_f} = \left\{ \begin{array}{l} a(T) + b(T)P + c(T)P^2 + cd(T) + C^2 e(T) \\ - PCf(T) - C^2 Pg(T) - \dfrac{h(T)}{2} P^2 \end{array} \right\} \tag{7}$$

$$\mu_f = \mu_o \left[1 + B\left(T, C\right) P\right] \tag{8}$$

where $a(T) - h(T)$ and $B(T, C)$ are, respectively, the $3rd$ and $4th$ order temperature and concentration dependent polynomials defined by Kestin et al., 1981. These polynomial expressions are valid for temperature ranges between 10 and $150\,^{\circ}\mathrm{C}$ and salinities between 0 and 6 molal NaCl. In general, fluid density is not as sensitive to changes in fluid pressure as changes in temperature and salinity for the range of conditions encountered in sedimentary basins. A critical issue in diagenetic studies is to relate changes in porosity due to precipitation/dissolution reactions to changes in permeability. Some permeability models included sediment

grain size as well as porosity. One such permeability model is based on the Kozeny-Carman equation (Bear, 1972; Scheidegger, 1974). Most have met with limited success, in part because the mixtures of grain sizes in most natural sediments create difficulties. However, Koltermann and Gorelick, 1995 have developed a so-called "fractional packing Kozeny-Carman model" and an approach for arriving at the appropriate representative grain size and porosity for mixtures of sediment sizes. This model is most appropriate before sediments are "lithified" by significant diagenesis. Maximum permeability (k_{max}) can then be calculated using the standard Kozeny-Carman equation and is given by:

$$k_{max} = \left\{ \frac{d^2\ \phi^3}{180\ (1\ -\ \phi)^2} \right\} \tag{9}$$

where d is the diameter of a representative grain.

(2) **<u>Heat Transfer:</u>**

Because temperature changes influence solubility of CO_2, solutions for conductive/convective heat transfer equations are needed. The governing equation for steady-state heat transfer is given by:

$$\left\{ \begin{array}{l} \frac{\partial}{\partial x}\left[\lambda_{xx}\frac{\partial T}{\partial x} + \lambda_{xy}\frac{\partial T}{\partial y} + \lambda_{xz}\frac{\partial T}{\partial z}\right] + \frac{\partial}{\partial y}\left[\lambda_{yx}\frac{\partial T}{\partial x} + \lambda_{yy}\frac{\partial T}{\partial y} + \lambda_{yz}\frac{\partial T}{\partial z}\right] \\ +\frac{\partial}{\partial z}\left[\lambda_{zx}\frac{\partial T}{\partial x} + \lambda_{zy}\frac{\partial T}{\partial y} + \lambda_{zz}\frac{\partial T}{\partial z}\right] \ -\ q_x\ \rho_f\ c_f\ \frac{\partial T}{\partial x}\ -\ q_z\ \rho_f\ c_f\ \frac{\partial T}{\partial z} \end{array} \right\} = 0 \tag{10}$$

where:

T — temperature;

q — Darcy flux;

cf — specific heat capacity of the fluid;

ρ_f — density of the fluid;

$\lambda_{xx}, \lambda_{xy}, \lambda_{yx}, \lambda_{yy}, \lambda_{yz}, \lambda_{zx}, \lambda_{zy}, \lambda_{zz}$ — components of the thermal conductivity-dispersion tensor of the porous medium;

x, y, z — spatial coordinates.

This equation is a representation of heat transport by conduction and convection. The components of the conduction tensor are given by:

$$\begin{aligned}
\lambda_{xx} &= \rho_f c_f \alpha_l \tfrac{q_x^2}{|q|} + \rho_f c_f \alpha_t \tfrac{q_z^2}{|q|} + \lambda_f \phi + (1-\phi)\lambda_s \\
\lambda_{yy} &= \rho_f c_f \alpha_t \tfrac{q_x^2}{|q|} + \rho_f c_f \alpha_t \tfrac{q_z^2}{|q|} + \lambda_f \phi + (1-\phi)\lambda_s \\
\lambda_{zz} &= \rho_f c_f \alpha_t \tfrac{q_x^2}{|q|} + \rho_f c_f \alpha_l \tfrac{q_z^2}{|q|} + \lambda_f \phi + (1-\phi)\lambda_s \\
\lambda_{yx} &= \lambda_{xy} = (\alpha_l - \alpha_t)\, \tfrac{q_x q_y}{|q|} \\
\lambda_{yz} &= \lambda_{zy} = (\alpha_l - \alpha_t)\, \tfrac{q_y q_z}{|q|} \\
\lambda_{zx} &= \lambda_{xz} = (\alpha_l - \alpha_t)\, \tfrac{q_x q_z}{|q|}
\end{aligned} \tag{11}$$

where:

α_l — longitudinal dispersivity;

α_t — transverse dispersivity;

ϕ — porosity;

λ_f — thermal conductivity of the fluid phase;

λ_s — thermal conductivity of the solid phase.

The above equation assumes that fluid and solid phases are in thermal equilibrium.

(3) **Solute Transport:**

The rate of change of mass of a species with respect to time equals the sum of the gradient of flux of that species (mass per unit volume per unit time) plus summation of rates (R) of all reactions involving that specific species. The flux term contains all modes of transport (diffusion, dispersion, and advection) of the particular solute being tracked. Calcite species are the focus of this dissertation. Other minerals, such as siderite ($FeCO_3$) are not present in quantitatively significant amounts to warrant including them in the models (Figure 10).

The governing transport equation for reactive solute transport models is given by:

$$\frac{dC_i}{dt} = \left\{ \begin{array}{l} \frac{\partial}{\partial x}\left[D_{xx}\frac{\partial C_i}{\partial x} + D_{xy}\frac{\partial C_i}{\partial y} + D_{xz}\frac{\partial C_i}{\partial z}\right] \\ +\frac{\partial}{\partial y}\left[D_{yx}\frac{\partial C_i}{\partial x} + D_{yy}\frac{\partial C_i}{\partial y} + D_{yz}\frac{\partial C_i}{\partial z}\right] \\ +\frac{\partial}{\partial z}\left[D_{zx}\frac{\partial C_i}{\partial x} + D_{zy}\frac{\partial C_i}{\partial y} + D_{zz}\frac{\partial C_i}{\partial z}\right] \\ -v_x\frac{\partial C_i}{\partial x} - v_y\frac{\partial C_i}{\partial y} - v_z\frac{\partial C_i}{\partial z} + \sum_{r=1}^{tr}\nu_i^r R^r \end{array} \right\} \tag{12}$$

where:

C_i — concentration in $(moles/m^3)$ of the ith species $\left(\mathrm{H}^+, \mathrm{Ca}_2^+, \mathrm{HCO}_3^-\right)$;

$D_{xx}, D_{xy}, D_{xz}, D_{yx}, D_{yy}, D_{yz}, D_{zx}, D_{zy}, D_{zz}$ — are elements of the hydrodynamic dispersion-diffusion tensor (m^2/s);

x, y, z — spatial coordinates;

v_x, v_y, v_z — flow velocities (m/s) in the x, y (horizontal) and z (vertical) directions, respectively;

t — time (s);

ν_i^r — stoichiometric coefficient of the tracked species in reaction (r); ν_i^r is positive for products and negative for reactants;

R^r — the kinetically controlled reaction rate for reaction (r), [$(moles/m3)/s$];

tr — total number of reactions involving each tracked species.

In order to quantify calcite concentration, we will solve a solute transport equation for each of basis species. The hydrodynamic dispersion tensor is given

by:

$$\begin{aligned}
D_{xx} &= \tfrac{v_x^2}{|v|}\alpha_l + \tfrac{v_z^2}{|v|}\alpha_t + D_d \\
D_{yy} &= \tfrac{v_x^2}{|v|}\alpha_l + \tfrac{v_y^2}{|v|}\alpha_l + D_d \\
D_{zz} &= \tfrac{v_x^2}{|v|}\alpha_t + \tfrac{v_z^2}{|v|}\alpha_l + D_d \\
D_{xy} &= D_{yx} = (\alpha_l - \alpha_t)\,\tfrac{v_x v_y}{|v|} \\
D_{yz} &= D_{zy} = (\alpha_l - \alpha_t)\,\tfrac{v_y v_z}{|v|} \\
D_{xz} &= D_{zx} = (\alpha_l - \alpha_t)\,\tfrac{v_x v_z}{|v|}
\end{aligned} \tag{13}$$

where:

$D_{xx}, D_{xy}, D_{xz}, D_{yx}, D_{yy}, D_{yz}, D_{zx}, D_{zy}, D_{zz}$ — the components of dispersion-diffusion tensor;

v_x, v_y, v_z — seepage velocity in the x, v and z directions defined as (q_x/ϕ, q_y/ϕ, and q_z/ϕ);

D_d — diffusion coefficient;

ϕ — porosity;

$|v|$ — the absolute value of the groundwater velocity defined by $(|v| = \sqrt{v_x^2 + v_z^2})$.

The kinetics of the calcite precipitation reaction will be represented by the general reaction rate expression (R^r):

$$R^r = k^r\, s\,(1 - \Omega^r) \tag{14}$$

where:

R^r — rate of precipitation $\{mole/[m^3$bulk volume $*$ time$(s)]\}$ of the rth reaction;

k^r — specific rate constant for the reaction;

s — reactive surface area (m^2) where reaction may take place (s equal to $V_d^{2/3}$ where V_d is the volume of mineral deposited in the element of volume);

Ω^r — saturation index of the solution with respect to a specific mineral of the rth reaction.

The saturation index (Ω^r) equals (IAP/K_{eqlbrm}), where IAP is the appropriate

product of activities, and $[\ln(K_{eqlbrm}) = A_o/R\,T]$. A_o is the standard state affinity of the mineral reaction; both IAP and K refer to the mineral in question.

The role of nucleation will be incorporated into the rate expression in the following fashion:

$$R^r = k^r \left(V_d^{2/3} \; + \; s_o\right) \; (1 - \Omega^r) \tag{15}$$

where s_o — small positive number if $IAP > 1.5\; K_{eqlbrm}$ and $V_d = 0$, otherwise $s_o = 0$. The 1.5 factor ensures that IAP exceeds K_{eqlbrm} by 50% for nucleation to take place.

The specific rate constant k in equations (14) and (15) is a function of temperature:

$$k \; = A_o^r \; \exp\left[-\frac{E_a^r}{R\,T}\right] \tag{16}$$

where:

A_o^r — the pre-exponential factor, also called the frequency factor. It is a dimensionless number related to the fraction of collision between reactants (with the appropriate orientation) to form the activation complex that leads to formation of the products;

E_a^r — the activation energy for the exchange reaction $(J/mole)$;

R — the universal gas constant $\{8.314 \; [(J/mole)/(K)]\}$;

T — temperature (K).

The volume fractions of the various species change over the course of each numerical experiment (Wang et al., 1995). The rate of change of V_i [the volume fraction of species (i)] is related to the rates of reactions in which this species is involved via molar density $[\rho_m; (mol/m^3)]$ of that species is as follows:

$$\frac{dV_i}{dt} \; = \frac{\sum\limits_{r=1}^{r} R_i^r}{\rho_{mi}} \tag{17}$$

The volume fractions of all species at any point in time must satisfy the following relationship:

$$\sum V_i \; + \phi \; = 1 \tag{18}$$

Additionally, porosity (ϕ) is related to the volume of the deposited material (V_d) via the following equations:

$$\phi \; = \left(\frac{V_T \; - \; V_d}{V_T} \right) \tag{19}$$

$$\frac{d\phi}{dt} \; = \left[- \; \left(\frac{dV_d}{dt} \right) \; \left(\frac{1}{V_T} \right) \right] \tag{20}$$

where V_T is the total volume. Therefore, the porosity lost due to precipitation is equal to the summation of V_d for all the grains in a volume element. i.e.,

$$\phi_{lost} \; = \sum V_d \tag{21}$$

1.2. Reaction. Tracking dissolved species in a fluid as it moves through porous media is a complex task. Concentrations of these species are affected by a variety of chemical and physical factors along the transport path. Reactive-transport models, in general, attempt to encapsulate all these factors for the purposes of quantitative determination of concentrations at every point along the path for the individual species being tracked.

The reactions considered for calcite precipitation are:

$$\underbrace{\mathrm{CaAl_2Si_2O_8}}_{Anorthite} + 8\,\mathrm{H^+} \longleftrightarrow \mathrm{Ca^{2+}_{(aq)}} \; + \; 2\,\mathrm{Al^{3+}_{(aq)}} \; + \; 2\,\mathrm{SiO_{2\,(aq)}} \; + \; 4\,\mathrm{H_2O} \tag{22}$$

Reaction (22), hereafter referred to as Reaction 1 ($Rxn1$), is a dissolution reaction of a Ca-plagioclase (anorthite). This reaction provides the Ca^+_2 necessary for the groundwater to reach supersaturation levels. Calcite precipitation occurs only from supersaturated solutions. The byproducts from $Rxn1$ (e.g., SiO_2 and Al^+_3) are not tracked in this study; and after dissolution, these two cations are left to move with the flowing water and discharged without any further reactions.

Calcite precipitation is a multistep reaction. Water infiltrating soils dissolves CO_2 to form carbonic acid (H_2CO_3), reaction (23), and carries it downward. Carbonic acid then dissociates to form the bicarbonate ion (HCO_3^-), reaction (24). Ca_2^+ from the dissolution reaction (22), combines with the bicarbonate to form calcite, reaction (25).

$$\mathrm{CO_2} + \mathrm{H_2O} \longleftrightarrow \mathrm{H_2CO_3} \tag{23}$$

$$\mathrm{H_2CO_3} \longleftrightarrow \mathrm{H^+} + \mathrm{HCO_3^-} \tag{24}$$

$$\mathrm{Ca^{2+}} + \mathrm{HCO_3^-} \longleftrightarrow \mathrm{H^+} + \mathrm{CaCO_3}\downarrow \tag{25}$$

The overall rate of the final reaction is determined by the slowest step in the series, also known as the rate-determining step. The slowest step in the precipitation reactions is (25). This reaction will be referred to hereafter as Reaction 2 ($Rxn2$). Understanding the physico-chemical behavior of the reactions is crucial to setting up a rigorous model to represent them accurately.

The finite element method is used to represent the solution domain. Computer codes written in FORTRAN 90/95 were developed to calculate concentrations of each of the various species. Chemical reactions alter these concentrations. Changes in concentration are tracked using the above mention computer subroutines. These reaction subroutines were then incorporated into an existing computer program used to study transport in porous media. The transport code was developed by (Person, 2005; Person et al., 2007).

The saturation index Ω {equations (14) and (15)} provides a measure of the likelihood that a specific solute will precipitate from solution or dissolve from the surrounding material. When solution is supersaturated (i.e., $\Omega > 1$), precipitation will occur; whereas when the solution is undersaturated ($\Omega < 1$), dissolution will take place. The Saturation index Ω is defined as follows:

$$\Omega = \frac{IAP}{K_{eqlbrm}} \tag{26}$$

where IAP is the ion activity product and K_{eqlbrm} is the thermodynamic equilibrium

constant. For anorthite dissolution, $Rxn1$ {equation (22)}, and calcite precipitation, $Rxn2$ {equation (25)}, IAP and K_{eqlbrm} are defined using the following equations:

$$IAP_{Rxn1} = \frac{a_{\mathrm{Ca}^{2+}}\ a^2_{\mathrm{Al}^{3+}}\ a^2_{\mathrm{SiO_2}}}{a^8_{\mathrm{H}^+}\ X_{\mathrm{CaAl_2Si_2O_8}}} \tag{27}$$

$$K_{eqlbrm(Rxn1)} = \frac{[\mathrm{Ca}^{2+}]\ [\mathrm{Al}^{3+}]^2\ [\mathrm{SiO_2}]^2}{[\mathrm{H}^+]^8} \tag{28}$$

$$IAP_{Rxn2} = \frac{a_{\mathrm{H}^+}}{a_{\mathrm{Ca}^{2+}}\ a_{\mathrm{HCO_3^-}}} \tag{29}$$

$$K_{eqlbrm(Rxn2)} = \frac{[\mathrm{H}^+]}{[\mathrm{Ca}^{2+}]\ [\mathrm{HCO_3^-}]} \tag{30}$$

where:

$[i]$ — equilibrium concentration of species i;

a_i — activity of species i;

X — mole fraction of the solid phase anorthite relative to other feldspar and glass constituents.

Activities are defined as follows, using a_{H^+} as an example:

$$a_{\mathrm{H}^+} = \gamma\, m_{\mathrm{H}^+} \tag{31}$$

where: γ — the activity coefficient (for H^+in this example)

m_{H^+} — its molality $(mol/kg\ solution)$.

Activity coefficients are most commonly defined using the Deby-Huckel equation in its simplest form:

$$-\log \gamma_{ion} = \frac{1}{2}\, Z^2_{ion} \sqrt{I} \tag{32}$$

where I is the ionic strength of the solution given by:

$$I = \frac{1}{2} \sum [C_{ion}]\, Z^2_{ion} \tag{33}$$

where $[C_{ion}]$ is the molar concentration (mol/L) of the ion of interest and Z_{ion} is its charge. A general assumption for dilute solutions, such as ones considered in this study, is that

activity coefficients for all basic species are set equal to unity.

The species that are tracked in this study are: $[\mathrm{H}^+]$, $[\mathrm{Ca}^{2+}]$, and $[\mathrm{HCO}_3^-]$. For the system under consideration, H_2CO_3 concentration will be set as a boundary condition because it is controlled by the $\mathrm{P}_{\mathrm{CO}_2}$ and CO_2 from soil horizons. To quantify calcite precipitation, we only need to represent the transport of three basic species (Ca^{2+}, HCO_3^-, and H^+). For Calcium (C_{Ca}):

$$\frac{dC_{\mathrm{Ca}}}{dt} = \left\{ \begin{array}{l} \frac{\partial}{\partial x}\left[D_{xx}\frac{\partial C_{\mathrm{Ca}}}{\partial x} + D_{xy}\frac{\partial C_{\mathrm{Ca}}}{\partial y} + D_{xz}\frac{\partial C_{\mathrm{Ca}}}{\partial z}\right] \\ +\frac{\partial}{\partial y}\left[D_{yx}\frac{\partial C_{\mathrm{Ca}}}{\partial x} + D_{yy}\frac{\partial C_{\mathrm{Ca}}}{\partial y} + D_{yz}\frac{\partial C_{\mathrm{Ca}}}{\partial z}\right] \\ +\frac{\partial}{\partial z}\left[D_{zx}\frac{\partial C_{\mathrm{Ca}}}{\partial x} + D_{zy}\frac{\partial C_{\mathrm{Ca}}}{\partial y} + D_{zz}\frac{\partial C_{\mathrm{Ca}}}{\partial z}\right] \\ -v_x\frac{\partial C_{\mathrm{Ca}}}{\partial x} - v_y\frac{\partial C_{\mathrm{Ca}}}{\partial y} - v_z\frac{\partial C_{\mathrm{Ca}}}{\partial z} - R_{Rxn1} - R_{Rxn2} \end{array} \right\} \tag{34}$$

For Hydrogen (C_H):

$$\frac{dC_{\mathrm{H}}}{dt} = \left\{ \begin{array}{l} \frac{\partial}{\partial x}\left[D_{xx}\frac{\partial C_{\mathrm{H}}}{\partial x} + D_{xy}\frac{\partial C_{\mathrm{H}}}{\partial y} + D_{xz}\frac{\partial C_{\mathrm{H}}}{\partial z}\right] \\ +\frac{\partial}{\partial y}\left[D_{yx}\frac{\partial C_{\mathrm{H}}}{\partial x} + D_{yy}\frac{\partial C_{\mathrm{H}}}{\partial y} + D_{yz}\frac{\partial C_{\mathrm{H}}}{\partial z}\right] \\ +\frac{\partial}{\partial z}\left[D_{zx}\frac{\partial C_{\mathrm{H}}}{\partial x} + D_{zy}\frac{\partial C_{\mathrm{H}}}{\partial y} + D_{zz}\frac{\partial C_{\mathrm{H}}}{\partial z}\right] \\ -v_x\frac{\partial C_{\mathrm{H}}}{\partial x} - v_y\frac{\partial C_{\mathrm{H}}}{\partial y} - v_z\frac{\partial C_{\mathrm{H}}}{\partial z} - 8\,R_{Rxn1} + R_{Rxn2} \end{array} \right\} \tag{35}$$

And for bicarbonate (C_{HCO_3}):

$$\frac{dC_{\mathrm{HCO}_3}}{dt} = \left\{ \begin{array}{l} \frac{\partial}{\partial x}\left[D_{xx}\frac{\partial C_{\mathrm{HCO}_3}}{\partial x} + D_{xy}\frac{\partial C_{\mathrm{HCO}_3}}{\partial y} + D_{xz}\frac{\partial C_{\mathrm{HCO}_3}}{\partial z}\right] \\ +\frac{\partial}{\partial y}\left[D_{yx}\frac{\partial C_{\mathrm{HCO}_3}}{\partial x} + D_{yy}\frac{\partial C_{\mathrm{HCO}_3}}{\partial y} + D_{yz}\frac{\partial C_{\mathrm{HCO}_3}}{\partial z}\right] \\ +\frac{\partial}{\partial z}\left[D_{zx}\frac{\partial C_{\mathrm{HCO}_3}}{\partial x} + D_{zy}\frac{\partial C_{\mathrm{HCO}_3}}{\partial y} + D_{zz}\frac{\partial C_{\mathrm{HCO}_3}}{\partial z}\right] \\ -v_x\frac{\partial C_{\mathrm{HCO}_3}}{\partial x} - v_y\frac{\partial C_{\mathrm{HCO}_3}}{\partial y} - v_z\frac{\partial C_{\mathrm{HCO}_3}}{\partial z} - R_{Rxn2} \end{array} \right\} \tag{36}$$

where $Rxn1$ and $Rxn2$ are calculated using the rate expression these reactions respectively as given by equation (15).

1.3. Finite-Element Method. Three-node triangular elements are used to approximate the unknown hydraulic heads, temperatures, and fluid isotopic composition. The shape functions are required to vary linearly across each triangular element (Figure 12), using the

standard Galerkin approach (Wang and Anderson, 1982; Reddy, 1984; Javandel et al., 1984; Istok, 1989; Thompson, 2005). For hydraulic heads (h), the trial solution ($\hat{h}$) is introduced:

$$\hat{h} = \sum_{n=1}^{nnode} \psi_n h_n \tag{37}$$

where $nnode$ is number of nodes of an element. For a three-node triangular element where $nnode = 3$, we have:

$$\hat{h} = \sum_{n=1}^{3} \psi_n h_n = \psi_1 h_1 + \psi_2 h_2 + \psi_3 h_3 \tag{38}$$

where ($\psi_n{}'s$) are the standard Lagrange shape functions defined as:

$$\psi_n = \frac{\alpha_n + \beta_n\, x + \gamma_n\, y}{2A_e} \tag{39}$$

The coefficients in equation (39) are calculated using the nodal coordinates of the vertices of the triangular elements:

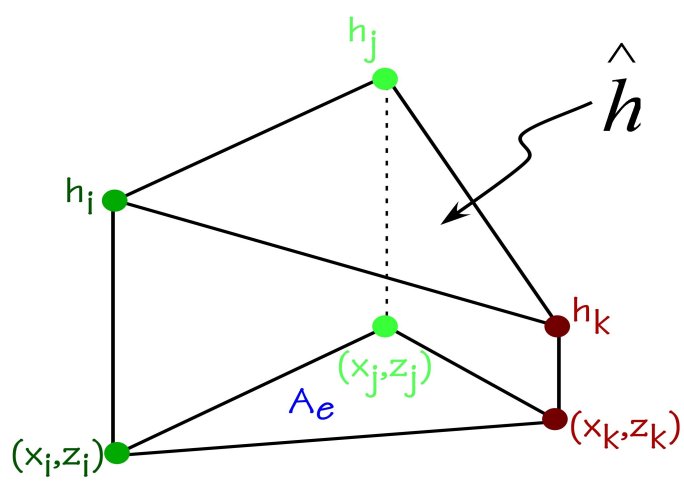

FIGURE 12. Schematic representation of the triangular elements used in the finite element method with the Galerkin approach. The trial solution for the example of hydraulic heads is shown here as $\hat{h}$. The area of the triangular element is represented by A_e.

$$\alpha_1 = x_2 z_3 - x_3 z_2 \qquad \alpha_2 = x_3 z_1 - x_1 z_3 \qquad \alpha_3 = x_1 z_2 - x_2 z_1 \tag{40}$$

$$\beta_1 = z_2 - z_3 \qquad \beta_2 = z_3 - z_1 \qquad \beta_3 = z_1 - z_2 \tag{41}$$

$$\gamma_1 = x_3 - x_2 \qquad \gamma_2 = x_1 - x_3 \qquad \gamma_3 = x_2 - x_1 \tag{42}$$

$$A_e = \frac{\beta_1\gamma_2 - \beta_2\gamma_1}{2} \tag{43}$$

The spatial derivatives of head trial solution ($\hat{h}$) are given by:

$$\frac{\partial \hat{h}}{\partial x} = \sum_{n=1}^{3} h_n \frac{\partial \psi_n}{\partial x} = \frac{b_1 h_1}{2A} + \frac{b_2 h_2}{2A} + \frac{b_3 h_3}{2A} \tag{44}$$

$$\frac{\partial \hat{h}}{\partial y} = \sum_{n=1}^{3} h_n \frac{\partial \psi_n}{\partial y} = \frac{c_1 h_1}{2A} + \frac{c_2 h_2}{2A} + \frac{c_3 h_3}{2A} \tag{45}$$

$$\frac{\partial \hat{h}}{\partial z} = \sum_{n=1}^{3} h_n \frac{\partial \psi_n}{\partial z} = \frac{d_1 h_1}{2A} + \frac{d_2 h_2}{2A} + \frac{d_3 h_3}{2A} \tag{46}$$

In the finite element method, the trial solution is subtituted into the governing groundwater flow equation. This results in some errors since the trial solution is linear while the change of the value of h is nonlinear. The weighted residual errors over an element are required to integrate to zero:

$$\int\int\int \nu \left\{ \begin{array}{l} \left[\frac{\partial}{\partial x}\left(K_{xx}\mu_r\rho_f\frac{\partial \hat{h}}{\partial x} + K_{xy}\mu_r\rho_f\frac{\partial \hat{h}}{\partial y} + K_{xz}\mu_r\rho_f\frac{\partial \hat{h}}{\partial z}\right)\right] \\ + \left[\frac{\partial}{\partial y}\left(K_{yx}\mu_r\rho_f\frac{\partial \hat{h}}{\partial x} + K_{yy}\mu_r\rho_f\frac{\partial \hat{h}}{\partial y} + K_{yz}\mu_r\rho_f\frac{\partial \hat{h}}{\partial z}\right)\right] \\ + \left[\frac{\partial}{\partial z}\left(K_{zx}\mu_r\rho_f\frac{\partial \hat{h}}{\partial x} + K_{zy}\mu_r\rho_f\frac{\partial \hat{h}}{\partial y} + K_{zz}\mu_r\rho_f\frac{\partial \hat{h}}{\partial z} + K_{zz}\mu_r\rho_f\rho_r\right)\right] \end{array} \right\} dx\,dy\,dz = 0 \tag{47}$$

The weighting function is of the form:

$$\nu = \sum_{m=1}^{3} \psi_m \tag{48}$$

Substituting the trial solution and weighting functions into the strong variational form (47) of the differential equation and applying integration by parts (assuming a fully implicit time

formulation) yields a matrix equation of the form, :

$$[A_{mn}]\, h_n = B_m \tag{49}$$

where:

$$A_{mn} = \int\int\int \left\{ \begin{array}{l} \left[K_{xx}\mu_r\rho_f \frac{\partial\psi_m}{\partial x}\frac{\partial\psi_n}{\partial x} + K_{xy}\mu_r\rho_f \frac{\partial\psi_m}{\partial x}\frac{\partial\psi_n}{\partial y} + K_{xz}\mu_r\rho_f \frac{\partial\psi_m}{\partial x}\frac{\partial\psi_n}{\partial z}\right] \\ + \left[K_{yx}\mu_r\rho_f \frac{\partial\psi_m}{\partial y}\frac{\partial\psi_n}{\partial x} + K_{yy}\mu_r\rho_f \frac{\partial\psi_m}{\partial y}\frac{\partial\psi_n}{\partial y} + K_{yz}\mu_r\rho_f \frac{\partial\psi_m}{\partial y}\frac{\partial\psi_n}{\partial z}\right] \\ + \left[K_{zx}\mu_r\rho_f \frac{\partial\psi_m}{\partial z}\frac{\partial\psi_n}{\partial x} + K_{zy}\mu_r\rho_f \frac{\partial\psi_m}{\partial z}\frac{\partial\psi_n}{\partial y} + K_{zz}\mu_r\rho_f \frac{\partial\psi_m}{\partial z}\frac{\partial\psi_n}{\partial z}\right] \end{array} \right\} dx\, dy\, dz \tag{50}$$

The buoyancy term (B_m) in equation (49) is given by:

$$B_m = \int\int \left[\frac{\partial\psi_m}{\partial z} K_{zz}\mu_r\rho_f\rho_r\right] dx\, dy\, dz \tag{51}$$

$$B_m = \left[2\, A \frac{0!}{2!}\, \frac{c_m}{2A}\, K_{zz}\, \mu_r\, \rho_f\, \rho_r\right] = \frac{c_m}{2}\, K_{zz}\, \mu_r\, \rho_f\, \rho_r \tag{52}$$

In matrix form, (B_m) is written as the following vector:

$$B_m = \frac{c_m}{2}\, K_{zz}\, \mu_r\, \rho_f\, \rho_r \begin{bmatrix} 1 \\ 1 \\ 1 \end{bmatrix} \tag{53}$$

Segerlind (1984), introduced the following integration formula that can be used to to evaluate integrals:

$$\int_{A_e} \Psi_m^a\, \Psi_n^b\, dA_e = 2\, A \left[\frac{a!\, b!}{(a+b+2)!}\right] \tag{54}$$

where a and b are the exponents of the interpolation functions.

As an example, assuming that the coordinate system is aligned with the principal directions of the permeability tensor, A_{11} can be found by applying the above integration formula (54) to equation (50):

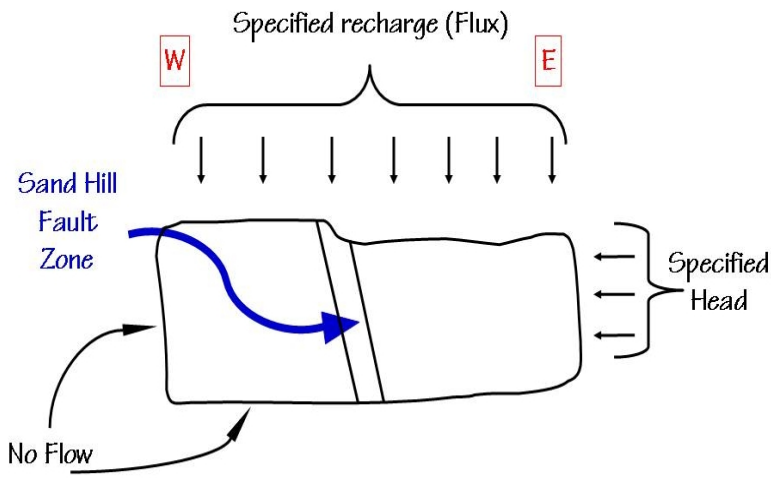

FIGURE 13. Schematic representation of the fluid flow boundary conditions.

$$
\begin{aligned}
A_{11} &= \int\int\int \left(K_{xx}\mu_r\rho_f \frac{\partial\Psi_1}{\partial x}\frac{\partial\Psi_1}{\partial x}\; K_{yy}\mu_r\rho_f \frac{\partial\Psi_1}{\partial y}\frac{\partial\Psi_1}{\partial y}\; K_{zz}\mu_r\rho_f \frac{\partial\Psi_1}{\partial z}\frac{\partial\Psi_1}{\partial z} \right) dx\, dy\, dz \\
A_{11} &= 2A\frac{0!\,0!}{(0+0+2)!}\left[K_{xx}\mu_r\rho_f \frac{\partial\Psi_1}{\partial x}\frac{\partial\Psi_1}{\partial x} \;+\; K_{yy}\mu_r\rho_f \frac{\partial\Psi_1}{\partial y}\frac{\partial\Psi_1}{\partial y} \;+\; K_{zz}\mu_r\rho_f \frac{\partial\Psi_1}{\partial z}\frac{\partial\Psi_1}{\partial z} \right] \\
A_{11} &= V\left[K_{xx}\mu_r\rho_f \frac{b_1^2}{4A^2} \;+\; K_{yy}\mu_r\rho_f \frac{c_1^2}{4A^2} \;+\; K_{zz}\mu_r\rho_f \frac{d_1^2}{4A^2} + \right] \\
A_{11} &= \frac{\mu_r\,\rho_f}{2\,A}\;[K_{xx}b_1^2 \;+\; K_{yy}c_1^2 \;+\; K_{zz}d_1^2]
\end{aligned}
\tag{55}
$$

Applying the integration formula to all components of the local A_{mn} matrix yields:

$$
A_{mn} = \frac{\mu_r\,\rho_f}{4\,A}\left\{ \begin{array}{l} [K_{xx}\,b_m\,b_n + K_{xy}\,b_m\,c_n + K_{xz}\,b_m\,d_n] \\ +\,[K_{yx}\,c_m\,b_n + K_{yy}\,c_m\,c_n + K_{yz}\,c_m\,d_n] \\ +\,[K_{zx}\,d_m\,b_n + K_{zy}\,d_m\,c_n + K_{zz}\,d_m\,d_n] \end{array} \right\} \tag{56}
$$

Solving the fluid flow differential equations above for a specific domain requires defined boundary conditions as shown in Figure 13. Values for hydraulic head are specified on the eastern side of solution domain. The base and western side of the domain are assumed to have very low permeability values that they are essentially barriers to flow. Recharge is specified for the top of the domain.

For heat transfer, we can similarly propose a piecewise linear trial solution into the

governing equation for heat transfer:

$$\int\int\int \nu \left\{ \begin{array}{l} \left[\frac{\partial}{\partial x}\left(\lambda_{xx}\frac{\partial \hat{T}}{\partial x} + \lambda_{xy}\frac{\partial \hat{T}}{\partial y} + \lambda_{xz}\frac{\partial \hat{T}}{\partial z}\right) - c_f \rho_f q_x \frac{\partial \hat{T}}{\partial x}\right] \\ + \left[\frac{\partial}{\partial y}\left(\lambda_{yx}\frac{\partial \hat{T}}{\partial x} + \lambda_{yy}\frac{\partial \hat{T}}{\partial y} + \lambda_{yz}\frac{\partial \hat{T}}{\partial z}\right) - c_f \rho_f q_y \frac{\partial \hat{T}}{\partial y}\right] \\ + \left[\frac{\partial}{\partial z}\left(\lambda_{zx}\frac{\partial \hat{T}}{\partial x} + \lambda_{zy}\frac{\partial \hat{T}}{\partial y} + \lambda_{zz}\frac{\partial \hat{T}}{\partial z}\right) - c_f \rho_f q_z \frac{\partial \hat{T}}{\partial z}\right] - (\rho c)\frac{\partial \hat{T}}{\partial t} \end{array} \right\} dx\, dy\, dz = 0 \tag{57}$$

As in the groundwater flow problem, for a triangular element (i.e., $nnode = 3$), a trial solution is substituted as follows:

$$\hat{T} = \sum_{n=1}^{nnode} \psi_n T_n = \sum_{n=1}^{3} \psi_n T_n = \psi_1 T_1 + \psi_2 T_2 + \psi_3 T_3 \tag{58}$$

The weighting function is identical to the one used in the groundwater flow problem. Applying integration by parts yields:

$$\sum_{m=1}^{3}\sum_{n=1}^{3} \left\{ \begin{array}{c} \left[\iiint \left(\begin{array}{c} \left(\lambda_{xx}\frac{\partial \psi_m}{\partial x}\frac{\partial \psi_n}{\partial x} T_n + \lambda_{xy}\frac{\partial \psi_m}{\partial x}\frac{\partial \psi_n}{\partial y} T_n + \lambda_{xz}\frac{\partial \psi_m}{\partial x}\frac{\partial \psi_n}{\partial z} T_n\right) \\ + \left(\lambda_{yx}\frac{\partial \psi_m}{\partial y}\frac{\partial \psi_n}{\partial x} T_n + \lambda_{yy}\frac{\partial \psi_m}{\partial y}\frac{\partial \psi_n}{\partial y} T_n + \lambda_{yz}\frac{\partial \psi_m}{\partial y}\frac{\partial \psi_n}{\partial z} T_n\right) \\ + \left(\lambda_{zx}\frac{\partial \psi_m}{\partial z}\frac{\partial \psi_n}{\partial x} T_n + \lambda_{zy}\frac{\partial \psi_m}{\partial z}\frac{\partial \psi_n}{\partial y} T_n + \lambda_{zz}\frac{\partial \psi_m}{\partial z}\frac{\partial \psi_n}{\partial z} T_n\right) \end{array} \right) dx\, dy\, dz \right] \\ + \left(c_f\, \rho_f\, q_x\, \psi_m \frac{\partial \psi_n}{\partial x} T_n + c_f\, \rho_f\, q_y\, \psi_m \frac{\partial \psi_n}{\partial y} T_n + c_f\, \rho_f\, q_z\, \psi_m \frac{\partial \psi_n}{\partial z} T_n\right) \end{array} \right\} = 0 \tag{59}$$

This results in a matrix equation of the form, assuming a fully implicit time formulation:

$$\sum_{m=1}^{3}\sum_{n=1}^{3} \left\{ [G_{mn}]\; T_n^{k+1} \right\} = 0 \tag{60}$$

where:

$$G_{mn} = \left\{ \begin{array}{c} \left[\frac{1}{4\,A}\left(\lambda_{xx}\, b_m\, b_n + \lambda_{xy}\, b_m\, c_n + \lambda_{xz}\, b_m\, d_n\right)\right] \\ + \left(\lambda_{yx}\; \mu_r\, c_n + \lambda_{yy}\, c_m\, c_n + \lambda_{yz}\, c_m\, d_n\right) \\ + \left(\lambda_{zx}\, \mu_r\, d_n + \lambda_{zy}\, d_m\, c_n + \lambda_{zz}\, d_m\, d_n\right) \\ + \left[\frac{\rho_f\; c_f}{24}\left(b_n\, q_x + c_n\, q_y + d_n\, q_z\right)\right] \end{array} \right\} \tag{61}$$

For heat transfer, a specified temperature is imposed at the top boundary (water table). Insulating conditions (no heat flow) are imposed on the two sides of the solution domain. At the base of the domain, a specified heat flux boundary condition is imposed. This set up is schematically depicted in Figure (14).

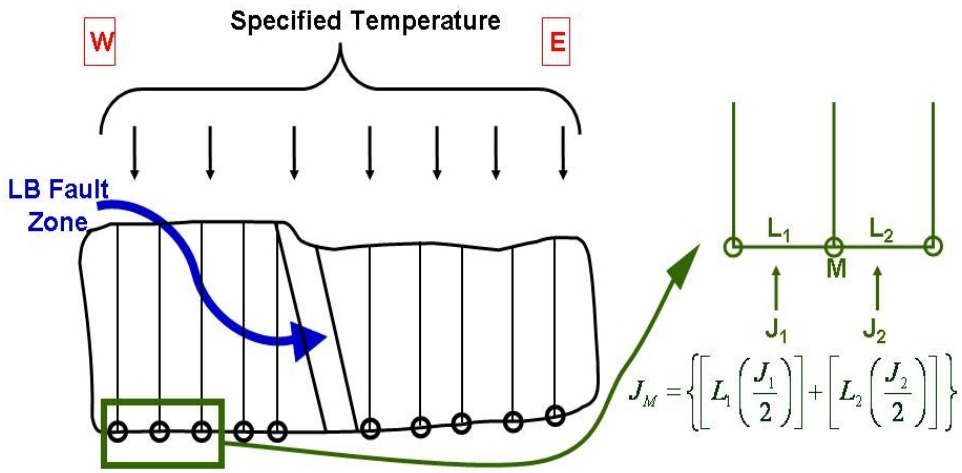

FIGURE 14. Schematic depiction of the boundary conditions for heat transfer equations. At point M, heat flux J_M is obtained from the heat flux values assigned to the neighboring elements as the equation in this figure shows.

For chemical mass transport, the following transport equation is proposed for Ca:

$$\frac{dC_{\mathrm{Ca}}}{dt} = \iiint \nu \left\{ \begin{array}{l} \left[\frac{\partial}{\partial x} \left(D_{xx} \frac{\partial \hat{C}_{\mathrm{Ca}}}{\partial x} + D_{xy} \frac{\partial \hat{C}_{\mathrm{Ca}}}{\partial y} + D_{xz} \frac{\partial \hat{C}_{\mathrm{Ca}}}{\partial z} \right) - c_f \, \rho_f \, q_x \frac{\partial \hat{C}_{\mathrm{Ca}}}{\partial x} \right] \\ + \left[\frac{\partial}{\partial y} \left(D_{yx} \frac{\partial \hat{C}_{\mathrm{Ca}}}{\partial x} + D_{yy} \frac{\partial \hat{C}_{\mathrm{Ca}}}{\partial y} + D_{yz} \frac{\partial \hat{C}_{\mathrm{Ca}}}{\partial z} \right) - c_f \, \rho_f \, q_y \frac{\partial \hat{C}_{\mathrm{Ca}}}{\partial y} \right] \\ + \left[\frac{\partial}{\partial z} \left(D_{zx} \frac{\partial \hat{C}_{\mathrm{Ca}}}{\partial x} + D_{zy} \frac{\partial \hat{C}_{\mathrm{Ca}}}{\partial y} + D_{zz} \frac{\partial \hat{C}_{\mathrm{Ca}}}{\partial z} \right) - c_f \, \rho_f \, q_z \frac{\partial \hat{C}_{\mathrm{Ca}}}{\partial z} - \left(\frac{\partial \hat{C}_{\mathrm{Ca}}}{\partial t} \right) \right] \\ + R_{Rxn1} - R_{Rxn2} \end{array} \right\} dx \, dy \, dz \tag{62}$$

For H^+, the equation is:

$$\frac{dC_{\mathrm{H}}}{dt} = \iiint \nu \left\{ \begin{array}{l} \left[\frac{\partial}{\partial x} \left(D_{xx} \frac{\partial \hat{C}_{\mathrm{H}}}{\partial x} + D_{xy} \frac{\partial \hat{C}_{\mathrm{H}}}{\partial y} + D_{xz} \frac{\partial \hat{C}_{\mathrm{H}}}{\partial z} \right) - c_f \, \rho_f \, q_x \frac{\partial \hat{C}_{\mathrm{H}}}{\partial x} \right] \\ + \left[\frac{\partial}{\partial y} \left(D_{yx} \frac{\partial \hat{C}_{\mathrm{H}}}{\partial x} + D_{yy} \frac{\partial \hat{C}_{\mathrm{H}}}{\partial y} + D_{yz} \frac{\partial \hat{C}_{\mathrm{H}}}{\partial z} \right) - c_f \, \rho_f \, q_y \frac{\partial \hat{C}_{\mathrm{H}}}{\partial y} \right] \\ + \left[\frac{\partial}{\partial z} \left(D_{zx} \frac{\partial \hat{C}_{\mathrm{H}}}{\partial x} + D_{zy} \frac{\partial \hat{C}_{\mathrm{H}}}{\partial y} + D_{zz} \frac{\partial \hat{C}_{\mathrm{H}}}{\partial z} \right) - c_f \, \rho_f \, q_z \frac{\partial \hat{C}_{\mathrm{H}}}{\partial z} - \left(\frac{\partial \hat{C}_{\mathrm{H}}}{\partial t} \right) \right] \\ - 8 \, R_{Rxn1} + R_{Rxn2} \end{array} \right\} dx \, dy \, dz \tag{63}$$

Similarly, for HCO_3^{2-}, the equation is:

$$\frac{dC_{\mathrm{HCO_3}}}{dt} = \iiint \nu \left\{ \begin{array}{l} + \left[\begin{array}{l} \frac{\partial}{\partial x}\left(D_{xx}\frac{\partial \hat{C}_{\mathrm{HCO_3}}}{\partial x} + D_{xy}\frac{\partial \hat{C}_{\mathrm{HCO_3}}}{\partial y} + D_{xz}\frac{\partial \hat{C}_{\mathrm{HCO_3}}}{\partial z}\right) - c_f \rho_f q_x \frac{\partial \hat{C}_{\mathrm{HCO_3}}}{\partial x} \\ \frac{\partial}{\partial y}\left(D_{yx}\frac{\partial \hat{C}_{\mathrm{HCO_3}}}{\partial x} + D_{yy}\frac{\partial \hat{C}_{\mathrm{HCO_3}}}{\partial y} + D_{yz}\frac{\partial \hat{C}_{\mathrm{HCO_3}}}{\partial z}\right) - c_f \rho_f q_y \frac{\partial \hat{C}_{\mathrm{HCO_3}}}{\partial y} \end{array} \right] \\ + \left[\begin{array}{l} \frac{\partial}{\partial z}\left(D_{zx}\frac{\partial \hat{C}_{\mathrm{HCO_3}}}{\partial x} + D_{zy}\frac{\partial \hat{C}_{\mathrm{HCO_3}}}{\partial y} + D_{zz}\frac{\partial \hat{C}_{\mathrm{HCO_3}}}{\partial z}\right) \\ -c_f \rho_f q_z \frac{\partial \hat{C}_{\mathrm{HCO_3}}}{\partial z} - \left(\frac{\partial \hat{C}_{\mathrm{HCO_3}}}{\partial t} \right) \end{array} \right] - R_{Rxn2} \end{array} \right\} dxdydz \tag{64}$$

As in the groundwater flow problem, a trial solution is substituted as follows :

$$\hat{C} = \sum_{n=1}^{nnode} \psi_n C_n = \sum_{n=1}^{3} \psi_n C_n = \psi_1 C_1 + \psi_2 C_2 + \psi_3 C_3 \tag{65}$$

The weighting function is identical to the one used in the groundwater flow problem. Substituting the trial solution and weighting function into the chemical mass transport equation yields:

$$\sum_{m=1}^{3}\sum_{n=1}^{3} \left\{ \begin{array}{c} \left[\iiint \left(\begin{array}{c} \left(\lambda_{xx}\frac{\partial \psi_m}{\partial x}\frac{\partial \psi_n}{\partial x} C_n + \lambda_{xy}\frac{\partial \psi_m}{\partial x}\frac{\partial \psi_n}{\partial y} C_n + \lambda_{xz}\frac{\partial \psi_m}{\partial x}\frac{\partial \psi_n}{\partial z} C_n \right) \\ + \left(\lambda_{yx}\frac{\partial \psi_m}{\partial y}\frac{\partial \psi_n}{\partial x} C_n + \lambda_{yy}\frac{\partial \psi_m}{\partial y}\frac{\partial \psi_n}{\partial y} C_n + \lambda_{yz}\frac{\partial \psi_m}{\partial y}\frac{\partial \psi_n}{\partial z} C_n \right) \\ + \left(\lambda_{zx}\frac{\partial \psi_m}{\partial z}\frac{\partial \psi_n}{\partial x} C_n + \lambda_{zy}\frac{\partial \psi_m}{\partial z}\frac{\partial \psi_n}{\partial y} C_n + \lambda_{zz}\frac{\partial \psi_m}{\partial z}\frac{\partial \psi_n}{\partial z} C_n \right) \end{array} \right) dx\,dy\,dz \right] \\ + \left(c_f\,\rho_f\,q_x\,\psi_m\,\frac{\partial \psi_n}{\partial x}\,C_n + c_f\,\rho_f\,q_y\,\psi_m\,\frac{\partial \psi_n}{\partial y}\,C_n + c_f\,\rho_f\,q_z\,\psi_m\,\frac{\partial \psi_n}{\partial z}\,C_n \right) \end{array} \right\} = 0 \tag{66}$$

This results in a matrix equation of the form, assuming a fully implicit time formulation:

$$\sum_{m=1}^{3}\sum_{n=1}^{3} \left\{ [S_{mn}]\; C_n^{k+1} \right\} = \sum_{M=1}^{3} L_M \tag{67}$$

where:

$$S_{mn} = \left\{ \begin{array}{c} \left[\frac{1}{4\,A} \left(\lambda_{xx}\,b_m\,b_n + \lambda_{xy}\,b_m\,c_n + \lambda_{xz}\,b_m\,d_n \right) \right] \\ + \left(\lambda_{yx}\;\mu_r\,c_n + \lambda_{yy}\,c_m\,c_n + \lambda_{yz}\,c_m\,d_n \right) \\ + \left(\lambda_{zx}\,\mu_r\,d_n + \lambda_{zy}\,d_m\,c_n + \lambda_{zz}\,d_m\,d_n \right) \\ + \left[\frac{\rho_f\,c_f}{24} \left(b_n\,q_x + c_n\,q_y + d_n\,q_z \right) \right] \end{array} \right\} \tag{68}$$

and L_M is given by:

$$L_M = \iiint \psi_M \left(R_{Rxn1} - R_{Rxn2} \right) dx\,dy\,dz \tag{69}$$

Evaluating the integral in equation (69) and putting the result in matrix form gives L_M as:

$$L_M = \left(\frac{A_e}{3}\right) \begin{bmatrix} 1 \\ 1 \\ 1 \end{bmatrix} (R_{Rxn1} - R_{Rxn2}) \tag{70}$$

The boundary conditions for the chemical mass transport are defined such that the boundaries east of the Loma Blanc fault zone are all advective. The area to the west of the fault zone are set differently. The bottom and western boundaries are set to allow no flux whereas the top boundary is set to have a specified equilibrium concentration; Figure (15). The equilibrium concentration on the western side of the domain will specified using atmospheric conditions.

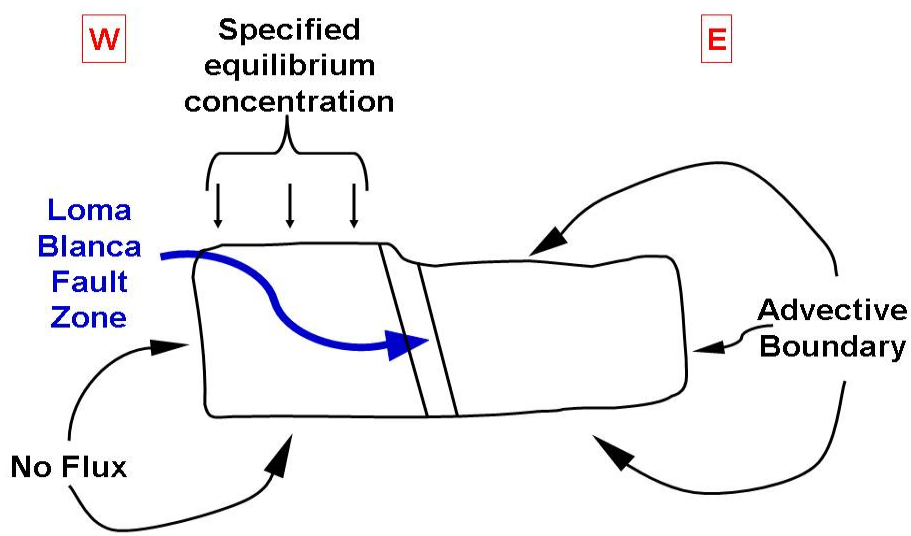

FIGURE 15. Schematic representation of the boundary conditions used in solving the chemical mass transport equations.

2. Mesh Generation

The mesh generator used in this study is modified from a computer program developed by Dina L. Lopez (López and Smith, 1995). The modifications introduced to the code by the author introduce the ability to create sub-domain finite element meshes that are of finer resolution than the overall domain. The modified FORTRAN code for this mesh generator is listed in Appendix A.1. An example input file for the modified mesh generator is presented in Appendix A.2.

3. Tracking Chemical Reactions

The author developed FORTRAN 90/95 computer code to calculate reaction rates of anorthite dissolution and calcite precipitation. This code is listed in Appendix B. This code has the capability to track porosity alteration (creation and destruction) and outputs net porosity changes. The author built this code based on equations {(15): page 26, (17) – (22): page 27, (25): page 28, and (27) – (29): page 29}.

4. Transport and Tracking of Chemical Species

Computer FORTRAN code was developed by the author to keep track of various chemical species while they undergo reactions throughout the life of simulations and as they get transported through the domain of simulation. The transport portions of the code were developed by (Person, 2005; Person et al., 2007).

4.1. Transport and Tracking of Ca^{2+}. The equations used to build this part of the code are: (34): page 30, (62): page 36, (65) – (70): page 38. The code is listed in Appendix C.1.

4.2. Transport and Tracking of H^{+}. For this part of the code, the equations used are: (35): page 30, (63): page 36, (65) – (70): page 38. The code is listed in Appendix C.2.

4.3. Transport and Tracking of HCO_3^-. The equations used to build this part of the code are: (36): page 30, (64): page 37, (65) – (70): page 38. The code is listed in Appendix C.3.

5. Results

This research project was a success in the sense that it incorporated field observations into a numerical model. The steps involved translating verbal descriptions into numerical values for various parameters. Another aspect of success for this project is the development of a number of computer subroutines that can be used to study reactions associated with dissolution of anorthite, equation (22) and deposition of calcite, equation (25). Appendices B and C list these subroutines. Additional contribution came in the form of added capabilities to a finite element mesh generator. that is capable of creating sub-meshes that have finer resolution compared to the original domain. This added functionality permits the user to assign different properties to different parts of the mesh. Thus allowing simultaneous experimentation with varying characteristic values for the property under study. Details are in Appendix A.1.

Initial results from this study were not sufficiently insightful to explain the mechanism under investigation even though the numerical representations of the reactions involved were correct. The numerical design of these experiments did not account for the potentially important effects of microbial biomass on calcite precipitation. In recent years, it has been shown that presence of biological activity enhances (*catalyzes?*) the precipitation of $CaCO_3$ (Kandianis et al., 2008). This revelation led to rethinking of the mechanisms of formation of calcite cementation and put focus on the role of microbial biomass in the cementation reactions (van der Kooij et al., 2010). The increase in the reaction rate due to presence of microbial biomass can be significant although it has not been well quantified (Kandianis et al., 2008; van der Kooij et al., 2010; Zaihua et al., 2010). Recent

findings by Fouke (2011) show that a complex relation exists between biotic and abiotic processes. Fouke (2011) has shown that rapid precipitation rates of travertine result from this complex interplay between these biotic and abiotic processes. Future reaction-transport models should take advantage of these recent advances and incorporate the role of microbial biomass in rate expressions, such as equation (15); page 26.

Part 2

Forward-Stratigraphic Modeling: Clore Formation, Mumford Hills, Indiana

CHAPTER 3

Introduction

This part of the dissertation discusses exploring the use of forward-stratigraphic modeling as a tool to gain insightful understanding of depositional seetings/environments (Griffiths, 2001). The investigation will be applied on the Clore Formation in the Mumford Hills oil field, southwestern Indiana (Potter, 1962; Swann, 1964; Treworgy, 1991; Droste and Keller, 1995). The study will probe the relationships between depositional settings on a semi regional scale and sediment preservation.

1. Geological Settings, Paleogeography, and Paleoclimate

The Mississippian Clore Formation is a part of the Buffalo Wallow Group (Droste and Keller, 1995). This group is part of the Chesterian Series (Weller, 1913; Swann, 1963; Droste and Keller, 1995) of the rock record of the Illinois Basin. The main lithological units of the Clore Formation in Indiana are limestone, sandstone, and shale. In Indiana, the most ubiquitous lithology is shale (Droste and Keller, 1995). The Clore Formation was deposited during the Late Mississippian (Figure 16). However, there are no studies that establish temporal constraints on its actual age range (Droste and Keller, 1995; Treworgy, 2004; May et al., 2009). The closest approximation available, to date, for the total time of deposition for the Clore Formation can be anywhere from 300 ky to 800 ky. The conodont species called *C. monoceras*, also known by the common name *Adetognathus unicornis*, has been reported in the Clore Formation. The same species has also been found in the overlying Kinkaid Limestone. To date, there is no reliable biostratigraphic data for the Degonia Formation that lies between the Clore and the Kinkaid. Therefore, the age of the Clore Formation is poorly constrained. (Swann, 1963, 1964; Norby, 1991; Treworgy, 2004; Rexroad et al., 2010).

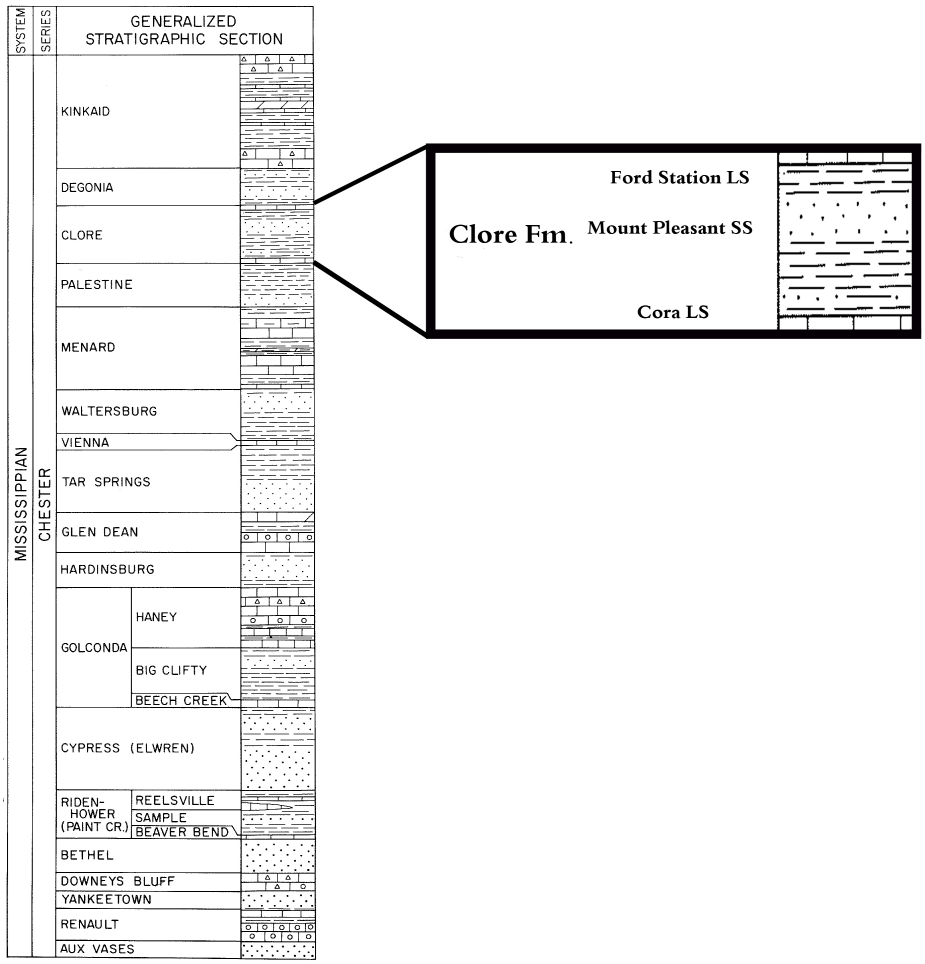

FIGURE 16. Stratigraphic column of the Chesterian Series of the Illinois Basin with emphasis on the Clore Formation — and its three members (modified from Atherton et al., 1960).

The Illinois Basin began its history as a rift complex. Thermal subsidence was the driving mechanism during the first part of the Paleozoic (520–350 mybp). From mid-Mississippian through Permian time, the Illinois basin underwent declining subsidence with the rate of sedimentation matched to the rate of subsidence and little or no accumulation of sedimentary units after the end of the Paleozoic (Siever, 1951; Swann, 1964; Heidlauf et al., 1986; Buschbach and Kolata, 1991). A sediment accumulation rate of $45\ m/10^6$ year has been report by Heidlauf et al. (1986) for the Pope megagroup which contains the Clore

Formation (Swann and Willman, 1961).

In Illinois, the Clore Formation is composed, in ascending order, of a lower carbonate member, called the Cora Limestone, a middle sandstone member, called the Mount Pleasant Sandstone, and an upper carbonate member called the Ford Station Limestone (Figure 16). These three members correspond generally to phases of transgression, regression, and another transgression, respectively (Swann, 1963; Treworgy, 1988; Craig and Varnes, 1979; Howard, 1991; Droste and Keller, 1995; Smith and Read, 2001; Treworgy, 2004).

Swann (1963) showed that the sediment supply during Chesterian time was from the northeast. He proposed the name Michigan River (Figure 17), for the drainage system that carried sediment from the Canadian highlands into the Illinois Basin. Swann (1964) illustrated that shallow-marine and coastal sediment accumulation was cyclical during the late Paleozoic in the Illinois Basin. Depositional settings alternated between shallow marine conditions indicated by conodonts, and terrestrial coastal conditions indicated by *Stigmaria* roots (Swann, 1964; Rexroad et al., 2010). The cyclic depositional nature of these rock units is a result of repeated advances and retreats of the shoreline (Swann and Willman, 1961; Potter and Pryor, 1961; Swann, 1964; Kahmann and Driese, 2008). During Clore deposition, the Cincinnati and Ozark Arches probably were submerged or only slightly elevated above sea level and the amount of sediment provided by these features is considered inconsequential (Siever, 1951; Swann, 1963). The Michigan River paleodelta is interpreted to have experienced large lateral shifts of some 200 miles, accompanied by roughly axial shoreline migration of 600–1000 miles (Figure 17), resulting in cyclic alternation of sedimentation patterns on the northern and northeastern margin in the basin (Swann and Bell, 1958; Potter and Pryor, 1961; Swann, 1963; Treworgy, 1988).

The location of the Illinois Basin during the time of Clore deposition (Figure 18) was south of the equator at an approximate paleolatitude of 5–15 degrees South i.e., in the tropicas (Craig and Varnes, 1979; Scotese and McKerrow, 1990; Smith and Read, 2001;

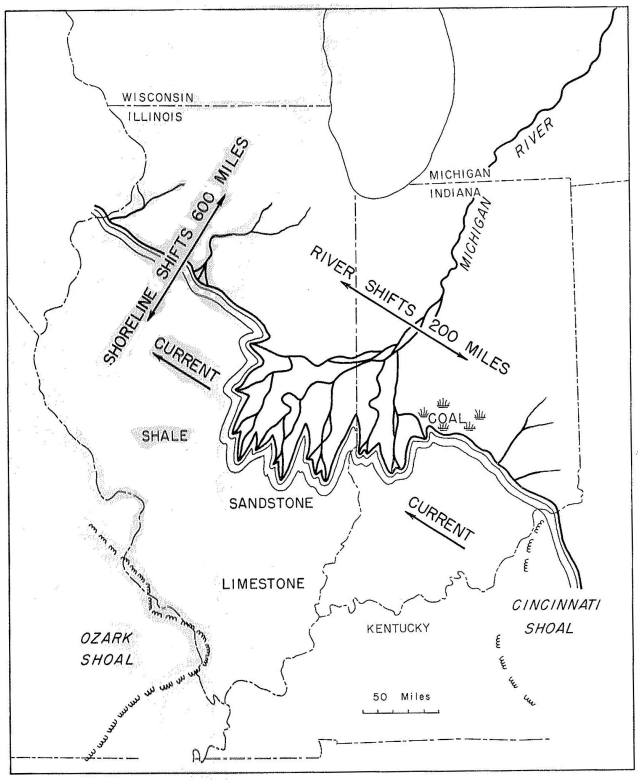

FIGURE 17. Paleogeographic map showing the Michigan River supplying sediment into the Illinois Basin from Canadian highlands during the Chestrian (after Swann, 1963).

Treworgy, 2004)). Globally, the time was one of change from greenhouse conditions to major continental glaciation (Smith and Read, 2001). The tropical climate is interpreted to indicate that the area experienced seasonal monsoonal flows similar to present-day southeast Asia.

The monsoonal interpretation is invoked here because of similarities in conditions to areas that experience monsoonal seasons at the present. During warm seasons, continental land masses across the land–sea thermal contrast undergoes thermal thawing. This results in the creation of zones of low surface pressure over land. Wind then flows from the relatively cold (high pressure) ocean into the low pressure continent. The wind in such situations carries excessive amounts of moisture with it. This moisture is then dropped on the continent

when the wind enters the low pressure zone in the form of monsoonal precipitation. These conditions are responsible for monsoonal seasons in places like India. In the Chesterian, the location of the AOI for this study (Figure 18) was in the tropics and therefore susceptible to receiving monsoonal precipitation when the North American land mass warmed.

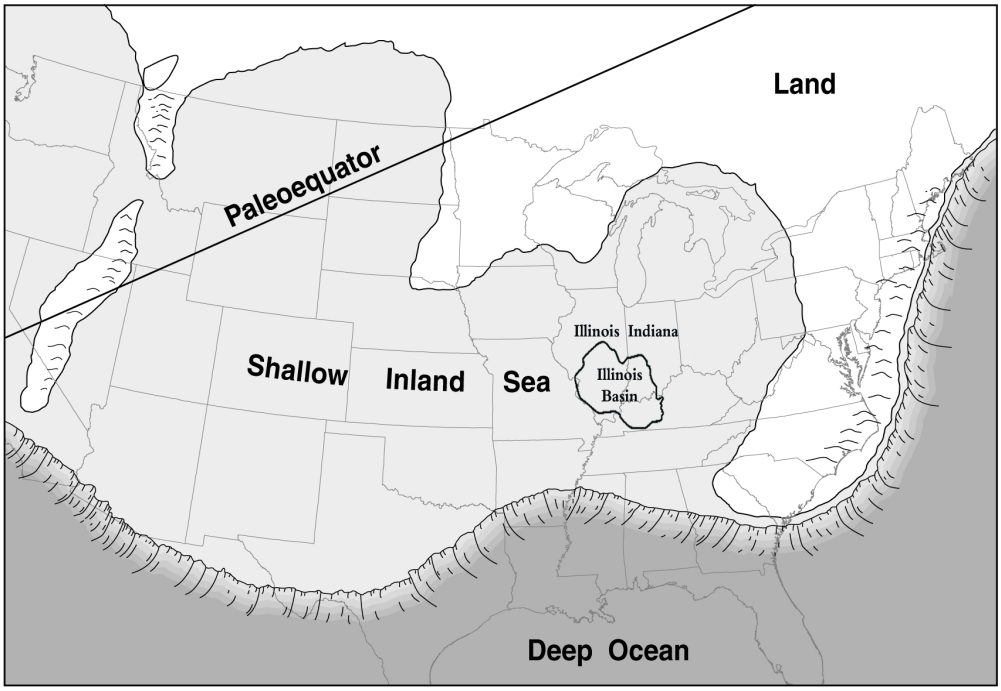

FIGURE 18. Paleogeographic map showing the location of the Illinois Basin and the State of Indiana relative to the equator during the Mississippian ∼ 350 million years ago (modified from Smith and Read, 2001; Treworgy, 2004).

During the middle–late Mississippian, the northern part of the Illinois Basin has been interpreted as a shallow, gently sloping ramp that dipped toward the southwest. (Heidlauf et al., 1986; Smith and Read, 2001) Sediment accumulation was not uniform throughout the basin. The unequal rate of sedimentation led to variations in thicknesses of sand bodies throughout the basin. Thicknesses of these sandstone bodies vary from approximately 10 m to 30 m. Wireline logs indicate that the thickest accumulations are found in the central part of the basin, in southern Illinois. These sand bodies have a distinguishing characteristic

related to grain size. They are described to have uniform grain sizes in the range of fine to very-fine sand (Potter and Pryor, 1961; Swann, 1963, 1964; Droste and Keller, 1995; Root, 2010)

2. Modern Analog

Simulating of a paleo-transportation and deposition system using stratigraphic-forward modeling (SFM) requires knowledge of the parameters that controlled the physical process in the system. The simulation parameters can come from previous studies, field data, or comparison with a modern analog environment. In order to apply SFM to an ancient system, modern analogs are often selected to represent the physical characteristics that may have influenced the ancient system. The laws of physics that govern geological processes have not changed throughout the life of the Earth. Therefore, understanding processes in the modern and the parameters associated with them provides the means to screen modern analogs. Selection of an appropriate modern analog for a sedimentary unit being studied by modeling is based on perceived similarities for climate, regional geography, local landscape and unusual sedimentary features such as the uniformly fine-grained nature of the sandstone bodies in the Clore Formation.

The modern analog should have similar characteristics to those thought to have prevailed during the times being modeled. For the present study, the modern analog that best meets key criteria is the Mekong River (Figure 19) of southeast Asia.

The Mekong River is an appropriate modern analog for modeling of the paleo-Michigan River. Direct comparison of the paleo-Michigan and the modern Mekong Rivers (Table 1) is hindered by the various unknown aspects of the paleo-Michigan River. However, the missing data do not reduce the suitability of the Mekong River as an appropriate modern analog given the inevitable difficulty in characterizing ancient depositional systems from the rock record. Both deltas are in the tropics but the Mekong delta is located north of the modern equator and

FIGURE 19. General location map of the Mekong River.

the paleo-Michigan delta was located south of the Late Paleozoic equator. Both river systems are sourced from highlands located in the mid-latitudes and discharge into deltas at low latitude. The Mekong River has its source in the Tibetan highlands and the paleo-Michigan River was sourced from the Canadian highlands. Both rivers carried sediment for long distances, although the Mekong River runs over a greater distance with some sinuosity in its path. For the Mekong River, the distance from its source to delta is approximately 5000 km. This river has a number of tributaries. For the paleo-Michigan River, however, its actual length, number of major tributaries, and sinuosity are unknown (Swann, 1964; Wolanski et al., 1998; Anikiyev et al., 1986).

The variables of interest that are to be gleaned from a modern system include flow

TABLE 1. Comparison of the Paleo-Michigan and the Mekong Rivers

	Paleo-Michigan River	Mekong River[1]
Latitude	Approximately $(5 - 10)^\circ$ south of the Paleo-Equator	Approximately 10° north of the Equator
Climate	Tropical: influenced by the ITCZ[2]	Tropical: influenced by the ITCZ
Vegetation	Vegetated at times	Vegetated
Source Height	High but not well-known	Average of 5000 m
River length	Long but not well-known	About 5000 km
Sediment load	Unknown	Average of 1200 (kg/m^3)
Flow velocity	Unknown	1 (m/s)
Number of tributaries	Unknown	Many

1:Values for the Mekong River are from (Anikiyev et al., 1986; Wolanski et al., 1998)

2:The ITCZ is the intertropical convergence zone where trade winds from north and south of the equator converge. It is characterized by seasonal shifts in wind direction and magnitude.

velocity, flux of water, sediment concentration, and seasonal variabilities. These values need, in most cases, to be adjusted in order to account for known or inferred dissimilarities between the analogue and the modeled system. Using as many parameters as possible, a conceptual framework is developed and translated into a numerical input using a modeling package. Multiple variations in the values used for major parameters can be established and run through the simulation program in order to assess sensitivity to a particular parameter such as flow velocity or proportion of grain sizes.

3. Methods

3.1. General Characteristics of the Numerical Experiments. The method used to test the plausibility of the multiple scenarios consisted of building input files using the values obtained from the Mekong River as a baseline. Of course, these values were adjusted for differences between the two systems such as, elevation of the source area and distance traveled. The Mekong River has an average annual fresh water discharge of 11,000 $m^3\ s^{-1}$ (Wolanski et al., 1998). This value was adjusted down to take into account that the Canadian highland source for the paleo-Michigan River is inferred to have had significantly less relief than

the Tibetan plateau, which sources the Mekong River. Another factor that necessitated adjustment is travel distance. The paleo-Michigan River has not been interpreted to have run for as large a distance as does the Mekong River today. (Swann, 1963; Wolanski et al., 1998)

Sediment concentration for the paleo-Michigan River was also adjusted down from the average values of the Mekong River. This was done for the same reason invoked in adjusting the flux values. The average concentration for the Mekong River is 1200 $kg\ m^{-3}$ (Wolanski et al., 1998). The range grain sizes carried by the Mekong River is in the fine to very fine grain sizes (Wolanski et al., 1998). The grain size range is the dominant range of sediment transported by the paleo-Michigan River. The specific values for simulation parameters are given in the next chapter on "Results, Discussions, and Conclusions" where each simulation is described individually.

The simulations were run using a software package called Sedsim that is sold and maintained by the Earth Science and Resource Engineering Group of the Commonwealth Scientific and Industrial Research Organization (CSIRO), in Australia. This software package has the capability to model changes in sedimentary structures as they evolve through time and space. The basis here is modeling the physical processes that erode, transport, and ultimately deposit sediment, i.e., stratigraphic-forwarding modeling is concerned with modeling physical processes rather deposits. The end result of the modeling is the deposits formed by the physical processes. Modeling in a forward sense allows the user to gain insights into the intermediary stages of evolution of the sedimentary system under investigation.

3.2. Fluid Flow. The commercial version of Sedsim is based on the original code that was published by Tetzlaff and Harbaugh (1989). The original code is a finite-difference FORTRAN code. The basic governing equations are the Navier-Stokes. These equations couple the continuity and momentum equations (71 and 72) to describe the Newtonian flow

of a fluid whose properties are spatially invariant. A fluid with such properties is called an isotropic fluid.

Tetzlaff and Harbaugh (1989) describe the system as follow: conservation of mass is handled by the continuity equation that is given by:

$$\frac{\partial \rho}{\partial t} + \nabla \cdot \rho q = 0 \tag{71}$$

where:

ρ = density of isotropic fluid

t = time

q = flow velocity vector

The momentum equation deals with changes in momentum caused by the fluid. This equation is given by:

$$\rho \left(\frac{\partial q}{\partial t} + (q \cdot \nabla) q \right) = -\nabla p + \nabla \cdot \mu U + \rho (g + \Omega q) \tag{72}$$

where:

p = pressure

μ = viscosity of fluid

U = Navier-Stokes tensor given by:

$$U = \begin{bmatrix} 2\frac{\partial u}{\partial x} - \frac{2}{3}\nabla \cdot q & \frac{\partial u}{\partial y} + \frac{\partial v}{\partial x} & \frac{\partial u}{\partial z} + \frac{\partial w}{\partial x} \\ \frac{\partial u}{\partial y} + \frac{\partial v}{\partial x} & 2\frac{\partial v}{\partial y} - \frac{2}{3}\nabla \cdot q & \frac{\partial v}{\partial z} + \frac{\partial w}{\partial y} \\ \frac{\partial u}{\partial z} + \frac{\partial w}{\partial x} & \frac{\partial v}{\partial z} + \frac{\partial w}{\partial y} & 2\frac{\partial w}{\partial z} - \frac{2}{3}\nabla \cdot q \end{bmatrix} \tag{73}$$

u, v, w = elements of the flow velocity vector q on the Cartesian x, y, and z axes, respectively.

Ω = Coriolis tensor given by:

$$\Omega = \begin{bmatrix} 0 & 2\omega \; sin \; \phi & -2\omega \; sin \; \phi \\ -2\omega \; sin \; \phi & 0 & 0 \\ -2\omega \; cos \; \phi & 0 & 0 \end{bmatrix} \tag{74}$$

ω = earth's angular rotational velocity

ϕ = latitude

g = earth's gravitational acceleration vector

Fluid density (ρ) and viscosity (μ) can be considered constant at constant temperature. In most cases, the application of Sedsim is over areas that are not large enough for the Coriolis effect to be significant. For this reason, (Ωq) can be neglected in these cases. However, for depositional systems that involve large scale circulation, the Coriolis effect cannot be neglected. The original code of Sedsim ignores the Coriolis effects. As a consequence, Sedsim cannot be used to simulate these systems.

The above simplifications allows us to write the continuity equation (71) in a simplified form as follows:

$$\nabla \cdot q = 0 \tag{75}$$

and the momentum equation (72) can be written as follows:

$$\frac{\partial q}{\partial t} + (q \cdot \nabla)q = -\nabla\Phi + \nu\nabla^2 q + g \tag{76}$$

where:

Φ = pressure to constant density ratio = p/ρ

ν =kinematic viscosity = μ/ρ

Fluid flow is represented in Sedsim by a system of equations composed of the simplified version of the continuity and momentum equations (75) and (76), respectively. This system can be solved in a deterministic fashion if initial and boundary conditions are known and well defined.

3.3. Sediment Transport. The basic notion in sediment transport is the principle of conservation of mass. For a fluid flowing over an erodible surface, the amount of sediment eroded from the surface must equal the amount added to the flow. The reverse holds true for deposition onto the surface. In the original code of Sedsim (Tetzlaff and Harbaugh, 1989),

this principle can be represented mathematically as follows:

$$(H - Z)\left(\frac{\partial l}{\partial t} + (Q \cdot \nabla)l\right) = -\frac{\partial Z}{\partial t} \tag{77}$$

where:

l = concentration of sediment

H = elevation of flow w.r.t. sea level

Z = topographic elevation w.r.t. sea level

t = time

Q = velocity of flow in the horizontal direction defined by:

$$Q = \overline{u}\mathbf{i} + \overline{v}\mathbf{j} \tag{78}$$

where:

$\mathbf{i}, \mathbf{j}$ = unit vectors in the x and y axes, respectively.

In Lagrangian form, equation (77) can be written as follows:

$$(H - Z)\frac{Dl}{Dt} = -\frac{\partial Z}{\partial t} \tag{79}$$

where D is the derivative in the direction of flow.

Flow conditions affect the amount of sediment carried in the flow. In a unit volume of flow, sediment suspended in the flow moves at different rate than sediment in the bed load (Tetzlaff and Harbaugh, 1989; Tetzlaff, 1991; Slingerland et al., 1994). Changes in flow characteristics that cause changes in the amount of sediment in the flow can be represented in the following mathematical form:

$$(H - Z)\frac{Dl}{Dt} = f(Q, \nabla H, \nabla Z, l, F) \tag{80}$$

where:

f = function representing variations in sediment load

F = coefficients of sediment properties array.

Tetzlaff and Harbaugh (1989) presents a number of functions (f) that can be used in equation (81). The one used by Sedsim for sediment transport is:

$$(H - Z)\frac{Dl}{Dt} = \begin{cases} (\Lambda - \Lambda_e) f_2 & \text{if } \Lambda - \frac{1}{f_l} < 0 \text{ or } \tau_0 \geq f_3 \\ 0 & \text{if } \tau_0 < f_3 \text{ and } \Lambda - \frac{1}{f_l} \geq 0 \end{cases} \tag{81}$$

where:

Λ = transport capacity; defined in equation (85)

$\Lambda_e = \frac{1}{f_1}$ = effective sediment concentration

f_1 = transportability of sediment

f_2 = erosion-deposition coefficient

f_3 = threshold shear stress for sediment movement

τ_0 = shear stress at the bed; defined as:

$$\tau_0 = c_1 |Q|^2 \rho \tag{82}$$

where c_1 is a friction coefficient for the bed. In SI units, it is defined as:

$$c_1 = g\frac{n^2}{h^{1/3}} \tag{83}$$

where:

n = Manning's roughness coefficient

h = depth of flow = $H - Z$.

Grain size (diameter of sediment particles), density, and shape control the functions $f_1, f_2,$ andf_3 of equation (81).

Tetzlaff and Harbaugh (1989) explains that quantification of sediment transport in Sedsim is accomplished by calculating the power lost by bed friction per unit volume of fluid. This power loss is what governs the capacity of the fluid to transport sediment. Thus,

$$\Lambda = c_t \frac{dP}{dV} = c_t \tau_0 \frac{|Q|}{h} \tag{84}$$

where:

P = power lost by bed friction

V = volume

c_t = coefficient of transport.

Using equations (83), (82), and (84), we get:

$$\Lambda = c_t g \frac{n^2}{h^{4/3}} \rho |Q|^3 \tag{85}$$

In Sedsim, erosion occurs when the transport capacity of the fluid is greater than the sediment load and the the fluid can overcome the shear stress of the bed. Deposition occurs when the sediment load exceeds the transport capacity of the fluid.

3.4. Initial Flow Boundary Conditions. Boundary conditions at the start of simulation time (t_0) must be defined for flow velocity and flow depth. These conditions must be defined at every point. So, for flow velocity Q, initial conditions are given by:

$$Q(x, y, t_0) = Q_0(x, y) \tag{86}$$

Similarly, initial flow depth h_0 is defined as:

$$h(x, y, t_0) = h_0(x, y) \tag{87}$$

At the shoreline, flow depth must be set to zero at all times. It is defined as follows:

$$h(x, y, t) = 0 \tag{88}$$

Other conditions, as discussed in (Tetzlaff, 1986), are set by methods described in the previous sections of this chapter. The initial surface grid used by Sedsim is a finite-difference grid. An example of such a grid is given in Appendix D.1.

CHAPTER 4

Results, Discussions, and Conclusions

Numerical experiments were set up to study the effects of multiple variables on the amount and location of preserved sediments. These experiments were applied to a paleo-depositional system of fine-grained Mississippian sediments in the Illinois Basin. Each series of experiments was designed to investigate how the system responds to changes in one variable at a time. For example, sediment concentration or proportion of particular grain sizes. The following section will present a description of the individual experiments and interpretation of the results from the respective simulations.

1. Results

1.1. Effects of Sediment Concentration on Preservation. This experiment was set up to investigate the role of the sediment concentration on the amount and location of preserved sediment. The area that was examined is part of the Illinois Basin. The current location of the this area is defined by a southwest corner located at 38.01 degrees North and 88.27 degrees West. The coordinates for the northeast corner are 38.37 degrees North and 87.48 degrees west. This area is 70 km x 40 km. The size of the simulation grid cell is 1 km x 1 km. In this experiment, two grain sizes were used for sediments in the model: fines represented by a grain diameter of 0.19 mm and clays which were given a diameter of 0.003 mm. Normally, one would use a range, such as 0.125–0.25 mm for fine-grained sand, to describe grain size. However, due to limitations of the modeling software, a single value was used to represent each grain size. Grains were dominantly in a grain size of fine-grained sand. 75% of the sediment load was set to the fine-grained sand and the remaining 25% was set to clay size.

The initial surface of deposition used in this simulation was smooth and gently dipping towards the southwest with a slope of approximately 2 degrees; (Appendix D.1). This surface was designed not to have any major preexisting topographical features. For changes in the global sea level, the curve from Haq and Schutter (2008) was used. The flux of flow was set to a value of 1600 $m^3\ s^{-1}$ representing monsoonal season and 950 $m^3\ s^{-1}$ for other seasons. The direction of flow was set initially from the northeast and then allowed to migrate westward for about 250 ka through the simulation domain. This movement from east to west ran for half the life of the experiment. The second 250 ka of the experiment was run with flow migrating from west to east back to the starting position. This behavior was designed to mimic the interpreted shift in the delta of the paleo-Michigan River. Total simulated time was set to 500 ky.

The baseline sediment sediment concentration was set to the value of average concentration in the Mekong River. This value is 1200 $kg\ m^{-3}$ (Appendix D.2). Values of experiment parameters are given in the example input file in Appendix D.2.

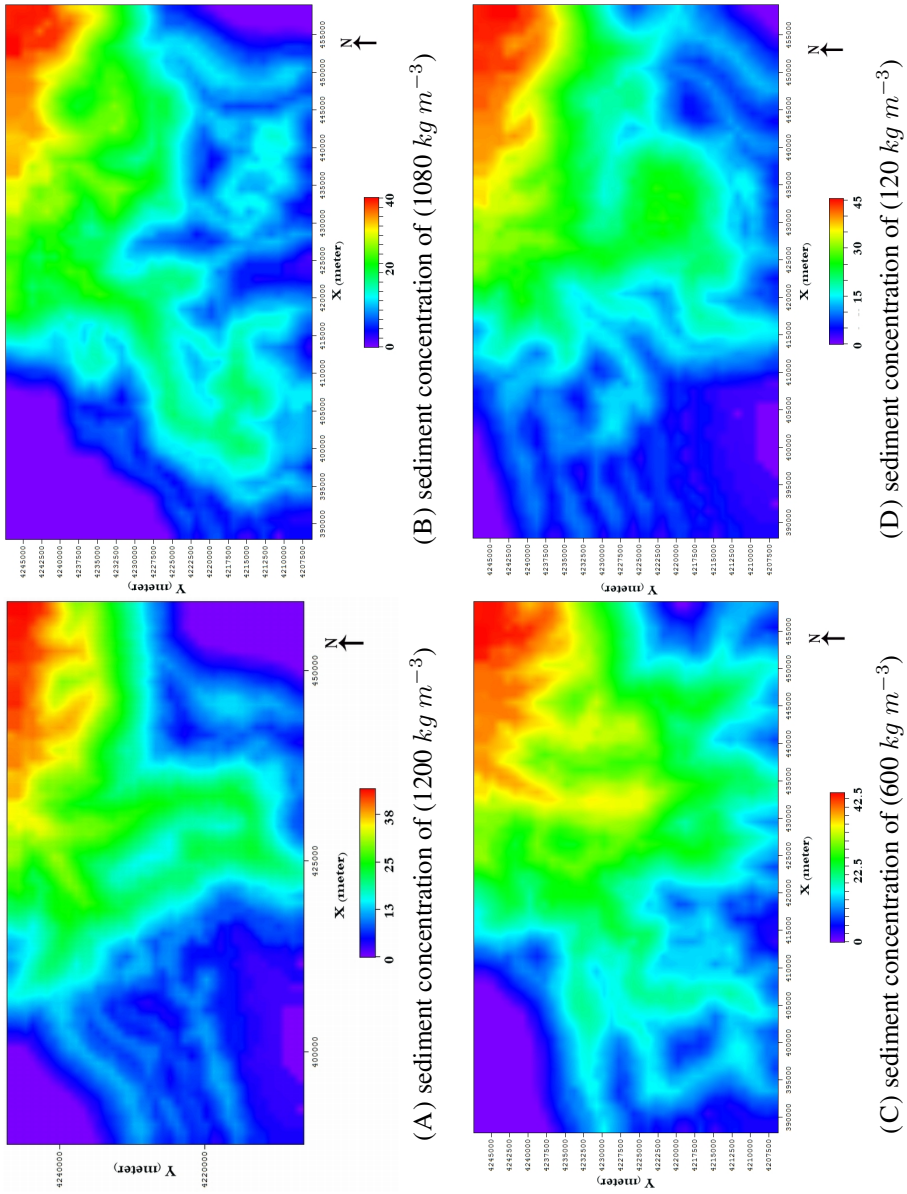

(A) sediment concentration of (1200 $kg\ m^{-3}$)

(B) sediment concentration of (1080 $kg\ m^{-3}$)

(C) sediment concentration of (600 $kg\ m^{-3}$)

(D) sediment concentration of (120 $kg\ m^{-3}$)

FIGURE 20. Simulated maps illustrating the preserved compacted sediment at various levels of sediment concentration.

Preserved compacted thicknesses showed a sensitive response to variations in sediment load (Figure 20). This response was tested and analyzed at the central part of the area of interest (AOI). This part is the location of the Mumford Hills petroleum field in Posey County, Indiana. The current coordinates of the center of the AOI are 38.19 degrees North and 87.87 degrees West. Model results show that of the amount for compacted sediment was the highest for this field at a sediment load of 50% (Figure 20C) that of average of the Mekong River. At this concentration level, the thickness of preserved sediment for this location was approximately 23 m. The area that contains most of the preserved sediment (NE corner of the AOI) shows a lesser degree of variability in areal extent compared to the central part of the AOI (Figure 20).

1.2. Effects of Grain-Size Proportion on Preservation. The numerical modeling experiment to study the effects of varying proportions of grain sizes within the sediment load of the paleo-Michigan River was conducted using the same values for the parameters discussed above. The only difference is that in the size-proportion experiment, proportions of grain sizes were changed between the different simulations while keeping the sediment concentration constant at 600 $kg\ m^{-3}$ i.e., 50% of the average value of the Mekong River. The size ratio of fine-grained sand to clay was varied in steps of 25%.

In the size-proportion experiment, as in the sediment-concentration experiment, it is seen that end members represented in Figures 21A and 21C exhibit close similarities in relation to the amount and location of sediment preservation. Another characteristic similarity between these results and those of the previous section, is that the area close to source, the NE corner of the model grid is the site of highest sediment accumulation for all combinations of grain size ratios (Figure 21).

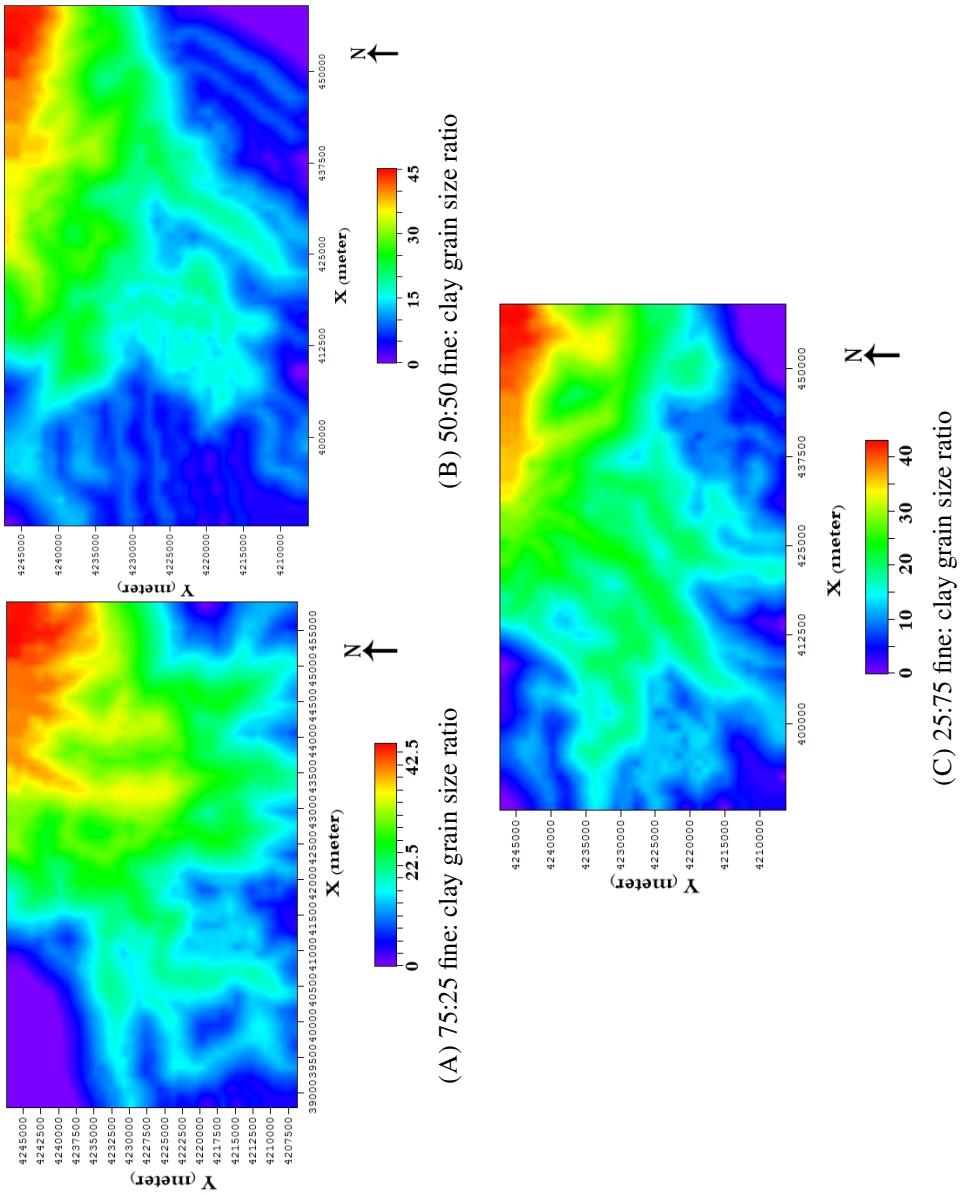

FIGURE 21. Simulated maps of preserved compacted sediment at different ratios of fine-grained:very fine-grained sediments.

Regardless of whether fine-grain sand or clay as the dominant fraction in the 3:1 ratio (Figures 21A and 21C), similar amounts of sediment become preserved in the central part of the AOI i.e, the location of the Mumford Hills petroleum field. The thickness here under both ratios is about 22 m. The same behavior is seen in the NE corner of the model grid. When the two grain sizes are present in equal proportions, the amount of sediment preserved in the central part of the AOI is less by about 30% (Figure 21B) compared to when grain sizes are in a 3:1 ratio.

2. Discussions

The results described above show that the thickness of preserved sediment after compaction did not match thickness data measured in log data (Figure 22). Model results also show a trend that is inconsistent with the actual preserved location of maximum thickness. Modeling results show that the NE part of the study site has maximum thickness of sand bodies; in contrast, outcrop descriptions (Potter, 1962; Swann, 1963, 1964) indicate that the SW part of the study site has maximum thickness of sand bodies preserved. There are a number of factors that can lead to this type of mismatch between model results and outcrop or borehole data. For the Clore study, the likely factors are scale of investigation, shape of the initial surface of deposition, flow velocity, distance from source, grain size proportions, and total elapsed time of deposition.

Values for parameters used in constructing the Clore model were derived from studies at varying scales (Anikiyev et al., 1986; Wolanski et al., 1998). Combining these values into one scale may create problems leading to inaccurate output from the model. The model presented in this study is a “first-pass” effort and despite the mismatch between results from the model and field data, positive conclusions can be drawn from the results for future simulations. Once a satisfactory match is achieved, the model then can be used in a predictive sense in order to assess, for example, thickness of sand in areas that have only

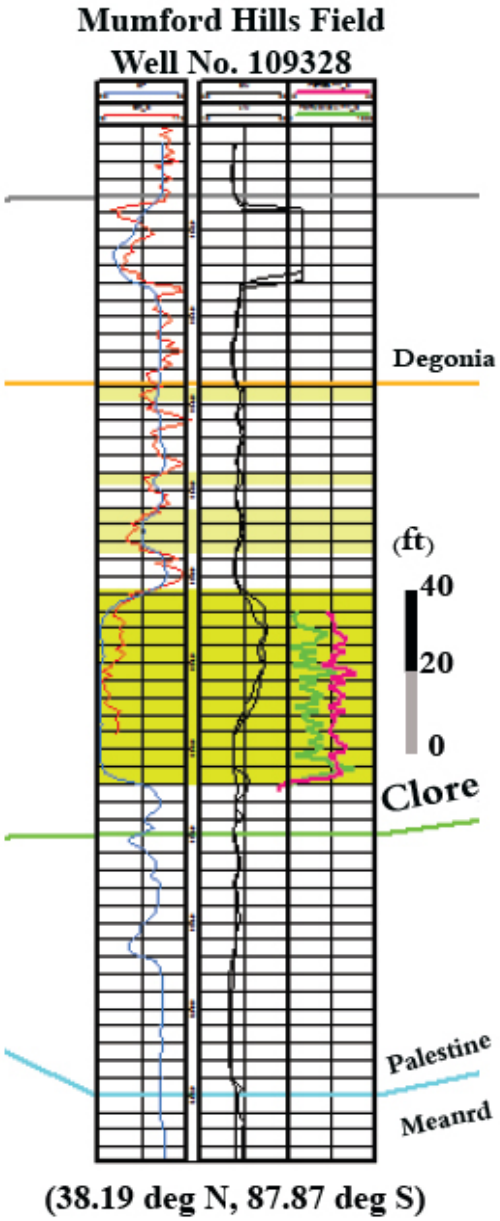

FIGURE 22. Example wireline log for a well from Mumford Hills field. The well is located near the center of the AOI; modified from IGSPDMS, 2011.

limited or no field data. Figure 23 shows the relationship between thickness of preserved sand and concentration of sediment for two locations within the AOI. In the Clore modeling study, sediment accumulations are thickest in the NE corner of the study area (Figure 23),

which is a result not in agreement with field data. However, the data show that the method applied here can be used to obtain the first derivative of thickness with respect to sediment concentration. This derivative can then be plotted against distance from flow source to calculate amount of sediment at a particular location. Sediment concentration in the river flows used in this study was derived from a modern analog and adjustments were made to account for differences between the modern analog, the Mekong River, and the ancient system, the paleo-Michigan River. Differences that were taken into account include length of travel and altitude of river source. That leaves other factors, such as sinuosity of flow path and tributaries in the delta that were not included in the adjustments. Discrepancies between model results and field data may stem from the manner in which the model was constructed.

The initial surface used in the model is gently dipping towards the southwest and is smooth, meaning that there are no preexisting positive or negative topographic features. Preexisting topography may affect accumulation of sediment if there are any forms of depressions in the initial surface. On the other hand, earlier topography may preclude sediment accumulation if it is present in the form of positive surface features.

Velocity of flow has a paramount role in controlling the distance that sediment travels. Seasonal variations in flow velocity have to be accounted for when building a model. In the Mumford Hills model, flow velocity was set at average values of 0.65 $m\ s^{-1}$ for monsoonal season and 0.35 $m\ s^{-1}$ for other seasons. Velocity in the Mekong River can reach average of 1 $m\ s^{-1}$. The values used in the model may not be high enough to move sediment to southwestern parts of the AOI. Hence, the relative low velocity of flow within the distributary channels of the paleo-Michigan River may be the reason for the area of maximum accumulation in the model's output occurring close to flow source. The flow in the simulations is affected by a constraint of the software. Sources of flow must be placed on the edge or inside of the simulation domain. Velocity needs to be adjusted for how far this domain is located relative to the source of sediment supply into the river.

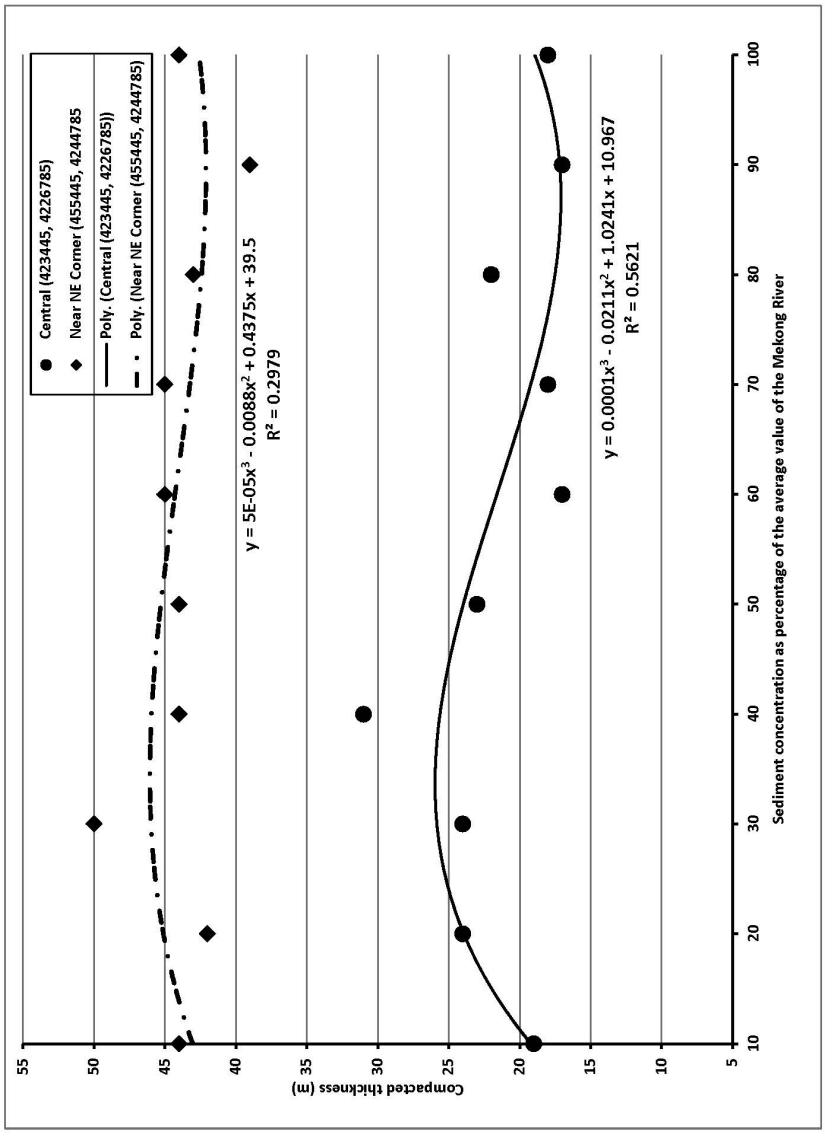

FIGURE 23. Relationship between preserved compacted thickness of sand and sediment concentration in the paleo-Michigan River.

Grain sizes used in the simulations were of two sizes only. The sizes used were average values for the fine-grained sand and an upper value for clay. Core data (Figure 24) show that the dominant grain sizes are the fractions used. More detailed petrographical work could lead to altering the grain diameters used. Proportion of grain sizes is another sedimentological parameter that should be considered in the Clore model. Given the presence of silt-sized grains in the sand bodies, average flow velocity and periods of unusually high and low flow will have a major impact on where sediments are continuously transported compared to where sediments are initially deposited and then eroded and further transported or are deposited and then buried. Interaction of these variables with flow velocity will have a major impact on how far from the source these sediments get carried by the river before they are ultimately deposited.

FIGURE 24. Photograph of a core from a Mumford Hills well showing the uniformity of grain size.

Localized changes in sea level are not well captured in the global sea level curve used in building the model. This curve is not of sufficiently high resolution to capture relatively short-lived fluctuations, especially those that may derive from climatic fluctuations. This is another example of the scale of investigation being a source of error. Absence of specific data on the local level for a study such as the Clore model, has more impact on the results

than on studies conducted on scales similar to the scale from which data are extracted. The pronounced effect here stems from the fact that the simulations attempt to model depositional processes of high frequency (Weller, 1956; Swann, 1964) using data that group high frequency information into low frequency data sets. The high frequency data are exemplified in changes in sea level that result from climatic cycles whose durations are shorter than what is captured in the sea level curve used in this study.

Total time of deposition used in the model may be incorrect. Age delineation of the interval of interest, the Mount Pleasant Sandstone, is not very accurate. In fact, time of deposition of the whole Clore formation is not well constrained due mainly to lack of distinct biostrtigraphical indicators (Norby, 1991; Rexroad et al., 2010).

The model did not account for effects of wind, tides, or waves. These two factors are powerful agents in moving sediment. Wind can carry sediments over large distance until its energy dissipates. Absence of wind influence may be the reason for maximum sediment preservation in the northeast as opposed to the southwest as observed in the field. Absence of wind effects could have a more pronounced effect here. This is because the finer grain sizes of the Mount Pleasant sandstones are composed mainly of fine-grained sand. These fine-grained sediments are more susceptible to eolian transport over large distance than larger-sized grains. The paleo-location of the study area could have amplified the role of the wind. This role is better understood in association with monsoonal influence over this paleo-tropical area. In the tropics, wind alternate between going from land to ocean and, during monsoonal season, from ocean to land. This alternation presents an extra level of complication while setting the input for the model. Accurate representation of wind influence requires information about wind speed, direction, and duration of each of the alternating episodes for the lifetime of the simulation.

Tidal influence may also have a role that is as equally important as that of the wind. Tides results from the gravitational pull exerted by the Moon and the Sun on the Earth. The

relative positions of the Moon and the Sun affects the strength of the tides. Tidal forces reach their maximum strength when these three bodies bodies are closely aligned (Kvale et al., 1999). Periods of the lunar cycles that affect tidal strength vary. The changes in periodicities of these lunar events are attributed to changes in the phases of the Moon and its declination relative to the equator. These cycles include: semidiurnal, diurnal, biweekly, monthly, yearly, and multi-yearly. (Williams, 1989; Feldman et al., 1993; Archer, 1996; Kvale et al., 1999)

Because each cycle has its own period, their effects can be with amplified, when they are in phase, or diminished, when they are out of phase (Williams, 1989; Kvale et al., 1999). Meteorological phenomena also affect tidal strength by interaction and influencing tidal cycles. Such meteorological factors include: monsoonal rain, wind, fluctuations in sea level. These latter factors can also be superimposed on tidal cycle in constructive and destructive ways. (Archer, 1996; Kvale et al., 1999) The complex interactions among all the above factors may affect the capacity of the current to carry sediment. These interactions may also impact the amount of sediment available for transport.

Evidence of tidally-influenced deposits have been identified in the rock record. They are called tidal rhythmites. They have identified in many basins spanning epochs of the geologic record of the Earth. These rhythmites have been identified in the Precamberian Elatina Formation in South Australia, the Mississippian Pride Shale of the Bluestone Formation in southern West Virginia, the Pennsylvanian Brazil Formation in Indiana, the Pennsylvanian Hindostan Whetstone beds of the Mansfield in Indiana, and the Carboniferous Francis Creek Shale in Illinois (Kvale et al., 1989; Williams, 1989; Kvale et al., 1994; Archer et al., 1995; Archer, 1996; Miller and Eriksson, 1997; Kvale et al., 1999). Tidal rhythmites have also been found in the Early Chesterian Bethel and Elwren Formations in Indiana (Thompson, 2011).

3. Conclusions

Numerical simulation is an effective approach to study evolution of sedimentary deposits. The process of preparing model input serves as a means to enhance geologists understanding of the system under study. This process stresses the need to comprehend all aspects related to the depositional system. This course of action represents an invaluable tool in achieving deeper insights into earth processes.

Results from the present study show that forward modeling allows for assessment of the effects of variables that control the physical process governing transportation and deposition of sediment in a complex system. This was achieved in the absence of information pertinent to this system, such as precise age delineation. In the modeling experiments, preservation of sediment is sensitive to concentration of sediment within a fluviodeltaic system. The amount of sediment preserved shows a complex relationship to sediment concentration.

Sediment preservation increased with increasing sediment load within the system to a certain point. Figure 23 shows that near the flow source, the preservation increased up until 30% the average concentration of the Mekong River. Beyond that concentration, preservation generally decreased. The same trend applies at the center of the AOI. Here, however, the concentration that produced the largest amount of preservation is 40%.

The location of preservation is also affected by concentration of sediment. The relationship between sediment concentration and location appears to be more complex than between sediment concentration and the amount preserved. Comparison between Figures 20A and 20B illustrates that at 90% concentration relative to the average of the Mekong River, there is a wider areal extent of preserved sediment than at 100%. The same approximate extent is seen at 50% (Figure 20C) as at 90%.

Proportions of different grain sizes affect the amount of preserved sediment in the central part of the AOI in such a way that emphasizes the relative ratio of grain sizes. At a ratio of 3:1 for either grain size, the amount preserved is about the same.

Further study of the system is recommended to investigate, in more detail, the roles sediment load and grain size proportions. Preexisting topography on the initial surface of deposition is a major variable recommended for further work. Additionally, improvements to the model would come from including the effects of wind and tides. Flow velocity and location of flow sources are also variables that need further experimentations. Since the duration of deposition of this system is not well constrained, experiments at different durations have the potential to enhance the model.

Looking at the results from the Clore model as a whole leads to the interpretation that such a study would be more useful by including the effects of wind, tides, and topography. The combined effect of wind and tides seems to be the factor that has the highest potential for improving the model output. The wind parameter is also the most difficult to quantify accurately for a paleo-system even with the use of a modern analog. Nevertheless, every effort should be taken to include thes two factors in the model input. Development of an *integrated* conceptual model is crucial. Integration here is meant to convey the sense that when translating the effects of a single variable in the conceptual model into numerical input, interaction of the other variable and how they affect this one variable should be considered carefully. Performing such analysis for all variables involved increases the potential for the output from the model to be meaningful and relevant.

The Clore model, in one aspect, raises questions for further work in both modeling as well as field studies. A major question that became clear from this study is: how is the ultimate fate of sediment impacted by wind and tides in the tropics?

Part 3

Appendices

APPENDIX A

Source Codes

1. Mesh Generation

The following section lists the modified code of the finite element mesh generator developed by the author based on original FORTRAN code developed by Dina L. Lopez (López and Smith, 1995). The author introduced new functionality that permits generating subdomains of finer resolution than the parent domain of the problem under study as mentioned in section 2 (Mesh Generation; page 39) of chapter 2. Output from this code is designed to be visualized using the commercially available software Tecplot™.

```
!   Last change: Mohammad R. Khadhrawi (MRK); 20:18 Monday, January 09, 2006
!
!   Mesh generation modified from package developed by:
!   Dinah Lopez.
!
!   Variables:
!
!   nrowx - number rows in x direction
!   nrowy - number rows in y direction
!   nrowz - number rows in z direction
!   delx - element width in x direction
!   dely - element width in y direction
!   delz - element width in z direction
!
    PROGRAM meshgen
    IMPLICIT NONE

    INTEGER :: mat(9000000),strat(700000), nnodeperface, h, f
    INTEGER :: nnx1, nnx2, nnx3, nny1, nny2, nny3, nnz1, nnz2, nnz3
    INTEGER :: i, j, k, l, node(4,9000000), nrowz, ncolx, ncoly, q, qqq, nnx
    INTEGER :: nny, nnz, kn, nelem, nnode,m,n
    INTEGER :: nnX1factor, nnX3factor, nnY1factor, nnY3factor
    REAL*8 :: qq, x(700000), y(700000), z(700000)
    REAL*8 :: stc, xx, yy, zz, xc, yc, zc
    REAL*8 :: xrefine, yrefine, zrefine, delxmin, delxmax, delymin, delymax
    REAL*8 :: delzmin, delzmax, delx, dely, delz, xmin, xmax, ymin, ymax
    REAL*8 :: zmin, zmax, xmin1, xmax1, concbc, concgrad
    REAL*8 :: head(500000),conc(500000),temp(500000), Vd(500000)
    REAL*8 :: chco3(500000),ch(500000),cal(500000), csio2(500000)
    REAL*8 :: cca(500000),XAnor(500000)
```

```
    REAL*8 :: high_head, low_head, low_head_factor, high_temp, low_temp
    REAL*8 :: low_temp_factor, high_conc, low_conc, low_conc_factor
    REAL*8 :: high_chco3, low_chco3, low_chco3_factor, high_ch, low_ch
    REAL*8 :: low_ch_factor, high_cal, low_cal, low_cal_factor, high_csio2
    REAL*8 :: low_csio2, low_csio2_factor, high_cca, low_cca, low_cca_factor
    REAL*8 :: head_grad, temp_grad, conc_grad, chco3_grad, ch_grad, cal_grad
    REAL*8 :: csio2_grad, cca_grad
    REAL*8 :: vol(9000000),voln(700000),d(4,9000000)
    CHARACTER(LEN=70) :: title
!*********************************************************************
    OPEN (unit = 7, file = "tetmeshgen.in")
    OPEN (unit = 8, file = "spec_bc.dat")
    OPEN (unit = 9, file = "geofe_data.dat")
    OPEN (unit = 10, file = "tetmesh.dat")
    OPEN (unit = 11, file = "tetmesh_tec.dat")
    OPEN (unit = 12, file = "mesh_parameters.dat")
!*********************************************************************
! Read Input Parameters from the file {tetmeshgen.in}
!*********************************************************************
! Read Domain Parameters:
read(7,111) title
write(12,111) title
read(7,111) title
write(12,111) title
read(7,*) ncolx, ncoly, nrowz
write(12,112) ncolx, ncoly, nrowz
write(12,*) '--------------'

! Read SubDomain Parameters:
read(7,111) title
```

```
write(12,111) title
read(7,111) title
write(12,111) title
read(7,*) xmin, xmax, ymin, ymax, zmin, zmax
write(12,113) xmin, xmax, ymin, ymax, zmin, zmax
write(12,*) '--------------'

! Read Adjustment Parameters for the SubDomain:
read(7,111) title
write(12,111) title
read(7,111) title
write(12,111) title
read(7,*) nnX1factor, nnX3factor, nnY1factor, nnY3factor
write(12,114) nnX1factor, nnX3factor, nnY1factor, nnY3factor
write(12,*) '--------------'

! Read Grid Refinement Parameters:
read(7,111) title
write(12,*) title
read(7,111) title
write(12,*) title
read(7,*) xrefine, delxmin, delxmax, yrefine, delymin, delymax
write(12,115) xrefine, delxmin, delxmax, yrefine, delymin, delymax
write(12,*) '--------------'

! Read Gradient Parameters:
read(7,111) title
write(12,*) title

read(7,111) title
```

```
write(12,*) title
read(7,*) high_head, low_head_factor
write(12,116) high_head, low_head_factor
write(12,*) ''

read(7,111) title
write(12,*) title
read(7,*) high_temp, low_temp_factor
write(12,116) high_temp, low_temp_factor
write(12,*) ''

read(7,111) title
write(12,*) title
read(7,*) high_conc, low_conc_factor
write(12,116) high_conc, low_conc_factor
write(12,*) ''

read(7,111) title
write(12,*) title
read(7,*) high_chco3, low_chco3_factor
write(12,116) high_chco3, low_chco3_factor
write(12,*) ''

read(7,111) title
write(12,*) title
read(7,*) high_ch, low_ch_factor
write(12,116) high_ch, low_ch_factor
write(12,*) ''

read(7,111) title
```

```
write(12,*) title
read(7,*) high_cal, low_cal_factor
write(12,116) high_cal, low_cal_factor
write(12,*) ''

read(7,111) title
write(12,*) title
read(7,*) high_csio2, low_csio2_factor
write(12,116) high_csio2, low_csio2_factor
write(12,*) ''

read(7,111) title
write(12,*) title
read(7,*) high_cca, low_cca_factor
write(12,116) high_cca, low_cca_factor
write(12,*) ''

close(unit=7)
!*************************************************************************
   k = 0
!*************************************************************************
! Check if the box should be a type A box (i+j+l odd)
! or a type B box (i+j+l even).
!Nodes are counterclockwise looking from 4.
!*************************************************************************
!  ncolx = 43     !Optimal ncolx = 100
!  ncoly = 15     !Optimal ncoly = 20
!  nrowz = 15     !Optimal nrowz = 20

!  xmin = 18.0    !Optimal xmin = 75
```

```
!  xmax = 30.0     !Optimal xmax = 100
!  ymin = 6.0      !Optimal ymin = 15
!  ymax = 8.0      !Optimal ymax = 20
!  zmin = 6.0      !Optimal zmin = 15
!  zmax = 8.0      !Optimal zmax = 20

!  concbc = 10.0
!  concgrad = concbc/189.0


   nnx = ncolx + 1
   nny = ncoly + 1
   nnz = nrowz + 1

      do 90 i = 1, nrowz
        do 60 j = 1, ncoly
          do 30 l = 1, ncolx
            q = l + j + i
            qq = q/2.0d0
            qqq = 2 *int(qq)
            if (qqq .eq. q) go to 15
            k = k + 1
 !           WRITE(12,*) ' k = ',k
            node(2,k) = (l-1)*nnz *nny + (j-1)*nnz + i
            node(1,k) = node(2,k) + 1
            node(3,k) = node(2,k) + nnz
            node(4,k) = node(2,k) + (nnz*nny)
            k = k + 1
            node(1,k) = node(4,k-1)
            node(2,k) = node(1,k) + 1
```

```
            node(3,k) = node(2,k) + nnz
            node(4,k) = node(1,k-1)
            k = k + 1
            node(1,k) = node(1,k-1)
            node(2,k) = node(3,k-2)
            node(3,k) = node(1,k-2)
            node(4,k) = node(3,k-1)
            k = k + 1
            node(1,k) = node(4,k-1)
            node(2,k) = node(1,k-1)
            node(3,k) = node(2,k-1)
            node(4,k) = node(2,k) + nnz
            k = k + 1
            node(1,k) = node(3,k-1)
            node(2,k) = node(3,k-2)
            node(3,k) = node(4,k-2)
            node(4,k) = node(1,k) + 1
            go to 30
 15         continue
            k = k + 1
            node(1,k) = (l-1)*nnz *nny + (j-1)*nnz + i
            node(2,k) = node(1,k) + 1
            node(3,k) = node(2,k) + nnz*nny
            node(4,k) = node(2,k) + nnz
            k = k + 1
            node(1,k) = node(3,k-1)
            node(2,k) = node(1,k) - 1
            node(3,k) = node(1,k-1)
            node(4,k) = node(2,k) + nnz
            k = k + 1
```

```
            node(1,k) = node(1,k-1)
            node(2,k) = node(1,k-2)
            node(3,k) = node(4,k-2)
            node(4,k) = node(4,k-1)
            k = k + 1
            node(1,k) = node(3,k-1)
            node(2,k) = node(4,k-1)
            node(3,k) = node(2,k-1)
            node(4,k) = node(1,k) -1
            k = k + 1
            node(1,k) = node(2,k-1)
            node(2,k) = node(1,k-2)
            node(3,k) = node(1,k) + 1
            node(4,k) = node(1,k-1)
   30     continue
   60   continue
   90 continue

       nelem = k

!*************************************************************************
! Read nodes coordenates
!*************************************************************************
  130 format ('␣', i5, 10x, 4i5)
!  set x direction
      xx = 0.0
      nnx2 = INT(nnx/2)
      nnx1 = nnx2 - nnX1factor
      nnx3 = nnx2 + nnX3factor
      delx = delxmax
```

```
!  set y direction
      yy = 0.0
      nny2 = INT(nny/2)
      nny1 = nny2 - nnY1factor
      nny3 = nny2 + nnY3factor
      dely = delymax

      kn = 1

      do 165 k = 1, nnx
        yy = 0.0
        dely = delymax
         do 160 j = 1, nny
        zz = 0.0
        delz = delymax
           do 150 i = 1, nnz
            x(kn) = xx
            y(kn) = yy
            z(kn) = zz
!            head(kn) = xx
            kn = kn + 1
           zz = zz + delz
!         conc(kn) = concbc - concgrad*xx
!         WRITE(12,*) 'nz=',i,'  delz = ',delz
        IF(i.lt.nny1) delz = delz*(1.0-yrefine)
        IF(i.gt.nny3) delz = delz*(1.0+yrefine)
        IF(delz.lt.delymin) delz = delymin
        IF(delz.gt.delymax) delz = delymax

  150     continue
```

```
          yy = yy + dely
!        WRITE(12,*) 'ny=',j,'  dely = ',dely
        IF(j.lt.nny1) dely = dely*(1.0-yrefine)
        IF(j.gt.nny3) dely = dely*(1.0+yrefine)
        IF(dely.lt.delymin) dely = delymin
        IF(dely.gt.delymax) dely = delymax

  160   continue
         xx = xx + delx
!        WRITE(12,*) 'nx=',k,'  delx = ',delx
        IF(k.lt.nnx1) delx = delx*(1.0-xrefine)
        IF(k.gt.nnx3) delx = delx*(1.0+xrefine)
        IF(delx.lt.delxmin) delx = delxmin
        IF(delx.gt.delxmax) delx = delxmax
  165 continue

       nnode = nnx*nny*nnz
       WRITE(11,444)
       WRITE(11,555) nnode,nelem
  232  FORMAT('nnode=',i6,1x,'nelem=',i9)

         do 1001 m=1,nelem
       i = node(1,m)
       j = node(2,m)
       k = node(3,m)
       l = node(4,m)
       xc = (x(i)+x(j)+x(k)+x(l))/4.0
       zc = (z(i)+z(j)+z(k)+z(l))/4.0
       yc = (y(i)+y(j)+y(k)+y(l))/4.0
```

```
      strat(i) = 1
      strat(j) = 1
      strat(k) = 1
      strat(l) = 1

      IF(xc.ge.xmin.and.xc.le.xmax .and. yc.ge.ymin.and.yc.le.ymax .and.&
     zc.ge.zmin.and.zc.le.zmax) THEN

      strat(i) = 2
      strat(j) = 2
      strat(k) = 2
      strat(l) = 2

      endif

 1001 continue
! ************************  volume insert begins here  ************************
! The following variables need to be dimensioned d,vol,voln.
! The change to the tecplot output statement added voln.
!
     do m=1,nelem
        i = node(1,m)
        j = node(2,m)
        k = node(3,m)
        l = node(4,m)

        d(1,m)   =    x(j) * y(k) * z(l)  - &
                     x(j) * y(l) * z(k)   - &
                     x(k) * y(j) * z(l)   + &
                     x(k) * y(l) * z(j)   + &
```

```
                        x(l) * y(j) * z(k)    - &
                        x(l) * y(k) * z(j)

          d(2,m)    =   -1.0d0 *  (x(i) * y(k) * z(l))   + &
                         x(i) * y(l) * z(k)   + &
                        x(k) * y(i) * z(l)    - &
                        x(k) * y(l) * z(i)    - &
                        x(l) * y(i) * z(k)    + &
                        x(l) * y(k) * z(i)

          d(3,m)    =    x(i) * y(j) * z(l)    - &
                        x(i) * y(l) * z(j)    - &
                        x(j) * y(i) * z(l)    + &
                        x(j) * y(l) * z(i)    + &
                        x(l) * y(i) * z(j)    - &
                        x(l) * y(j) * z(i)

          d(4,m)    =  -1.0d0 *  (x(i) * y(j) * z(k))   + &
                        x(i) * y(k) * z(j)    + &
                        x(j) * y(i) * z(k)    - &
                        x(j) * y(k) * z(i)    - &
                        x(k) * y(i) * z(j)    + &
                        x(k) * y(j) * z(i)

!*********************************************************************
! calculate volume of tetrahedral element
!
! vol(m) = dabs(d(1) -d(2) + d(3) -d(4))/6.0d0
! dohc Take absolute value of addition.
! Wed Mar.9 07:29:05 EST 2005
```

```
! vol(m) = dabs(d(1,m) - d(2,m) + d(3,m) - d(4,m))/6.0d0
! volume formula from the volume subroutine used by GeoFE.
   vol(m) = (d(1,m) + d(2,m) + d(3,m) + d(4,m))/6.0d0
       voln(i) = vol(m)
       voln(j) = vol(m)
       voln(k) = vol(m)
       voln(l) = vol(m)

!  if(m .eq. 2) then
!  write(*,*) 'volume of element 2  = ',  vol(m)
!      write(*,*) i,x(i),y(i),z(i)
!      write(*,*) j,x(j),y(j),z(j)
!      write(*,*) k,x(k),y(k),z(k)
!      write(*,*) l,x(l),y(l),z(l)
!  end if

   if (vol(m).lt.0.0d0) then

       WRITE(*,*) 'warning: volume < 0, check node ordering ', m
       write(*,*) i,x(i),y(i),z(i)
       write(*,*) j,x(j),y(j),z(j)
       write(*,*) k,x(k),y(k),z(k)
       write(*,*) l,x(l),y(l),z(l)

           stop
   end if

      end do

!************************Begin MRK-01****************************************
```

```
!         high_head = 2.0
          low_head = (low_head_factor*high_head)
          head_grad = ((high_head - low_head)/(ncolx*delx))
!         high_temp = 10.0
          low_temp = (low_temp_factor*high_temp)
!         temp_grad = ((high_temp - low_temp)/(ncolx*delx))
!         high_conc = 0.2
          low_conc = (low_conc_factor*high_conc)
          conc_grad = ((high_conc - low_conc)/(ncolx*delx))
!         high_chco3 = 1.8
          low_chco3 = (low_chco3_factor*high_chco3)
          chco3_grad = ((high_chco3 - low_chco3)/(ncolx*delx))
!         high_ch = 4.00E-05
          low_ch = (low_ch_factor*high_ch)
          ch_grad = ((high_ch - low_ch)/(ncolx*delx))
!         high_cal = 6.60E-07
          low_cal = (low_cal_factor*high_cal)
          cal_grad = ((high_cal - low_cal)/(ncolx*delx))
!         high_csio2 = 2.22E-03
          low_csio2 = (low_csio2_factor*high_csio2)
          csio2_grad = ((high_csio2 - low_csio2)/(ncolx*delx))
!         high_cca = 1.64E-03
          low_cca = (low_cca_factor*high_cca)
          cca_grad = ((high_cca - low_cca)/(ncolx*delx))

          XAnor = 0.12
          temp = 10.0
          Vd = 0.0
```

```
      write(12,*) ''
      write(12,1818)'head_grad␣=␣', head_grad
!     write(12,1818)'temp_grad = ', temp_grad
      write(12,1818)'conc_grad␣=␣', conc_grad
      write(12,1818)'chco3_grad␣=␣', chco3_grad
      write(12,1818)'ch_grad␣=␣', ch_grad
      write(12,1818)'cal_grad␣=␣', cal_grad
      write(12,1818)'csio2_grad␣=␣', csio2_grad
      write(12,1818)'cca_grad␣=␣', cca_grad

!************************End MRK-01*****************************************

!        WRITE(*,*) 'before 2000 loop'

       do 2000 n=1,nnode
! WRITE(11,*) x(n),y(n),z(n),conc(n),strat(n)
       WRITE(11,2323) x(n),y(n),z(n),REAL(strat(n)),voln(n)
       conc(n) = 0.0
       temp(n) = 10.0
! write(10,313) x(n),y(n),z(n),head(n),temp(n),conc(n),strat(n)
100    continue
17    FORMAT(6(f9.2,3x),2x,i9)
333   FORMAT(3(f13.2,1x),2x,i9)
18    FORMAT(5(i5,1x))
2000  continue
!************************Begin MRK-02*****************************************
!   WRITE(9,1414)
!   WRITE(9,555) nnode,nelem

   nnodeperface = (nnode/nnx)
```

```
setvalues:  do n=1,nnode,nnodeperface
!     WRITE(11,333) x(n),y(n),z(n)

      if(n .eq. 1) then
         head(n:n+nnodeperface-1) = high_head
!        temp(n:n+nnodeperface-1) = high_temp
         conc(n:n+nnodeperface-1) = high_conc
         chco3(n:n+nnodeperface-1) = high_chco3
         ch(n:n+nnodeperface-1) = high_ch
         cal(n:n+nnodeperface-1) = high_cal
         csio2(n:n+nnodeperface-1) = high_csio2
         cca(n:n+nnodeperface-1) = high_cca
      else
         head(n:n+nnodeperface-1) = head(n-1) - head_grad
!        temp(n:n+nnodeperface-1) = temp(n-1) - temp_grad
         conc(n:n+nnodeperface-1) = conc(n-1) - conc_grad
         chco3(n:n+nnodeperface-1) = chco3(n-1) - chco3_grad
         ch(n:n+nnodeperface-1) = ch(n-1) - ch_grad
         cal(n:n+nnodeperface-1) = cal(n-1) - cal_grad
         csio2(n:n+nnodeperface-1) = csio2(n-1) - csio2_grad
         cca(n:n+nnodeperface-1) = cca(n-1) - cca_grad
      endif
!        temp(n) = 10.0
!        Vd(n) = 0.0

datainput:  do f = n,n+nnodeperface-1

   write(9,1717) x(f),y(f),z(f),head(f),temp(f),conc(f),&
   chco3(f),   ch(f),cal(f),csio2(f),cca(f),Vd(f),XAnor(f)
```

```
!  if(f.eq.1) write (10,1002) 'Face #', 'Starts @ Node #',&
! 'Ends @ Node #'
!   if(f.eq.n)then
!    write(10,1001) ((x(f))+1), n, n+nnodeperface-1
!   end if
         end do datainput
!     write(10,*) ''
   end do setvalues
!************************End MRK-02*****************************************
      do 1000 m=1,nelem
        mat(m) = 1
        i = node(1,m)
        j = node(2,m)
        k = node(3,m)
        l = node(4,m)
        stc = real(strat(i)+strat(j)+strat(k)+strat(l))/4.0
        IF(stc.gt.1.0) mat(m) = 2

     WRITE(9,18) node(1,m),node(2,m),node(3,m),node(4,m),mat(m)
! write(10,18) node(1,m),node(2,m),node(3,m),node(4,m),mat(m)
       WRITE(11,222) node(1,m),node(2,m),node(3,m),node(4,m)

 1000 continue
!************************Begin MRK-03*****************************************
   xmin1 = minval(x)
   xmax1 = maxval(x)

spec_head:  do h = 1,nnode
      if(h .eq. 1) then
```

```
         write(8,*) 'NH␣HB'
      endif
      if(x(h) .eq. xmin1)then
         write(8,666) h, high_head
      elseif(x(h) .eq. xmax1)then
         write(8,666) h, low_head
      endif
   end do spec_head

spec_temp:  do h = 1,nnode
      if(h .eq. 1) then
         write(8,*) 'NT␣TB'
      endif
      if(x(h) .eq. xmin1)then
         write(8,666) h, temp(h) !high_temp
      elseif(x(h) .eq. xmax1)then
         write(8,666) h, temp(h) !low_temp
      endif
   end do spec_temp

spec_chem:  do h = 1,nnode
   if(h .eq. 1) then
    write(8,*) 'Nc␣␣␣hco3aspec(mol/L)␣␣hspec(mol/L)␣␣␣alspec(mol/L)&
␣␣␣␣sio2spec(mol/L)␣␣caspec␣(mol/L)␣concSpec'
   endif

   if(x(h) .eq. xmin1)then
    write(8,666) h, high_chco3, high_ch, high_cal, high_csio2, high_cca,&
    high_conc
   elseif(x(h) .eq. xmax1)then
```

```
    write(8,666) h, low_chco3, low_ch, low_cal, low_csio2, low_cca, low_conc
   endif
   end do spec_chem

   write(12,*) ''
        write(12,*) 'Number␣of␣Nodes␣=␣', nnode
        write(12,*) 'Number␣of␣Elements␣=␣',nelem
        write(12,*) 'Number␣of␣Nodes␣per␣X-Face␣=␣', nnodeperface
        write(12,*) '[2*(Number␣of␣Nodes␣per␣X-Face)]␣=␣', 2*nnodeperface
        write(12,*) ''
        write(12,*) 'DONE␣:-)'

        write(*,*) ''
        write(*,*) 'Number␣of␣Nodes␣=␣', nnode
        write(*,*) 'Number␣of␣Elements␣=␣',nelem
        write(*,*) 'Number␣of␣Nodes␣per␣X-Face␣=␣', nnodeperface
        write(*,*) '[2*(Number␣of␣Nodes␣per␣X-Face)]␣=␣', 2*nnodeperface
        write(*,*) ''
        write(*,*) 'DONE␣:-)'

!************************End MRK-03*****************************************

 111 FORMAT (A70)
 112 FORMAT (3(i5,3x))
 113 FORMAT (6(f6.2,2x))
 114 FORMAT (4(i5,11x))
 115 FORMAT (6(f6.2,8x))
 116 FORMAT (2(f6.2,8x))

 222 FORMAT (4(i5,1x))
```

```
313 FORMAT (6(f6.2,2x),2x,i6)
444 format ('VARIABLES␣=␣"X",␣"Y","Z","Strat","Volume"␣')
555 FORMAT ('ZONE␣N=',i5,',E=',i9,',F=FEPOINT,␣ET=TETRAHEDRON')
666 FORMAT (I8,3x,f6.2,2x,4(ES8.2,2x),f6.2)

1414 FORMAT ('VARIABLES␣=␣"X",␣"Y",␣"Z",␣"Head","Temp","Conc","CHCO3",&
␣"H+","AL3+","SiO2","Ca","Vd","XAnor"')
1717 FORMAT (13(ES10.2,2x))
1818 FORMAT (A20,2x,e12.3)
2323 FORMAT (5(1pe12.5,2x))


  close(unit=8)
  close(unit=9)
  close(unit=10)
  close(unit=11)
  stop
  end
```

2. Input for Mesh Generation

An example of an input file for the above mesh generator is given below. This example highlights the functionality added by the author as described in section 2 (Mesh Generation; page 39) of chapter 2.

```
Domain Parameters:
ncolx ncoly    nrowz
30    12    12
SubDomain Parameters:
xmin  xmax  ymin  ymax  zmin  zmax
17.0  23.0  5.0   7.0   5.0   7.0
Grid Adjustment Parameters for the SubDomain:
nnX1factor  nnX3factor  nnY1factor  nnY3factor
6     12    6     5
Grid Refinement Parameters:
xrefine     delxmin     delxmax     yrefine     delymin  delymax
0.65     1.0      2.6      0.25     1.0      1.0
Gradient Parameters (Low factors should be < 1.0):
high_head   low_head_factor
2.0      0.45
high_temp   low_temp_factor
10.0     0.45
high_conc   low_conc_factor
0.2      0.45
high_chco3  low_chco3_factor
1.8      0.45
high_ch     low_ch_factor
4.00E-05 0.45
high_cal low_cal_factor
6.60E-07 0.45
high_csio2  low_csio2_factor
2.22E-03 0.45
high_cca low_cca_factor
1.64E-03 0.45
```

APPENDIX B

Reaction Rates

The FORTRAN 90/95 computer code, developed in this study, to calculate reaction rates i.e., dissolution of anorthite and precipitation of calcite is listed below. This computer code tracks porosity alteration and outputs net porosity changes accounting for porosity created and lost. The basis of this part of the code is described in section 3 (Tracking Chemical Reactions; page 39) of chapter 2. Output from this code is designed to be visualized using the commercially available software Tecplot™.

```
!^-^-^-^-^-^-^-^-^-^-^-^-^- SUBROUTINE: RXN_Rate ^-^-^-^-^-^-^-^-^-^-^-^-^-
! Last change: by Mohammad R. Khadhrawi (MRK) on:
! Thu., Oct 13, 2005 @ 8:50 AM
! These updates are:
! 1- The reaction rate subroutine (rxn_rate.f90) is updated to
! reflect the Calcite precipitation reaction written as:
!  CaCO3 + (H+) = (Ca2+) + (HCO3-)
! instead of the previously written reaction:
!  (Ca2+) + (HCO3-) = CaCO3 + (H+).
! This change will result in the ion-activity product for this
! reaction (IPA2)  being written as follows:
!  iap2(n) = (cca(n)*chco3(n))/ch(n); instead of:
!  iap2(n) = ch(n)/(cca(n)*chco3(n)).

! The rate law for this reaction (R2) has now to be written
! as follows:
! Rate2(n) = -(1.0/1000.0)*krxn2*s0*(1.0-omega2(n)); where
! the negative sign infront of the RHS is needed such the
! Rate2 is positive for growth and negative for dissolution.
! This rate expression can be written as:
! Rate2(n) = (1.0/1000.0)*krxn2*s0*(omega2(n)-1)

! Calculate the rates of anorthite dissolution and
! calcite deposition

SUBROUTINE RXN_Rate(it, nnode, nelem, ntime, x, a01, a02, Ea1, Ea2, keq1,&
keq2, krxn1, krxn2, rhocal, rhomcal, MWcal, chco3, ch, cal, csio2, cca, xanor,&
Temp, Vd, s0, R, iap1, iap2, omega1, omega2, delt, Rate1, Rate2, SA1, SA2,&
phi, iout,hco3_snap,h_snap,al_snap,sio2_snap,ca_snap)
```

```
use splib_data
IMPLICIT NONE


INTEGER:: nnode, nelem, ntime
INTEGER:: n, m, l, it, iout, c, y

REAL*8 :: a01, a02, Ea1, Ea2, keq1, keq2, krxn1, krxn2, rhocal,
REAL*8 :: rhomcal, MWcal
REAL*8 :: x(maxnodes), chco3(maxnodes), ch(maxnodes),
REAL*8 :: cal(maxnodes), csio2(maxnodes)
REAL*8 :: cca(maxnodes), xanor(maxnodes), Temp(maxnodes),
REAL*8 :: Vd(maxnodes), s0, R, delt, SA1, SA2, phi(maxmats)
REAL*8 :: iap1(maxnodes), iap2(maxnodes), omega1(maxnodes),
REAL*8 :: omega2(maxnodes), Rate1(maxnodes), Rate2(maxnodes)
REAL*8 :: hco3_snap,h_snap,al_snap,sio2_snap,ca_snap

character :: NaN


DO n=1,nnode

!  if(it .gt. 1) then

IF (ch(n) .lt. h_snap) then
   write(*,*) 'Top␣of␣RXN_Rate:␣NNODE␣␣NTIME␣H+␣H_ini'
   write(*,321) n, it, ch(n), h_snap
   ch(n) = h_snap
endif
```

```
IF (cal(n) .lt. al_snap) then
   write(*,*) 'Top␣of␣RXN_Rate:␣NNODE␣␣NTIME␣AL␣AL_ini'
   write(*,321) n, it, cal(n), al_snap
   cal(n) = al_snap
endif

IF (csio2(n) .lt. sio2_snap) then
   write(*,*) 'Top␣of␣RXN_Rate:␣NNODE␣␣NTIME␣SiO2␣␣SiO2_ini'
   write(*,321) n, it, csio2(n), sio2_snap
   csio2(n) = sio2_snap
endif

IF (cca(n) .lt. ca_snap) then
   write(*,*) 'Top␣of␣RXN_Rate:␣NNODE␣␣NTIME␣Ca␣Ca_ini'
   write(*,321) n, it, cca(n), ca_snap
   cca(n) = ca_snap
endif

IF (chco3(n) .lt. hco3_snap) then
   write(*,*) 'Top␣of␣RXN_Rate:␣NNODE␣␣NTIME␣HCO3␣␣HCO3_ini'
   write(*,321) n, it, chco3(n), hco3_snap
   chco3(n) = hco3_snap
endif

!IF (Vd(n) .lt. 0.0) then
!  write(*,*) 'Top of RXN_Rate: NNODE  NTIME SiO2  Vd_ini'
!  write(*,321) n, it, Vd(n), Vd(n)
!  Vd(n) = 0.0
!endif
```

```
!  endif

!if (rate1(n) .gt. 2.8E-08) rate1(n) = 2.8E-08
!if (rate1(n) .lt. 0.0) rate1(n) = 0.0

!if (rate2(n) .gt. 0.05) rate2(n) = 0.05
!if (rate2(n) .lt. 0.0) rate2(n) = 0.0

if(iout .ge. 1) then
WRITE(8,*) ''
WRITE(8,*) 'RXN_Rate␣Subroutine:␣node␣#', n, '␣and␣ntime␣=␣', it
WRITE(8,*) 'Pre-Calculation␣----------'

WRITE(8,19) 'Node␣#␣␣X(m)␣␣␣␣␣␣chco3(mol/L)␣␣ch(mol/L)
cal(mol/L)␣csio2(mol/L)␣cca␣(mol/L)␣Temp.(C)␣Vd␣XAnor'
endif
!DO l = 1, nnode
!  WRITE(8,11) l, x(l), chco3(l), ch(l),  cal(l),  csio2(l),
cca(l), Temp(l), Vd(l), xanor(l)
!END DO

10 FORMAT(2(f10.4,2x))
11 FORMAT(I5,2x,9(ES12.4,2x))

if(iout .ge. 1) then
WRITE(8,*) 'iap1,␣omega1,␣Rate1'
WRITE(8,25) iap1(n), omega1(n), Rate1(n)
WRITE(8,*) ''
WRITE(8,*) 'iap2,␣omega2,␣Rate2'
```

```
WRITE(8,25) iap2(n), omega2(n), Rate2(n)
WRITE(8,*) ''
endif

25 FORMAT(ES14.4,2x,2(ES12.4))


!  iap1(n) = (cca(n)*((cal(n))**2.0)*(csio2(n))**2.0)/(((ch(n))**8.0)*xanor(n))
   iap1(n) = (cca(n)*((cal(n))**2.0)*(csio2(n))**2.0)/(((ch(n))**8.0))
   omega1(n) = iap1(n)/keq1
!  krxn1(n) = a01*(EXP(-Ea1/(R*Temp(n))))
   Rate1(n) = (1.0/1000.0)*krxn1*SA1*(ch(n)**(0.5))*(1.0-omega1(n))

!        if(rate1(n) .eq. len(NaN))then
        if(rate1(n) .eq. len(NaN) .or. ch(n) .eq. len(NaN) .or. chco3(n) .eq.&
      len(NaN) .or. cca(n) .eq. len(NaN) .or. cal(n) .eq. len(NaN) .or.&
      csio2(n) .eq. len(NaN)) then
          write(*,*) 'Rxn_Rate␣Subroutine:␣'
          write(*,*) 'NTIME␣=␣', it

          write(*,*) 'Reaction␣Parameters␣at␣the␣Previous␣Node:'
          write(*,*) 'Previous␣NNODE␣=␣', n-1
          write(*,*) 'CA␣␣␣␣␣␣␣␣AL␣␣␣␣␣␣SiO2␣␣␣␣H+␣␣␣␣␣␣XAnor'
          write(*,171) cca(n-1), cal(n-1), csio2(n-1), ch(n-1), xanor(n-1)
          write(*,*) 'SA1␣␣␣␣␣␣␣delt␣␣␣␣IAP1␣␣␣␣Omega1␣␣Rate1'
   endif

if(iout .ge. 1) then
WRITE(8,*) 'iap1,␣omega1,␣Rate1'
WRITE(8,25) iap1(n), omega1(n), Rate1(n)
```

```
WRITE(8,*) ''
WRITE(8,*) 'iap2, omega2, Rate2'
WRITE(8,25) iap2(n), omega2(n), Rate2(n)
WRITE(8,*) ''
endif



!  iap1(n) = (cca(n)*((cal(n))**2.0)*(csio2(n))**2.0)/(((ch(n))**8.0)*xanor(n))
   iap1(n) = (cca(n)*((cal(n))**2.0)*(csio2(n))**2.0)/(((ch(n))**8.0))
   omega1(n) = iap1(n)/keq1
!  krxn1(n) = a01*(EXP(-Ea1/(R*Temp(n))))
   Rate1(n) = (1.0/1000.0)*krxn1*SA1*(ch(n)**(0.5))*(1.0-omega1(n))

!        if(rate1(n) .eq. len(NaN))then
        if(rate1(n) .eq. len(NaN) .or. ch(n) .eq. len(NaN) .or. chco3(n) .eq.&
      len(NaN) .or. cca(n) .eq. len(NaN) .or. cal(n) .eq. len(NaN) .or.&
      csio2(n) .eq. len(NaN)) then
          write(*,*) 'Rxn_Rate Subroutine: '
          write(*,*) 'NTIME = ', it

          write(*,*) 'Reaction Parameters at the Previous Node:'
          write(*,*) 'Previous NNODE = ', n-1
          write(*,*) 'CA        AL      SiO2    H+      XAnor'
          write(*,171) cca(n-1), cal(n-1), csio2(n-1), ch(n-1), xanor(n-1)
          write(*,*) 'SA1       delt    IAP1    Omega1  Rate1'
          write(*,171) sa1,delt,iap1(n-1), omega1(n-1), rate1(n-1)
        write(*,*) '______________________'
          write(*,*) 'Reaction Parameters at the Current Node'
          write(*,*) 'Current NNODE =', n
```

```
          write(*,*) 'CA␣␣␣␣␣␣␣␣AL␣␣␣␣␣␣SiO2␣␣␣␣H+␣␣␣␣␣␣XAnor'
          write(*,171) cca(n), cal(n), csio2(n), ch(n), xanor(n)
          write(*,*) 'SA2␣␣␣␣␣␣␣delt␣␣␣␣IAP1␣␣␣␣Omega1␣␣Rate1'
          write(*,171) sa1,delt,iap1(n), omega1(n), rate1(n)
          write(*,*) 'GeoFE␣is␣STOPPING␣now␣!'
          STOP
        endif
171 FORMAT(5(ES12.4,2x))


!Update concentrations

!  ch(n) = ch(n) - (8.0*Rate1(n)*delt)
!  cal(n) = cal(n) + (2.0*Rate1(n)*delt)
!  csio2(n) = csio2(n) + (2.0*Rate1(n)*delt)
!  cca(n) = cca(n) + (Rate1(n)*delt)

!  IF (ch(n) .lt. h_snap) ch(n) = h_snap
!  IF (cal(n) .lt. al_snap) cal(n) = al_snap
!  IF (csio2(n) .lt. sio2_snap) csio2(n) = sio2_snap
!  IF (cca(n) .lt. ca_snap) cca(n) = ca_snap


if (iout .ge. 1) then
WRITE(8,*) ''
WRITE(8,*) 'RXN_Rate␣Subroutine:␣node␣#', n, '␣and␣ntime␣=␣', it
WRITE(8,*) 'Concentrations␣updated␣after␣Rxn␣1:␣----------'

WRITE(8,19) 'Node␣#␣␣X(m)␣chco3(mol/L)␣ch(mol/L)␣␣␣cal(mol/L)␣csio2(mol/L)&
cca␣(mol/L)␣Temp.(C)␣Vd␣XAnor'
```

```
WRITE(8,11) n, x(n), chco3(n), ch(n), cal(n), csio2(n), cca(n), Temp(n),&
Vd(n), xanor(n)
endif

! Calculate Rate for Calcite Deposition (Reaction 2):

   iap2(n) = (cca(n)*chco3(n))/ch(n)
   !See UPDATE note of Oct. 13, 2005 above.
!  iap2(n) = ch(n)/(cca(n)*chco3(n));
!  See UPDATE note of Oct. 13, 2005 above.
   omega2(n) = iap2(n)/keq2
!  krxn2(n) = a02*(EXP(-Ea2/(R*Temp(n))))


   !IF (Vd(n) .eq. 0.0 .and. omega2(n) .lt. 0.999) THEN
!See UPDATE note of Oct. 13, 2005 above.
   IF (Vd(n) .eq. 0.0 .and. omega2(n) .gt. 1.3) THEN
!See UPDATE note of Oct. 13, 2005 above.
      Rate2(n) = (1.0/1000.0)*krxn2*s0*(ch(n)**(0.5))*(omega2(n)-1.0)
!See UPDATE note of Oct. 13, 2005 above.
!  Rate2(n) = (1.0/1000.0)*krxn2*s0*(1.0-omega2(n))
!See UPDATE note of Oct. 13, 2005 above.
   ENDIF

 IF (Vd(n) .ne. 0.0) THEN
 Rate2(n) = (1.0/1000.0)*krxn2*(ch(n)**(0.5))*((Vd(n)**(2/3)))*(omega2(n)-1.0)
!See UPDATE note of Oct. 13, 2005 above.
!Rate2(n) = (1.0/1000.0)*krxn2*((Vd(n)**(2/3)))*(1.0-omega2(n))
!See UPDATE note of Oct. 13, 2005 above.
   ENDIF
```

```
!         if(rate2(n) .eq. len(NaN))then
        if(rate2(n) .eq. len(NaN) .or. ch(n) .eq. len(NaN) .or. chco3(n) .eq.&
      len(NaN) .or. cca(n) .eq. len(NaN) .or. cal(n) .eq. len(NaN) .or.&
      csio2(n) .eq. len(NaN))then
     write(*,*) 'Rxn_Rate␣Subroutine:␣'
     write(*,*) 'NTIME␣=␣', it

     write(*,*) 'Reaction␣Parameters␣at␣the␣Previous␣Node:'
     write(*,*) 'Previous␣NNODE␣=␣', n-1
     write(*,*) 'CA␣␣AL␣SiO2␣␣H+␣XAnor'
     write(*,171) cca(n-1), cal(n-1), csio2(n-1), ch(n-1), xanor(n-1)
     write(*,*) 'SA2␣delt␣␣IAP2␣␣Omega2␣␣␣Rate2'
     write(*,171) sa1,delt,iap2(n-1), omega2(n-1), rate2(n-1)
     write(*,*) '_____________________'
     write(*,*) 'Reaction␣Parameters␣at␣the␣Current␣Node'
     write(*,*) 'Current␣NNODE␣=', n
     write(*,*) 'CA␣␣AL␣SiO2␣␣H+␣XAnor'
     write(*,171) cca(n), cal(n), csio2(n), ch(n), xanor(n)
     write(*,*) 'SA2␣delt␣␣IAP2␣␣Omega2␣␣␣Rate2'
          write(*,*) 'GeoFE␣is␣STOPPING␣now␣!'
          STOP
   endif

!  IF (ch(n) .lt. h_snap) ch(n) = h_snap
!  IF (cal(n) .lt. al_snap) cal(n) = al_snap
!  IF (csio2(n) .lt. sio2_snap) csio2(n) = sio2_snap
!  IF (cca(n) .lt. ca_snap) cca(n) = ca_snap
!  IF (Vd(n) .lt. 0.0) Vd(n) = 0.0
```

```
!  if(it .gt. 1) then

IF (ch(n) .lt. h_snap) then
   write(*,*) 'Bottom␣of␣RXN_Rate:␣NNODE␣␣NTIME␣H+␣H_ini'
   write(*,321) n, it, ch(n), h_snap
   ch(n) = h_snap
endif


IF (cal(n) .lt. al_snap) then
   write(*,*) 'Bottom␣of␣RXN_Rate:␣NNODE␣␣NTIME␣AL␣AL_ini'
   write(*,321) n, it, cal(n), al_snap
   cal(n) = al_snap
endif

IF (csio2(n) .lt. sio2_snap) then
   write(*,*) 'Bottom␣of␣RXN_Rate:␣NNODE␣NTIME␣SiO2␣SiO2_ini'
   write(*,321) n, it, csio2(n), sio2_snap
   csio2(n) = sio2_snap
endif

IF (cca(n) .lt. ca_snap) then
   write(*,*) 'Bottom␣of␣RXN_Rate:␣NNODE␣␣NTIME␣Ca␣Ca_ini'
   write(*,321) n, it, cca(n), ca_snap
   cca(n) = ca_snap
endif

IF (chco3(n) .lt. hco3_snap) then
   write(*,*) 'Bottom␣of␣RXN_Rate:␣NNODE␣NTIME␣HCO3␣HCO3_ini'
```

```
   write(*,321) n, it, chco3(n), hco3_snap
   chco3(n) = hco3_snap
endif

!IF (Vd(n) .lt. 0.0) then
!  write(*,*) 'Bottom of RXN_Rate: NNODE NTIME SiO2 Vd_ini'
!  write(*,321) n, it, Vd(n), Vd(n)
!  Vd(n) = 0.0
!endif

!  endif

if (iout .ge. 1) then
WRITE(8,*) ''

WRITE(8,*) 'RXN_Rate␣Subroutine:␣node␣#', n, '␣and␣ntime␣=␣', it
WRITE(8,*) 'Concentrations␣updated␣after␣Rxn␣2:␣----------'

WRITE(8,19) 'Node␣#␣␣X(m)␣chco3(mol/L)␣ch(mol/L)␣cal(mol/L)␣csio2(mol/L)␣cca&
mol/L)␣Temp.(C)␣Vd␣␣␣XAnor'
WRITE(8,11) n, x(n), chco3(n), ch(n), cal(n), csio2(n), cca(n), Temp(n),&
Vd(n), xanor(n)

WRITE(8,*) ''

WRITE(8,*) 'Post-Calculation'
WRITE(8,*) 'iap1,␣omega1,␣Rate1'
WRITE(8,25) iap1(n), omega1(n), Rate1(n)
WRITE(8,*) ''
WRITE(8,*) 'iap2,␣omega2,␣Rate2'
```

```
WRITE(8,25) iap2(n), omega2(n), Rate2(n)
WRITE(8,*) ''
endif

if (n .eq. nnode)then
   write (*,*) '-------Bottom␣of␣Rxn␣SubRoutine------Node␣#␣', n,'␣NTIME=␣',it
   write (8,*) '-------Bottom␣of␣Rxn␣SubRoutine------Node␣#␣', n,'␣NTIME=␣',it
endif

!^-^-^-^-^-^-^-^-^-^-^-^-^-^- TecPlot Output ^-^^-^-^-^-^-^-^-^-^-^-^-^-

!  IF (it .eq. 1) THEN
!     WRITE(9,*) 'variables = "Distance", "Rate1", "Rate2"'
!     WRITE(9,19) 'variables = "Distance", "HCO3", "H",&
!     "Al", "SiO2", "Ca", "Temp", "Vd","Rate1", "Rate2"'
!  END IF
19 Format(A90)


!  IF (MODULO(it,4) .eq. 0) THEN
!     IF (n .eq. 1) THEN
!        WRITE (9,*) "Zone"
!     END IF

!     WRITE (9,21) x(n), chco3(n), ch(n), cal(n), csio2(n), cca(n), Vd(n),&
      Rate1(n), Rate2(n), Temp(n)
!     WRITE (9,20) x(n), Rate1(n), Rate2(n)
!  END IF

20 FORMAT(3(ES12.4,2x))
```

```
21 FORMAT(10(ES12.4,2x))
321 FORMAT(2(I7,2x),2x,2(ES14.3,2x))

END DO

End Subroutine RXN_Rate

!^_^_^_^_^_^_^_^_^_^_^_^_^_^_^_^_^_^_^_^_^_^_^_^_^_^_^_^_^_^_^_^_^_^_^_^_^_^_
```

APPENDIX C

Transport of Chemical Species

1. Transport and Tracking of Ca^{2+}

The basis of this part of the code is described in section 4.1 (Transport and Tracking of Ca^{2+}; page 39) of chapter 2.

```
subroutine catran (x,y,z,ni,nj,nk,nl,phi,ldis,tdis,rhof,vol,concpca,ireact,&
a,b,c,tetxyz,nelem,gt,mat,iout,delt,vx,vy,vz,dif,rate1,rate2)
!
      use splib_data
      implicit none

!      integer maxnodes,maxelems,maxbnds,maxmats,maxflts,maxwdt

       real*8 vol(maxelems),tetxyz(maxelems),rhof(maxnodes)
       real*8 a(4,maxelems),b(4,maxelems),c(4,maxelems)
       real*8 x(maxnodes),y(maxnodes),z(maxnodes)
       real*8 phi(maxmats),dif(maxmats)
       real*8 ldis(maxmats),tdis(maxmats)
       REAL*8 vx(maxelems),vy(maxelems),vz(maxelems)
       real*8 rate1(maxnodes),rate2(maxnodes)
       real*8 exx,eyy,ezz,exz,eyz,exy
       real*8 concpca(maxnodes),delt
!       real*8 concp(maxnodes),delt
       real*8 rvise,rrho,vise,coef,rhofe  !,rho0
!       REAL*8 r(MAXNB,MAXNODES),gt(MAXNODES)
       real*8 gt(MAXNODES)
       REAL*8 dd,p(4,4),aa(4,4),be(4)
       REAL*8 snp(maxnodes)                !rvis(maxnodes),
!
       integer ni(maxelems),nj(maxelems),nk(maxelems),nl(maxelems)
       integer nelem,i,j,k,l,node(4),qq,mat(maxelems)
!      integer in(4,maxelems)
   integer :: inode, iout, jband, jnode, m, mm, np, nq
   real*8  :: acoef1, acoef2, vbar, vx2, vy2, vz2, ireact

```

```
!     r(:,:) = 0.0d0
        splibA(:)=0.0d0
   gt(:)  = 0.0d0

   do 100 m=1, nelem
        node(1) = ni(m)
        node(2) = nj(m)
        node(3) = nk(m)
        node(4) = nl(m)
        qq=mat(m)
        i = ni(m)
        j = nj(m)
        k = nk(m)
        l = nl(m)

        vx2 = vx(m)*vx(m)/(phi(qq)*phi(qq))
        vy2 = vy(m)*vy(m)/(phi(qq)*phi(qq))
        vz2 = vz(m)*vz(m)/(phi(qq)*phi(qq))
        vbar = dsqrt(vx2+vy2+vz2)

        if(vbar.eq.0.0d+00) then
    write(8,401) m
!  if(iout.eq.1) write(8,401) m
           exx = dif(qq)
           eyy = dif(qq)
           ezz = dif(qq)
           exz = 0.0d+00
           eyz = 0.0d+00
           exy = 0.0d+00

```

```
      else

          exx = ( (ldis(qq)*vx2+tdis(qq)*vy2+tdis(qq)*vz2) ) / vbar + dif(qq)
          eyy = ( (tdis(qq)*vx2+ldis(qq)*vy2+tdis(qq)*vz2) ) / vbar + dif(qq)
          ezz = ( (tdis(qq)*vx2+tdis(qq)*vy2+ldis(qq)*vz2) ) / vbar + dif(qq)
          exz = (ldis(qq)-tdis(qq)) * vx(m) * vz(m) / vbar
          eyz = (ldis(qq)-tdis(qq)) * vy(m) * vz(m) / vbar
          exy = (ldis(qq)-tdis(qq)) * vx(m) * vy(m) / vbar

        end if

        acoef1= vol(m)/4.0d0
        acoef2= 1.0d+0/(36.0d0*vol(m))

                do 101 i = 1, 4
                 !inode=in(i,m)
              select case (i)
               case(1)
                 inode = ni(m)
               case(2)
                 inode = nj(m)
               case(3)
                 inode = nk(m)
               case(4)
                 inode = nl(m)
                end select

              np = node(i)
                  dd = 0.0d+0
                     do 80 j = 1,4
```

```
                    !jnode=in(j,m)
                 select case (j)
                  case(1)
                    jnode = ni(m)
                  case(2)
                    jnode = nj(m)
                  case(3)
                    jnode = nk(m)
                  case(4)
                    jnode = nl(m)
                     end select

                  nq = node(j)
          IF(i.EQ.j)THEN
!
            P(i,j)= acoef1/(delt)
          ELSE IF (i.NE.j)THEN
            P(i,j)=0.0D+00
          END IF
!
! form local Stiffness matrix, fully implicit
!

                    aa(i,j) = acoef2*          &
                  ((Exx*a(i,m)*a(j,m))         &
                + (Eyy*b(i,m)*b(j,m))          &
                + (Ezz*c(i,m)*c(j,m))          &
                + (Exy*a(i,m)*b(j,m))          &
                + (Exz*a(i,m)*c(j,m))          &
                + (Exy*b(i,m)*a(j,m))          &
```

```
                 + (Eyz*b(i,m)*c(j,m))        &
                 + (Exz*c(i,m)*a(j,m))        &
                 + (Eyz*c(i,m)*b(j,m)))


          dd = dd + p(i,j)*concpca(node(j))

!          dd = dd + p(i,j)*concp(node(j))

          aa(i,j) = aa(i,j) + p(i,j)

      call find (inode,jnode,jband)
!
! add stiffness matrix to global r matrix using
! crank nicholson formulation
!
!      r(jband,inode) = r(jband,inode) + aa(i,j)
       splibA(jband)=splibA(jband)+aa(i,j)

   80                continue
!
! add explicit contribution of capacitance matrix
! and bouyancy term to right hand side

   if(ireact.eq.1)then
           be(i) =  dd + (acoef1*((rate1(inode)*0.12*.3)-rate2(inode)))
         elseif(ireact.lt.1) then
          be(i) =  dd
         endif
! 0.12 = mole fraction of anorthite in the plageoclase
```

```
! 0.30 = fraction of plageoclase in the snad.

      gt(inode) =  gt(inode)+be(i)

 101            continue
 120          continue
 140        continue
 160      continue
 180    continue
!
!
!     PRINT OUT LOCAL AA MATRIX & B VECTOR IF IOUT > 0
!
      IF (iout.lt.1) GO TO 300
      WRITE(8,*) 'catran: stiffness matrix'
      DO 250 L=1,4
      WRITE (8,20) (AA(L,MM),MM=1,4)
  250 CONTINUE
      WRITE(8,*) 'catran: capacitance matrix'
      DO 251 L=1,4
      WRITE (8,20) (p(L,MM),MM=1,4)
  251 CONTINUE
!
!     PRINT OUT B VECTOR
!
      WRITE(8,*) 'catran: b vector'
      WRITE (8,30) (be(L),L=1,4)
  300 CONTINUE
!
```

```
  100 CONTINUE


!       do 117 m=1,1722
!           if (gt(m) .ne. 0.0d0) write(*,*) m, gt(m)
!117    continue


   10 FORMAT (/,1X,'SUBROUTINE␣catran',/,1X,'AA␣MATRIX:')
   20 FORMAT (11(1PE12.4))
   30 FORMAT (//,1X,'B␣VECTOR',10(1PE12.4))
  401 format('***in␣catran:␣warning␣vbar␣equals␣zero␣for␣elememt',i4)
!
       return
end subroutine catran
```

2. Transport and Tracking of H^+

The basis of this part of the code is described in section 4.2 (Transport and Tracking of H^+; page 39) of chapter 2.

```
subroutine htran (x,y,z,ni,nj,nk,nl,phi,ldis,tdis,rhof,vol,concph,ireact,a,b,&
c,tetxyz,nelem,gt,mat,iout,delt,vx,vy,vz,dif,rate1,rate2)
!
      use splib_data
      implicit none

!      integer maxnodes,maxelems,maxbnds,maxmats,maxflts,maxwdt

       real*8 vol(maxelems),tetxyz(maxelems),rhof(maxnodes)
       real*8 a(4,maxelems),b(4,maxelems),c(4,maxelems)
       real*8 x(maxnodes),y(maxnodes),z(maxnodes)
       real*8 phi(maxmats),dif(maxmats)
       real*8 ldis(maxmats),tdis(maxmats)
       REAL*8 vx(maxelems),vy(maxelems),vz(maxelems)
       real*8 rate1(maxnodes),rate2(maxnodes)
       real*8 exx,eyy,ezz,exz,eyz,exy
       real*8 concph(maxnodes),delt
       real*8 rvise,rrho,vise,coef,rhofe  !,rho0
!      REAL*8 r(MAXNB,MAXNODES),gt(MAXNODES)
       real*8 gt(MAXNODES)
       REAL*8 dd,p(4,4),aa(4,4),be(4)
       REAL*8 snp(maxnodes)                !rvis(maxnodes),
!
       integer ni(maxelems),nj(maxelems),nk(maxelems),nl(maxelems)
       integer nelem,i,j,k,l,node(4),qq,mat(maxelems)
!      integer in(4,maxelems)
   integer :: inode, iout, jband, jnode, m, mm, np, nq
   real*8  :: acoef1, acoef2, vbar, vx2, vy2, vz2, ireact

!    r(:,:) = 0.0d0
```

```
      splibA(:)=0.0d0
gt(:)  = 0.0d0

do 100 m=1, nelem
      node(1) = ni(m)
      node(2) = nj(m)
      node(3) = nk(m)
      node(4) = nl(m)
      qq=mat(m)
      i = ni(m)
      j = nj(m)
      k = nk(m)
      l = nl(m)

      vx2 = vx(m)*vx(m)/(phi(qq)*phi(qq))
      vy2 = vy(m)*vy(m)/(phi(qq)*phi(qq))
      vz2 = vz(m)*vz(m)/(phi(qq)*phi(qq))
      vbar = dsqrt(vx2+vy2+vz2)

      if(vbar.eq.0.0d+00) then
 write(8,401) m
!  if(iout.eq.1) write(8,401) m
         exx = dif(qq)
         eyy = dif(qq)
         ezz = dif(qq)
         exz = 0.0d+00
         eyz = 0.0d+00
         exy = 0.0d+00

else
```

```
            exx = ( (ldis(qq)*vx2+tdis(qq)*vy2+tdis(qq)*vz2) ) / vbar + dif(qq)
            eyy = ( (tdis(qq)*vx2+ldis(qq)*vy2+tdis(qq)*vz2) ) / vbar + dif(qq)
            ezz = ( (tdis(qq)*vx2+tdis(qq)*vy2+ldis(qq)*vz2) ) / vbar + dif(qq)
            exz = (ldis(qq)-tdis(qq)) * vx(m) * vz(m) / vbar
            eyz = (ldis(qq)-tdis(qq)) * vy(m) * vz(m) / vbar
            exy = (ldis(qq)-tdis(qq)) * vx(m) * vy(m) / vbar

        end if

        acoef1= vol(m)/4.0d0
        acoef2= 1.0d+0/(36.0d0*vol(m))

                do 101 i = 1, 4
                 !inode=in(i,m)
            select case (i)
             case(1)
               inode = ni(m)
             case(2)
               inode = nj(m)
             case(3)
               inode = nk(m)
             case(4)
               inode = nl(m)
                end select

            np = node(i)
                dd = 0.0d+0
                   do 80 j = 1,4
                    !jnode=in(j,m)
```

```
                  select case (j)
                   case(1)
                     jnode = ni(m)
                   case(2)
                     jnode = nj(m)
                   case(3)
                     jnode = nk(m)
                   case(4)
                     jnode = nl(m)
                      end select

                   nq = node(j)
          IF(i.EQ.j)THEN
!
            P(i,j)= acoef1/(delt)
          ELSE IF (i.NE.j)THEN
            P(i,j)=0.0D+00
          END IF
!
! form local Stiffness matrix, fully implicit
!

                    aa(i,j) = acoef2*          &
                  ((Exx*a(i,m)*a(j,m))         &
                 + (Eyy*b(i,m)*b(j,m))         &
                 + (Ezz*c(i,m)*c(j,m))         &
                 + (Exy*a(i,m)*b(j,m))         &
                 + (Exz*a(i,m)*c(j,m))         &
                 + (Exy*b(i,m)*a(j,m))         &
                 + (Eyz*b(i,m)*c(j,m))         &
```

```
                 + (Exz*c(i,m)*a(j,m))        &
                 + (Eyz*c(i,m)*b(j,m)))


          dd = dd + p(i,j)*concph(node(j))

          aa(i,j) = aa(i,j) + p(i,j)

      call find (inode,jnode,jband)
!
! add stiffness matrix to global r matrix using
! crank nicholson formulation
!
!      r(jband,inode) = r(jband,inode) + aa(i,j)
       splibA(jband)=splibA(jband)+aa(i,j)

   80                continue
!
! add explicit contribution of capacitance matrix
! and bouyancy term to right hand side
!
!      be(i) =  dd

   if(ireact.eq.1) then
          be(i) =  dd + (acoef1*(-1*rate2(inode)))
        elseif(ireact.lt.1) then
          be(i) =  dd
        endif

      be(i) =  dd + (acoef1*(rate2(inode)-(8*rate1(inode)*0.12*0.3)))
```

```
! 0.12 = mole fraction of anorthite in the plageoclase
! 0.30 = fraction of plageoclase in the snad.

      gt(inode) =  gt(inode)+be(i)

 101            continue
 120          continue
 140        continue
 160      continue
 180    continue
!
!
!     PRINT OUT LOCAL AA MATRIX & B VECTOR IF IOUT > 0
!
      IF (iout.lt.1) GO TO 300
      WRITE(8,*) 'htran␣stiffness␣matrix'
      DO 250 L=1,4
      WRITE (8,20) (AA(L,MM),MM=1,4)
  250 CONTINUE
      WRITE(8,*) 'htran␣capacitance␣matrix'
      DO 251 L=1,4
      WRITE (8,20) (p(L,MM),MM=1,4)
  251 CONTINUE
!
!     PRINT OUT B VECTOR
!
      WRITE(8,*) 'htran␣b␣vector'
      WRITE (8,30) (be(L),L=1,4)
```

```
  300 CONTINUE
!
  100 CONTINUE


!      do 117 m=1,1722
!          if (gt(m) .ne. 0.0d0) write(*,*) m, gt(m)
!117   continue


   10 FORMAT (/,1X,'SUBROUTINE htran',/,1X,'AA MATRIX:')
   20 FORMAT (11(1PE12.4))
   30 FORMAT (//,1X,'B VECTOR',10(1PE12.4))
  401 format('***in htran: warning vbar equals zero for elememt',i4)
!
       return
       end subroutine htran
```

3. Transport and Tracking of HCO_3^-

The basis of this part of the code is described in section 4.3 (Transport and Tracking of HCO_3^-; page 40) of chapter 2.

```
subroutine hco3tran (x,y,z,ni,nj,nk,nl,phi,ldis,tdis,rhof,vol,concphco3,&
ireact,a,b,c,tetxyz,nelem,gt,mat,iout,delt,vx,vy,vz,dif,rate1,rate2)
!
      use splib_data
      implicit none
!      integer maxnodes,maxelems,maxbnds,maxmats,maxflts,maxwdt

       real*8 vol(maxelems),tetxyz(maxelems),rhof(maxnodes)
       real*8 a(4,maxelems),b(4,maxelems),c(4,maxelems)
       real*8 x(maxnodes),y(maxnodes),z(maxnodes)
       real*8 phi(maxmats),dif(maxmats)
       real*8 ldis(maxmats),tdis(maxmats)
       REAL*8 vx(maxelems),vy(maxelems),vz(maxelems)
      real*8 rate1(maxnodes),rate2(maxnodes)
       real*8 exx,eyy,ezz,exz,eyz,exy
       real*8 concphco3(maxnodes),delt
       real*8 rvise,rrho,vise,coef,rhofe  !,rho0
!       REAL*8 r(MAXNB,MAXNODES),gt(MAXNODES)
       real*8 gt(MAXNODES)
       REAL*8 dd,p(4,4),aa(4,4),be(4)
       REAL*8 snp(maxnodes)                !rvis(maxnodes),
!
       integer ni(maxelems),nj(maxelems),nk(maxelems),nl(maxelems)
       integer nelem,i,j,k,l,node(4),qq,mat(maxelems)
!      integer in(4,maxelems)
   integer :: inode, iout, jband, jnode, m, mm, np, nq
   real*8  :: acoef1, acoef2, vbar, vx2, vy2, vz2, ireact

!    r(:,:) = 0.0d0
        splibA(:)=0.0d0
```

```
   gt(:)  = 0.0d0

   do 100 m=1, nelem
        node(1) = ni(m)
        node(2) = nj(m)
        node(3) = nk(m)
        node(4) = nl(m)
        qq=mat(m)
        i = ni(m)
        j = nj(m)
        k = nk(m)
        l = nl(m)

        vx2 = vx(m)*vx(m)/(phi(qq)*phi(qq))
        vy2 = vy(m)*vy(m)/(phi(qq)*phi(qq))
        vz2 = vz(m)*vz(m)/(phi(qq)*phi(qq))
        vbar = dsqrt(vx2+vy2+vz2)

        if(vbar.eq.0.0d+00) then
    write(8,401) m
!  if(iout.eq.1) write(8,401) m
           exx = dif(qq)
           eyy = dif(qq)
           ezz = dif(qq)
           exz = 0.0d+00
           eyz = 0.0d+00
           exy = 0.0d+00

      else
```

```
      exx = ( (ldis(qq)*vx2+tdis(qq)*vy2+tdis(qq)*vz2) ) / vbar + dif(qq)
      eyy = ( (tdis(qq)*vx2+ldis(qq)*vy2+tdis(qq)*vz2) ) / vbar + dif(qq)
      ezz = ( (tdis(qq)*vx2+tdis(qq)*vy2+ldis(qq)*vz2) ) / vbar + dif(qq)
      exz = (ldis(qq)-tdis(qq)) * vx(m) * vz(m) / vbar
      eyz = (ldis(qq)-tdis(qq)) * vy(m) * vz(m) / vbar
      exy = (ldis(qq)-tdis(qq)) * vx(m) * vy(m) / vbar

   end if

   acoef1= vol(m)/4.0d0
   acoef2= 1.0d+0/(36.0d0*vol(m))

         do 101 i = 1, 4
          !inode=in(i,m)
     select case (i)
      case(1)
        inode = ni(m)
      case(2)
        inode = nj(m)
      case(3)
        inode = nk(m)
      case(4)
        inode = nl(m)
         end select

     np = node(i)
         dd = 0.0d+0
            do 80 j = 1,4
             !jnode=in(j,m)
         select case (j)
```

```
                  case(1)
                    jnode = ni(m)
                  case(2)
                    jnode = nj(m)
                  case(3)
                    jnode = nk(m)
                  case(4)
                    jnode = nl(m)
                     end select

                  nq = node(j)
          IF(i.EQ.j)THEN
!
            P(i,j)= acoef1/(delt)
          ELSE IF (i.NE.j)THEN
            P(i,j)=0.0D+00
          END IF
!
! form local Stiffness matrix, fully implicit
!

                   aa(i,j) = acoef2*          &
                 ((Exx*a(i,m)*a(j,m))         &
               + (Eyy*b(i,m)*b(j,m))          &
               + (Ezz*c(i,m)*c(j,m))          &
               + (Exy*a(i,m)*b(j,m))          &
               + (Exz*a(i,m)*c(j,m))          &
               + (Exy*b(i,m)*a(j,m))          &
               + (Eyz*b(i,m)*c(j,m))          &
               + (Exz*c(i,m)*a(j,m))          &
```

```
                + (Eyz*c(i,m)*b(j,m)))

          dd = dd + p(i,j)*concphco3(node(j))

          aa(i,j) = aa(i,j) + p(i,j)

      call find (inode,jnode,jband)
!
! add stiffness matrix to global r matrix using
! crank nicholson formulation
!
!      r(jband,inode) = r(jband,inode) + aa(i,j)
       splibA(jband)=splibA(jband)+aa(i,j)

   80                continue
!
! add explicit contribution of capacitance matrix
! and bouyancy term to right hand side

   if(ireact.eq.1)then
     be(i) =  dd + (acoef1*(-1*rate2(inode)))
   elseif(ireact.lt.1) then
     be(i) =  dd
   endif

      gt(inode) =  gt(inode)+be(i)

 101            continue
 120          continue
```

```
 140        continue
 160      continue
 180    continue
!
!
!     PRINT OUT LOCAL AA MATRIX & B VECTOR IF IOUT > 0
!
      IF (iout.lt.1) GO TO 300
      WRITE(8,*) 'hco3ctran:␣stiffness␣matrix'
      DO 250 L=1,4
      WRITE (8,20) (AA(L,MM),MM=1,4)
  250 CONTINUE
      WRITE(8,*) 'hco3ctran:␣capacitance␣matrix'
      DO 251 L=1,4
      WRITE (8,20) (p(L,MM),MM=1,4)
  251 CONTINUE
!
!     PRINT OUT B VECTOR
!
      WRITE(8,*) 'hco3tran:␣b␣vector'
      WRITE (8,30) (be(L),L=1,4)
  300 CONTINUE
!
  100 CONTINUE


!      do 117 m=1,1722
!          if (gt(m) .ne. 0.0d0) write(*,*) m, gt(m)
!117   continue
```

```
   10 FORMAT (/,1X,'SUBROUTINE␣hco3tran',/,1X,'AA␣MATRIX:')
   20 FORMAT (11(1PE12.4))
   30 FORMAT (//,1X,'B␣VECTOR',10(1PE12.4))
  401 format('***in␣haco3tran:␣warning␣vbar␣equals␣zero␣for␣elememt',i4)
!
      return
      end subroutine hco3tran
```

APPENDIX D

Input Files for Stratigraphic-Forward Modeling

The following input file contains all the parameters used in investigating the effects of sediment concentration on preservation. This particular simulation was run with concentration value of 1200 $kg\ m^{-3}$. Discussion of this simulation and others related to the same experiment is in section 4.1.2 (Effects of Grain-Size Proportion on Preservation; page 60).

1. Grid of Initial Surface of Deposition

The initial surface grid that was used in the simulations is given in the file below:

```
  685.80   685.80   685.76   685.76   685.76   685.76   685.76   685.76   685.76   685.72   685.72   685.72   685.72   685.72
685.72   685.72   685.72   685.68   685.68   685.68   685.68   685.68   685.68   685.68   685.68   685.68   685.64   685.64
685.64   685.64   685.64   685.64   685.64   685.68   685.68   685.68   685.68   685.68   685.68   685.72   685.72   685.72
685.72   685.72   685.76   685.76   685.76   685.80   685.80   685.84   685.84   685.88   685.92   685.92   685.96   686.00
686.00   686.04   686.08   686.12   686.12   686.16   686.20   686.24   686.24   686.28   686.32   686.32   686.36   686.36
686.36
  685.76   685.76   685.76   685.76   685.76   685.72   685.72   685.72   685.72   685.72   685.68   685.68   685.68   685.68
685.68   685.68   685.64   685.64   685.64   685.64   685.64   685.64   685.60   685.60   685.60   685.60   685.60   685.60
685.60   685.56   685.60   685.60   685.60   685.60   685.60   685.60   685.64   685.64   685.64   685.68   685.68   685.68
685.68   685.72   685.72   685.72   685.76   685.76   685.80   685.80   685.84   685.88   685.88   685.92   685.96   685.96
686.00   686.04   686.08   686.08   686.12   686.16   686.20   686.20   686.24   686.28   686.28   686.32   686.36   686.36
686.36
  685.72   685.72   685.72   685.72   685.72   685.68   685.68   685.68   685.64   685.64   685.64   685.64   685.60   685.60
685.60   685.60   685.56   685.56   685.56   685.56   685.56   685.52   685.52   685.52   685.52   685.48   685.48   685.48
685.48   685.48   685.48   685.48   685.48   685.48   685.52   685.52   685.56   685.56   685.56   685.60   685.60   685.64
685.64   685.68   685.68   685.68   685.72   685.72   685.76   685.80   685.80   685.84   685.88   685.88   685.92   685.96
685.96   686.00   686.04   686.08   686.12   686.12   686.16   686.20   686.24   686.24   686.28   686.28   686.32   686.32
686.36
  685.68   685.68   685.68   685.64   685.64   685.64   685.60   685.60   685.60   685.56   685.56   685.56   685.56   685.52
685.52   685.52   685.48   685.48   685.48   685.44   685.44   685.44   685.44   685.40   685.40   685.40   685.36   685.36
685.36   685.36   685.36   685.36   685.36   685.40   685.40   685.44   685.44   685.48   685.48   685.52   685.52   685.56
685.60   685.60   685.64   685.64   685.68   685.68   685.72   685.76   685.76   685.80   685.84   685.84   685.88   685.92
685.96   686.00   686.00   686.04   686.08   686.12   686.12   686.16   686.20   686.20   686.24   686.28   686.28   686.32
686.32
  685.64   685.60   685.60   685.60   685.56   685.56   685.56   685.52   685.52   685.52   685.48   685.48   685.48   685.44
685.44   685.44   685.40   685.40   685.40   685.36   685.36   685.36   685.32   685.32   685.32   685.28   685.28   685.28
685.28   685.28   685.28   685.28   685.28   685.32   685.32   685.36   685.36   685.40   685.44   685.44   685.48   685.52
685.52   685.56   685.56   685.60   685.64   685.64   685.68   685.72   685.72   685.76   685.80   685.84   685.84   685.88
685.92   685.96   686.00   686.00   686.04   686.08   686.08   686.12   686.16   686.16   686.20   686.24   686.24   686.28
686.28
  685.56   685.56   685.52   685.52   685.52   685.48   685.48   685.48   685.48   685.44   685.44   685.44   685.40   685.40
685.36   685.36   685.36   685.32   685.32   685.32   685.28   685.28   685.28   685.24   685.24   685.24   685.20   685.20
685.20   685.20   685.20   685.20   685.24   685.24   685.28   685.28   685.32   685.36   685.36   685.40   685.44   685.44
685.48   685.52   685.52   685.56   685.60   685.60   685.64   685.68   685.72   685.72   685.76   685.80   685.84   685.84
685.88   685.92   685.96   685.96   686.00   686.04   686.08   686.08   686.12   686.16   686.16   686.20   686.20   686.24
686.24
  685.48   685.48   685.48   685.44   685.44   685.44   685.44   685.40   685.40   685.40   685.36   685.36   685.36   685.32
685.32   685.32   685.28   685.28   685.28   685.24   685.24   685.24   685.20   685.20   685.20   685.16   685.16   685.16
685.16   685.16   685.16   685.16   685.16   685.20   685.20   685.24   685.28   685.28   685.32   685.36   685.36   685.40
685.44   685.48   685.48   685.52   685.56   685.60   685.60   685.64   685.68   685.72   685.72   685.76   685.80   685.84
685.84   685.88   685.92   685.96   685.96   686.00   686.04   686.04   686.08   686.12   686.12   686.16   686.20   686.20
686.20
```

```
8   685.40   685.40   685.40   685.40   685.36   685.36   685.36   685.36   685.36   685.32   685.32   685.32   685.28   685.28
685.24   685.24   685.24   685.24   685.20   685.20   685.20   685.16   685.16   685.16   685.12   685.12   685.12   685.12
685.12   685.12   685.12   685.12   685.12   685.16   685.16   685.20   685.24   685.24   685.28   685.32   685.36   685.36
685.40   685.44   685.44   685.48   685.52   685.56   685.56   685.60   685.64   685.68   685.72   685.72   685.76   685.80
685.84   685.84   685.88   685.92   685.92   685.96   686.00   686.00   686.04   686.08   686.08   686.12   686.16   686.16
686.20
  685.36   685.36   685.32   685.32   685.32   685.32   685.28   685.28   685.28   685.28   685.24   685.24   685.24   685.20
685.20   685.20   685.16   685.16   685.16   685.16   685.12   685.12   685.12   685.12   685.08   685.08   685.08   685.08
685.08   685.08   685.08   685.08   685.08   685.12   685.12   685.16   685.20   685.20   685.24   685.28   685.32   685.32
685.36   685.40   685.44   685.44   685.48   685.52   685.56   685.56   685.60   685.64   685.68   685.68   685.72   685.76
685.80   685.80   685.84   685.88   685.88   685.92   685.96   685.96   686.00   686.04   686.08   686.08   686.12   686.12
686.16
10  685.28   685.28   685.28   685.24   685.24   685.24   685.24   685.24   685.20   685.20   685.20   685.16   685.16   685.16
685.16   685.12   685.12   685.12   685.12   685.08   685.08   685.08   685.08   685.04   685.04   685.04   685.04   685.04
685.00   685.04   685.04   685.04   685.04   685.08   685.08   685.12   685.16   685.16   685.20   685.24   685.28   685.28
685.32   685.36   685.40   685.40   685.44   685.48   685.52   685.56   685.56   685.60   685.64   685.64   685.68   685.72
685.76   685.76   685.80   685.84   685.84   685.88   685.92   685.96   685.96   686.00   686.04   686.04   686.08   686.12
686.12
  685.20   685.20   685.20   685.20   685.16   685.16   685.16   685.16   685.16   685.12   685.12   685.12   685.12   685.08
685.08   685.08   685.08   685.08   685.04   685.04   685.04   685.04   685.04   685.00   685.00   685.00   685.00   684.96
684.96   684.96   685.00   685.00   685.00   685.04   685.04   685.08   685.12   685.16   685.16   685.20   685.24   685.28
685.28   685.32   685.36   685.40   685.40   685.44   685.48   685.52   685.52   685.56   685.60   685.64   685.64   685.68
685.72   685.72   685.76   685.80   685.80   685.84   685.88   685.92   685.92   685.96   686.00   686.04   686.04   686.08
686.08
12  685.12   685.12   685.12   685.12   685.12   685.12   685.08   685.08   685.08   685.08   685.08   685.04   685.04   685.04
685.04   685.04   685.00   685.00   685.00   685.00   685.00   685.00   684.96   684.96   684.96   684.96   684.96   684.92
684.92   684.92   684.96   684.96   684.96   685.00   685.04   685.04   685.08   685.12   685.12   685.16   685.20   685.24
685.24   685.28   685.32   685.36   685.36   685.40   685.44   685.48   685.48   685.52   685.56   685.60   685.60   685.64
685.68   685.68   685.72   685.76   685.80   685.80   685.84   685.88   685.92   685.92   685.96   686.00   686.04   686.04
686.04
  685.08   685.08   685.04   685.04   685.04   685.04   685.04   685.04   685.00   685.00   685.00   685.00   685.00   685.00
684.96   684.96   684.96   684.96   684.96   684.96   684.92   684.92   684.92   684.92   684.92   684.92   684.88   684.88
684.88   684.88   684.92   684.92   684.92   684.96   685.00   685.00   685.04   685.08   685.08   685.12   685.16   685.20
685.20   685.24   685.28   685.32   685.32   685.36   685.40   685.44   685.44   685.48   685.52   685.56   685.56   685.60
685.64   685.68   685.68   685.72   685.76   685.76   685.80   685.84   685.88   685.92   685.92   685.96   686.00   686.00
686.04
14  685.00   685.00   685.00   685.00   684.96   684.96   684.96   684.96   684.96   684.96   684.96   684.92   684.92   684.92
684.92   684.92   684.92   684.92   684.88   684.88   684.88   684.88   684.88   684.88   684.88   684.84   684.84   684.84
684.84   684.84   684.88   684.88   684.88   684.92   684.96   684.96   685.00   685.04   685.04   685.08   685.12   685.16
685.16   685.20   685.24   685.28   685.28   685.32   685.36   685.40   685.40   685.44   685.48   685.52   685.52   685.56
685.60   685.64   685.64   685.68   685.72   685.76   685.76   685.80   685.84   685.88   685.92   685.92   685.96   685.96
686.00
```

```
  684.92   684.92   684.92   684.92   684.92   684.92   684.92   684.88   684.88   684.88   684.88   684.88   684.88   684.88
684.88   684.84   684.84   684.84   684.84   684.84   684.84   684.84   684.84   684.84   684.80   684.80   684.80   684.80
684.80   684.80   684.84   684.84   684.84   684.88   684.92   684.92   684.96   685.00   685.00   685.04   685.08   685.12
685.12   685.16   685.20   685.24   685.24   685.28   685.32   685.36   685.36   685.40   685.44   685.48   685.52   685.52
685.56   685.60   685.64   685.64   685.68   685.72   685.76   685.76   685.80   685.84   685.88   685.88   685.92   685.96
685.96
  684.84   684.84   684.84   684.84   684.84   684.84   684.84   684.84   684.84   684.84   684.84   684.84   684.80   684.80
684.80   684.80   684.80   684.80   684.80   684.80   684.80   684.80   684.76   684.76   684.76   684.76   684.76   684.76
684.76   684.76   684.80   684.80   684.80   684.84   684.88   684.88   684.92   684.96   684.96   685.00   685.04   685.08
685.08   685.12   685.16   685.20   685.24   685.24   685.28   685.32   685.36   685.36   685.40   685.44   685.48   685.48
685.52   685.56   685.60   685.64   685.64   685.68   685.72   685.76   685.76   685.80   685.84   685.88   685.88   685.92
685.92
  684.80   684.80   684.80   684.76   684.76   684.76   684.76   684.76   684.76   684.76   684.76   684.76   684.76   684.76
684.76   684.76   684.76   684.76   684.76   684.72   684.72   684.72   684.72   684.72   684.72   684.72   684.72   684.72
684.72   684.72   684.76   684.76   684.80   684.80   684.84   684.84   684.88   684.92   684.96   684.96   685.00   685.04
685.08   685.08   685.12   685.16   685.20   685.20   685.24   685.28   685.32   685.36   685.36   685.40   685.44   685.48
685.48   685.52   685.56   685.60   685.60   685.64   685.68   685.72   685.76   685.76   685.80   685.84   685.88   685.88
685.88
  684.72   684.72   684.72   684.72   684.72   684.72   684.72   684.72   684.72   684.72   684.72   684.72   684.72   684.68
684.68   684.68   684.68   684.68   684.68   684.68   684.68   684.68   684.68   684.68   684.68   684.68   684.68   684.68
684.68   684.68   684.72   684.72   684.76   684.76   684.80   684.80   684.84   684.88   684.92   684.92   684.96   685.00
685.04   685.04   685.08   685.12   685.16   685.20   685.20   685.24   685.28   685.32   685.36   685.36   685.40   685.44
685.48   685.48   685.52   685.56   685.60   685.60   685.64   685.68   685.72   685.76   685.76   685.80   685.84   685.84
685.88
  684.64   684.64   684.64   684.64   684.64   684.64   684.64   684.64   684.64   684.64   684.64   684.64   684.64   684.64
684.64   684.64   684.64   684.64   684.64   684.64   684.64   684.64   684.64   684.64   684.64   684.64   684.64   684.64
684.64   684.64   684.68   684.68   684.72   684.72   684.76   684.76   684.80   684.84   684.88   684.88   684.92   684.96
685.00   685.04   685.04   685.08   685.12   685.16   685.20   685.20   685.24   685.28   685.32   685.32   685.36   685.40
685.44   685.48   685.48   685.52   685.56   685.60   685.60   685.64   685.68   685.72   685.76   685.76   685.80   685.84
685.84
  684.56   684.56   684.60   684.60   684.60   684.60   684.60   684.60   684.60   684.60   684.60   684.60   684.60   684.60
684.60   684.60   684.60   684.60   684.60   684.60   684.60   684.60   684.60   684.60   684.60   684.60   684.60   684.60
684.60   684.60   684.64   684.64   684.68   684.68   684.72   684.72   684.76   684.80   684.84   684.84   684.88   684.92
684.96   685.00   685.00   685.04   685.08   685.12   685.16   685.16   685.20   685.24   685.28   685.32   685.32   685.36
685.40   685.44   685.48   685.48   685.52   685.56   685.60   685.60   685.64   685.68   685.72   685.72   685.76   685.80
685.80
  684.52   684.52   684.52   684.52   684.52   684.52   684.52   684.52   684.52   684.52   684.52   684.52   684.52   684.52
684.52   684.52   684.52   684.52   684.52   684.52   684.52   684.52   684.52   684.52   684.52   684.52   684.56   684.56
684.56   684.56   684.60   684.60   684.64   684.64   684.68   684.68   684.72   684.76   684.80   684.80   684.84   684.88
684.92   684.96   684.96   685.00   685.04   685.08   685.12   685.16   685.16   685.20   685.24   685.28   685.32   685.32
685.36   685.40   685.44   685.48   685.48   685.52   685.56   685.60   685.60   685.64   685.68   685.72   685.72   685.76
685.76
```

```
22   684.44   684.44   684.44   684.44   684.44   684.44   684.44   684.44   684.44   684.44   684.44   684.48   684.48   684.48
684.48   684.48   684.48   684.48   684.48   684.48   684.48   684.48   684.48   684.48   684.48   684.48   684.48   684.52
684.52   684.52   684.52   684.56   684.56   684.60   684.64   684.64   684.68   684.72   684.76   684.76   684.80   684.84
684.88   684.92   684.92   684.96   685.00   685.04   685.08   685.12   685.12   685.16   685.20   685.24   685.28   685.28
685.32   685.36   685.40   685.44   685.44   685.48   685.52   685.56   685.60   685.60   685.64   685.68   685.72   685.72
685.72
   684.36   684.36   684.36   684.40   684.40   684.40   684.40   684.40   684.40   684.40   684.40   684.40   684.40   684.40
684.40   684.40   684.44   684.44   684.44   684.44   684.44   684.44   684.44   684.44   684.44   684.44   684.44   684.44
684.48   684.48   684.48   684.52   684.52   684.56   684.60   684.60   684.64   684.68   684.72   684.76   684.76   684.80
684.84   684.88   684.92   684.92   684.96   685.00   685.04   685.08   685.08   685.12   685.16   685.20   685.24   685.28
685.28   685.32   685.36   685.40   685.44   685.44   685.48   685.52   685.56   685.60   685.60   685.64   685.68   685.68
685.72
24   684.28   684.32   684.32   684.32   684.32   684.32   684.32   684.32   684.32   684.32   684.36   684.36   684.36   684.36
684.36   684.36   684.36   684.36   684.36   684.36   684.40   684.40   684.40   684.40   684.40   684.40   684.40   684.40
684.44   684.44   684.44   684.48   684.48   684.52   684.56   684.60   684.60   684.64   684.68   684.72   684.72   684.76
684.80   684.84   684.88   684.88   684.92   684.96   685.00   685.04   685.04   685.08   685.12   685.16   685.20   685.24
685.24   685.28   685.32   685.36   685.40   685.44   685.44   685.48   685.52   685.56   685.60   685.60   685.64   685.64
685.68
   684.24   684.24   684.24   684.24   684.24   684.24   684.28   684.28   684.28   684.28   684.28   684.28   684.28   684.28
684.32   684.32   684.32   684.32   684.32   684.32   684.32   684.36   684.36   684.36   684.36   684.36   684.36   684.36
684.40   684.40   684.40   684.44   684.48   684.48   684.52   684.56   684.56   684.60   684.64   684.68   684.72   684.72
684.76   684.80   684.84   684.88   684.88   684.92   684.96   685.00   685.04   685.04   685.08   685.12   685.16   685.20
685.20   685.24   685.28   685.32   685.36   685.40   685.44   685.44   685.48   685.52   685.56   685.56   685.60   685.64
685.64
26   684.16   684.16   684.16   684.16   684.20   684.20   684.20   684.20   684.20   684.20   684.24   684.24   684.24   684.24
684.24   684.24   684.24   684.28   684.28   684.28   684.28   684.28   684.28   684.32   684.32   684.32   684.32   684.32
684.36   684.36   684.36   684.40   684.44   684.44   684.48   684.52   684.52   684.56   684.60   684.64   684.68   684.68
684.72   684.76   684.80   684.84   684.84   684.88   684.92   684.96   685.00   685.00   685.04   685.08   685.12   685.16
685.20   685.20   685.24   685.28   685.32   685.36   685.40   685.40   685.44   685.48   685.52   685.56   685.56   685.60
685.60
   684.08   684.08   684.12   684.12   684.12   684.12   684.12   684.16   684.16   684.16   684.16   684.16   684.16   684.20
684.20   684.20   684.20   684.20   684.20   684.24   684.24   684.24   684.24   684.24   684.28   684.28   684.28   684.28
684.32   684.32   684.32   684.36   684.40   684.40   684.44   684.48   684.48   684.52   684.56   684.60   684.64   684.68
684.68   684.72   684.76   684.80   684.84   684.84   684.88   684.92   684.96   685.00   685.00   685.04   685.08   685.12
685.16   685.16   685.20   685.24   685.28   685.32   685.36   685.40   685.40   685.44   685.48   685.52   685.56   685.56
685.56
28   684.04   684.04   684.04   684.04   684.04   684.08   684.08   684.08   684.08   684.08   684.12   684.12   684.12   684.12
684.12   684.16   684.16   684.16   684.16   684.16   684.20   684.20   684.20   684.20   684.20   684.24   684.24   684.24
684.28   684.28   684.28   684.32   684.36   684.36   684.40   684.44   684.44   684.48   684.52   684.56   684.60   684.64
684.64   684.68   684.72   684.76   684.80   684.84   684.84   684.88   684.92   684.96   685.00   685.00   685.04   685.08
685.12   685.16   685.16   685.20   685.24   685.28   685.32   685.36   685.40   685.40   685.44   685.48   685.52   685.52
685.56
```

```
  683.96   683.96   683.96   683.96   684.00   684.00   684.00   684.00   684.04   684.04   684.04   684.04   684.04   684.08
684.08   684.08   684.08   684.12   684.12   684.12   684.12   684.16   684.16   684.16   684.16   684.20   684.20   684.20
684.20   684.24   684.24   684.28   684.32   684.32   684.36   684.40   684.40   684.44   684.48   684.52   684.56   684.60
684.60   684.64   684.68   684.72   684.76   684.80   684.80   684.84   684.88   684.92   684.96   684.96   685.00   685.04
685.08   685.12   685.12   685.16   685.20   685.24   685.28   685.32   685.36   685.40   685.40   685.44   685.48   685.48
685.52
30  683.88   683.88   683.88   683.92   683.92   683.92   683.92   683.96   683.96   683.96   683.96   684.00   684.00   684.00
684.00   684.04   684.04   684.04   684.08   684.08   684.08   684.08   684.12   684.12   684.12   684.12   684.16   684.16
684.16   684.20   684.20   684.24   684.28   684.28   684.32   684.36   684.40   684.40   684.44   684.48   684.52   684.56
684.56   684.60   684.64   684.68   684.72   684.76   684.76   684.80   684.84   684.88   684.92   684.96   684.96   685.00
685.04   685.08   685.12   685.12   685.16   685.20   685.24   685.28   685.32   685.36   685.40   685.40   685.44   685.48
685.48
  683.80   683.80   683.84   683.84   683.84   683.84   683.88   683.88   683.88   683.92   683.92   683.92   683.92   683.96
683.96   683.96   684.00   684.00   684.00   684.04   684.04   684.04   684.04   684.08   684.08   684.08   684.12   684.12
684.12   684.16   684.16   684.20   684.24   684.24   684.28   684.32   684.36   684.36   684.40   684.44   684.48   684.52
684.52   684.56   684.60   684.64   684.68   684.72   684.76   684.76   684.80   684.84   684.88   684.92   684.96   684.96
685.00   685.04   685.08   685.12   685.12   685.16   685.20   685.24   685.28   685.32   685.36   685.40   685.40   685.44
685.44
32  683.76   683.76   683.76   683.76   683.76   683.80   683.80   683.80   683.84   683.84   683.84   683.88   683.88   683.88
683.92   683.92   683.92   683.96   683.96   683.96   684.00   684.00   684.00   684.04   684.04   684.04   684.08   684.08
684.08   684.12   684.12   684.16   684.20   684.20   684.24   684.28   684.32   684.32   684.36   684.40   684.44   684.48
684.52   684.52   684.56   684.60   684.64   684.68   684.72   684.72   684.76   684.80   684.84   684.88   684.92   684.96
684.96   685.00   685.04   685.08   685.12   685.12   685.16   685.20   685.24   685.28   685.32   685.36   685.36   685.40
685.40
  683.68   683.68   683.68   683.72   683.72   683.72   683.72   683.76   683.76   683.76   683.80   683.80   683.84   683.84
683.84   683.88   683.88   683.88   683.92   683.92   683.92   683.96   683.96   684.00   684.00   684.00   684.04   684.04
684.08   684.08   684.12   684.12   684.16   684.16   684.20   684.24   684.28   684.32   684.32   684.36   684.40   684.44
684.48   684.52   684.52   684.56   684.60   684.64   684.68   684.72   684.72   684.76   684.80   684.84   684.88   684.92
684.96   684.96   685.00   685.04   685.08   685.12   685.12   685.16   685.20   685.24   685.28   685.32   685.36   685.36
685.40
34  683.64   683.64   683.64   683.64   683.64   683.68   683.68   683.68   683.72   683.72   683.72   683.76   683.76   683.80
683.80   683.80   683.84   683.84   683.88   683.88   683.88   683.92   683.92   683.96   683.96   683.96   684.00   684.00
684.04   684.04   684.08   684.08   684.12   684.16   684.16   684.20   684.24   684.28   684.32   684.36   684.36   684.40
684.44   684.48   684.52   684.52   684.56   684.60   684.64   684.68   684.72   684.76   684.76   684.80   684.84   684.88
684.92   684.96   684.96   685.00   685.04   685.08   685.12   685.12   685.16   685.20   685.24   685.28   685.32   685.36
685.36
  683.56   683.56   683.60   683.60   683.60   683.64   683.64   683.64   683.64   683.68   683.68   683.72   683.72   683.76
683.76   683.80   683.80   683.80   683.84   683.84   683.88   683.88   683.88   683.92   683.92   683.96   683.96   684.00
684.00   684.04   684.04   684.08   684.08   684.12   684.16   684.16   684.20   684.24   684.28   684.32   684.36   684.40
684.44   684.44   684.48   684.52   684.56   684.56   684.60   684.64   684.68   684.72   684.76   684.80   684.84   684.84
684.88   684.92   684.96   685.00   685.00   685.04   685.08   685.12   685.16   685.20   685.24   685.24   685.28   685.32
685.32
```

```
36   683.52   683.56   683.56   683.56   683.56   683.60   683.60   683.60   683.60   683.64   683.64   683.68   683.68   683.72
683.76   683.76   683.80   683.80   683.80   683.84   683.84   683.88   683.88   683.92   683.92   683.92   683.96   683.96
684.00   684.00   684.04   684.04   684.08   684.12   684.12   684.16   684.20   684.24   684.28   684.32   684.32   684.36
684.40   684.44   684.48   684.52   684.52   684.56   684.60   684.64   684.68   684.68   684.72   684.76   684.80   684.84
684.88   684.92   684.92   684.96   685.00   685.04   685.04   685.08   685.12   685.16   685.20   685.24   685.28   685.28
685.32
   683.52   683.52   683.52   683.56   683.56   683.56   683.56   683.56   683.60   683.60   683.64   683.64   683.68   683.72
683.76   683.76   683.80   683.80   683.80   683.84   683.84   683.88   683.88   683.92   683.92   683.92   683.96   683.96
684.00   684.00   684.04   684.04   684.08   684.12   684.12   684.16   684.20   684.24   684.28   684.32   684.32   684.36
684.40   684.44   684.48   684.48   684.52   684.56   684.60   684.60   684.64   684.68   684.72   684.76   684.80   684.84
684.84   684.88   684.92   684.96   685.00   685.00   685.04   685.08   685.12   685.16   685.20   685.20   685.24   685.28
685.28
38   683.52   683.52   683.52   683.52   683.52   683.52   683.56   683.56   683.56   683.56   683.60   683.64   683.68   683.72
683.76   683.76   683.80   683.80   683.84   683.84   683.88   683.88   683.88   683.92   683.92   683.96   683.96   683.96
684.00   684.00   684.04   684.08   684.08   684.12   684.16   684.16   684.20   684.24   684.28   684.32   684.36   684.36
684.40   684.44   684.48   684.52   684.52   684.56   684.60   684.64   684.64   684.68   684.72   684.76   684.80   684.84
684.84   684.88   684.92   684.96   684.96   685.00   685.04   685.08   685.12   685.12   685.16   685.20   685.24   685.24
685.28
   683.48   683.48   683.52   683.52   683.52   683.52   683.52   683.52   683.52   683.56   683.60   683.64   683.68   683.72
683.76   683.80   683.80   683.84   683.84   683.88   683.88   683.92   683.92   683.92   683.96   683.96   683.96   684.00
684.00   684.04   684.04   684.08   684.12   684.12   684.16   684.20   684.20   684.24   684.28   684.32   684.36   684.40
684.40   684.44   684.48   684.52   684.52   684.56   684.60   684.64   684.68   684.68   684.72   684.76   684.80   684.84
684.84   684.88   684.92   684.96   684.96   685.00   685.04   685.08   685.12   685.12   685.16   685.20   685.24   685.24
685.28
40   683.48   683.48   683.48   683.48   683.52   683.52   683.52   683.52   683.52   683.56   683.56   683.64   683.68   683.72
683.80   683.80   683.84   683.84   683.88   683.88   683.92   683.92   683.92   683.96   683.96   684.00   684.00   684.00
684.04   684.04   684.08   684.08   684.12   684.16   684.16   684.20   684.24   684.28   684.28   684.32   684.36   684.40
684.44   684.48   684.48   684.52   684.56   684.56   684.60   684.64   684.68   684.72   684.72   684.76   684.80   684.84
684.84   684.88   684.92   684.96   684.96   685.00   685.04   685.08   685.08   685.12   685.16   685.20   685.24   685.24
685.24
   683.48   683.48   683.48   683.48   683.48   683.52   683.52   683.52   683.52   683.52   683.56   683.64   683.68   683.76
683.80   683.84   683.84   683.88   683.88   683.88   683.92   683.92   683.96   683.96   683.96   684.00   684.00   684.04
684.04   684.08   684.08   684.12   684.12   684.16   684.20   684.20   684.24   684.28   684.32   684.32   684.36   684.40
684.44   684.48   684.48   684.52   684.56   684.60   684.60   684.64   684.68   684.72   684.72   684.76   684.80   684.84
684.84   684.88   684.92   684.96   684.96   685.00   685.04   685.08   685.08   685.12   685.16   685.20   685.24   685.24
685.24
```

2. Example of Master Input File for Sediment Concentration Investigation

```
#start of sedsim input file
##############################################################
#                       Required parameters section            #
##############################################################
# SedSim_Pack_20110218.exe input file
# One-line title / comment on experiment                   (required)
#
mumford_hills_34_k.sif Clore Fm.
#AOI:
#TopRight Corner (meters):
#  X  458445
#  Y  4246785
#LowerLeft Corner (meters):
#  X  388445
#  Y  4206785
# Lenght in X-Direction = 70 km
# Lenght in X-Direction = 40 km
# Simulation Properties:
#1) Based on mumford_hills_33_i.sif.
#2) Sediment concentration value equla avg. of the Mekong River: 1200 kg/m3.
#3) Grain size percentages are 75% fine and 25% very fine.
#4) Depth of post depo burial by sediment was reduced from 1000 to 500 (m);
#   this was done to match SSTVD from logs.
#5) Depth of post depo burial by water was reduced from 500 to 250 (m).
#6) Reversed the order of mouth river movement: first 35 sources move E->W
#   and the next last 35 sources move W-> E.
#7) All 70 sources are active.
#-------------------------------------------------------------
TIME
# Time parameters                                          (required)
# Middle Carboniferous to Early Permian
# Simulation start time [years]   End time [years]
       -330000000                  -329500000
#
# i.e. 500 ky starting from mid-mississippian (visean) to simulate deposition
```

```
# of the Mount PLeasant Sandstone in the AoI.  Bear in mind the total
# deposition time for the Clore Fm. is about 2 Ma.
#
# Display interval [years]      Flow sampling interval [years]
         1000                           500
#
# Display interval decides how often the results files are updated
# Flow sampling interval decides how often fluid elements are
# released from the source
#-----------------------------------------------------------------
GRID
# Grid size definitions and geometry
#
# Grid spacing [m]   Number of rows    Number of columns
    1000.0                 41               71
# Lower left (SW) corner coordinates   Base level elevation
    388445        4206785                        685
# Topography grid file name
71x41_UNYZ_B_Topc60x4_smoothed_MH_Centered.top
#---------------------------------------------------------------
#SEA LEVEL
# Define sea level curve        (optional)
#
# Sea level curve file
haq_and_schutter_2008.sl
#-------------------------------------------------------
SEDIMENTS
# Sediment Parameters                                    (required)
# Line 1: Diameter of each grain size   [mm]
# Line 2: Density of each grain size    [kg/m3]
# Line 3: 1 - suspension (normal type),  0 - bed load (new)
#
# pebble 4-64 mm, granule 2-4 mm, vcse 1-2 mm, cse 0.5-1 mm, med 0.25-0.5 mm,
#  fn 0.125-0.25, vfn 0.062-0.125 mm, slt 0.0039-0.062 mm, clay < 0.0039 mm
#    Coarse      Medium        Fine      Finest
```

```
      0.7        0.35           0.19       0.003
     2650.00     2650.00      2700.00    2700.00
        1           1           1          1
#-------------------------------------------------------
SOURCES
# Definition of sources that are constant throughout the experiment (required)
#
# One line per source, entries are:
# Source location            (x,y)            [m]
# Velocity at source         (vx,vy)          [m/sec]
# Discharge rate             (Q)              [m3/sec]
# Sediment concentration     (c)              [kg/m3]
# Sediment composition       (C coarse,       [%]
#                             M medium,
#                             F fine,
#                             FF finest)
#
# ID  t1       t2    x     y     vx    vy    Q     c  %C %M %F %FF
# src  (mm)                                            0.7 0.35 0.19 0.003
#
101   -329992500  -329991500  457445   4245785  -0.2  -0.3  950       1200 0  0  75 25
102   -329984000  -329983500  456445   4245785  -0.6  -0.4  1600     1200  0  0  75 25
103   -329978500  -329977500  455445   4245785  -0.1  -0.4  950       1200 0  0  75 25
104   -329970000  -329969500  454445   4245785  -0.3  -0.5  1600     1200  0  0  75 25
105   -329964500  -329963500  453445   4245785  -0.1  -0.4  950       1200 0  0  75 25
106   -329956000  -329955500  452445   4245785  -0.3  -0.6  1600     1200  0  0  75 25
107   -329950500  -329949500  451445   4245785  -0.2  -0.3  950       1200 0  0  75 25
108   -329942000  -329941500  450445   4245785  -0.6  -0.8  1600     1200  0  0  75 25
109   -329936500  -329935500  449445   4245785  -0.3  -0.4  950       1200 0  0  75 25
110   -329928000  -329927500  448445   4245785  -0.5  -0.4  1600     1200  0  0  75 25
201   -329922500  -329921500  447445   4245785  -0.2  -0.3  950       1200 0  0  75 25
202   -329914000  -329913500  446445   4245785  -0.6  -0.4  1600     1200  0  0  75 25
203   -329908500  -329907500  445445   4245785  -0.1  -0.4  950       1200 0  0  75 25
204   -329900000  -329899500  444445   4245785  -0.3  -0.5  1600     1200  0  0  75 25
205   -329894500  -329893500  443445   4245785  -0.1  -0.4  950       1200 0  0  75 25
```

```
    206   -329886000  -329885500  442445   4245785  -0.3  -0.6  1600     1200  0  0  75 25
107 207   -329880500  -329879500  441445   4245785  -0.2  -0.3  950       1200 0  0  75 25
    208   -329872000  -329871500  440445   4245785  -0.6  -0.8  1600     1200  0  0  75 25
109 209   -329866500  -329865500  439445   4245785  -0.3  -0.4  950       1200 0  0  75 25
    210   -329858000  -329857500  438445   4245785  -0.5  -0.4  1600     1200  0  0  75 25
111 301   -329852500  -329851500  437445   4245785  -0.2  -0.3  950       1200 0  0  75 25
    302   -329844000  -329843500  436445   4245785  -0.6  -0.4  1600     1200  0  0  75 25
113 303   -329838500  -329837500  435445   4245785  -0.1  -0.4  950       1200 0  0  75 25
    304   -329830000  -329829500  434445   4245785  -0.3  -0.5  1600     1200  0  0  75 25
115 305   -329824500  -329823500  433445   4245785  -0.1  -0.4  950       1200 0  0  75 25
    306   -329816000  -329815500  432445   4245785  -0.3  -0.6  1600     1200  0  0  75 25
117 307   -329810500  -329809500  431445   4245785  -0.2  -0.3  950       1200 0  0  75 25
    308   -329802000  -329801500  430445   4245785  -0.6  -0.8  1600     1200  0  0  75 25
119 309   -329796500  -329795500  429445   4245785  -0.3  -0.4  950       1200 0  0  75 25
    310   -329788000  -329787500  428445   4245785  -0.5  -0.4  1600     1200  0  0  75 25
121 401   -329782500  -329781500  427445   4245785  -0.2  -0.3  950       1200 0  0  75 25
    402   -329774000  -329773500  426445   4245785  -0.6  -0.4  1600     1200  0  0  75 25
123 403   -329768500  -329767500  425445   4245785  -0.1  -0.4  950       1200 0  0  75 25
    404   -329760000  -329759500  424445   4245785  -0.3  -0.5  1600     1200  0  0  75 25
125 405   -329754500  -329753500  423445   4245785  -0.1  -0.4  950       1200 0  0  75 25
    406   -329746000  -329745500  423445   4245785  -0.3  -0.6  1600     1200  0  0  75 25
127 407   -329740500  -329739500  424445   4245785  -0.2  -0.3  950       1200 0  0  75 25
    408   -329732000  -329731500  425445   4245785  -0.6  -0.8  1600     1200  0  0  75 25
129 409   -329726500  -329725500  426445   4245785  -0.3  -0.4  950       1200 0  0  75 25
    410   -329718000  -329717500  427445   4245785  -0.5  -0.4  1600     1200  0  0  75 25
131 501   -329712500  -329711500  428445   4245785  -0.2  -0.3  950       1200 0  0  75 25
    502   -329704000  -329703500  429445   4245785  -0.6  -0.4  1600     1200  0  0  75 25
133 503   -329698500  -329697500  430445   4245785  -0.1  -0.4  950       1200 0  0  75 25
    504   -329690000  -329689500  431445   4245785  -0.3  -0.5  1600     1200  0  0  75 25
135 505   -329684500  -329683500  432445   4245785  -0.1  -0.4  950       1200 0  0  75 25
    506   -329676000  -329675500  433445   4245785  -0.3  -0.6  1600    1200   0  0  75 25
137 507   -329670500  -329669500  434445   4245785  -0.2  -0.3  950       1200 0  0  75 25
    508   -329662000  -329661500  435445   4245785  -0.6  -0.8  1600    1200   0  0  75 25
139 509   -329656500  -329655500  436445   4245785  -0.3  -0.4  950       1200 0  0  75 25
    510   -329648000  -329647500  437445   4245785  -0.5  -0.4  1600    1200   0  0  75 25
```

```
601   -329642500  -329641500  438445   4245785  -0.2  -0.3  950       1200 0  0  75 25
602   -329634000  -329633500  439445   4245785  -0.6  -0.4  1600    1200   0  0  75 25
603   -329628500  -329627500  440445   4245785  -0.1  -0.4  950       1200 0  0  75 25
604   -329620000  -329619500  441445   4245785  -0.3  -0.5  1600    1200   0  0  75 25
605   -329614500  -329613500  442445   4245785  -0.1  -0.4  950       1200 0  0  75 25
606   -329606000  -329605500  443445   4245785  -0.3  -0.6  1600    1200   0  0  75 25
607   -329600500  -329599500  444445   4245785  -0.2  -0.3  950       1200 0  0  75 25
608   -329592000  -329591500  445445   4245785  -0.6  -0.8  1600    1200   0  0  75 25
609   -329586500  -329585500  446445   4245785  -0.3  -0.4  950       1200 0  0  75 25
610   -329578000  -329577500  447445   4245785  -0.5  -0.4  1600    1200   0  0  75 25
701   -329572500  -329571500  448445   4245785  -0.2  -0.3  950       1200 0  0  75 25
702   -329564000  -329563500  449445   4245785  -0.6  -0.4  1600    1200   0  0  75 25
703   -329558500  -329557500  450445   4245785  -0.1  -0.4  950       1200 0  0  75 25
704   -329550000  -329549500  451445   4245785  -0.3  -0.5  1600    1200   0  0  75 25
705   -329544500  -329543500  452445   4245785  -0.1  -0.4  950       1200 0  0  75 25
706   -329536000  -329535500  453445   4245785  -0.3  -0.6  1600    1200   0  0  75 25
707   -329530500  -329529500  454445   4245785  -0.2  -0.3  950       1200 0  0  75 25
708   -329522000  -329521500  455445   4245785  -0.6  -0.8  1600    1200   0  0  75 25
709   -329516500  -329515500  456445   4245785  -0.3  -0.4  950       1200 0  0  75 25
710   -329508000  -329507500  457445   4245785  -0.5  -0.4  1600    1200   0  0  75 25
*
#-------------------------------------------------------------
SOURCE HEIGHTS
# list ends in '*'
# flow types 0=normal 1=turbidite 2=debris flow
# for debris flows the concentration must be high enough, otherwise will
# transition to a turbidite (default transition at 60 kg/m3)
#
# Source ID#  flow height(m)    flow type
101   2.0   0
102   2.0   0
103   2.0   0
104   2.0   0
105   2.0   0
106   2.0   0
```

```
107   2.0   0
108   2.0   0
109   2.0   0
110   2.0   0
201   2.0   0
202   2.0   0
203   2.0   0
204   2.0   0
205   2.0   0
206   2.0   0
207   2.0   0
208   2.0   0
209   2.0   0
210   2.0   0
301   2.0   0
302   2.0   0
303   2.0   0
304   2.0   0
305   2.0   0
306   2.0   0
307   2.0   0
308   2.0   0
309   2.0   0
310   2.0   0
401   2.0   0
402   2.0   0
403   2.0   0
404   2.0   0
405   2.0   0
406   2.0   0
407   2.0   0
408   2.0   0
409   2.0   0
410   2.0   0
501 2.0  0
```

```
502 2.0  0
503 2.0  0
504 2.0  0
505 2.0  0
506 2.0  0
507 2.0  0
508 2.0  0
509 2.0  0
510 2.0  0
601 2.0  0
602 2.0  0
603 2.0  0
604 2.0  0
605 2.0  0
606 2.0  0
607 2.0  0
608 2.0  0
609 2.0  0
610 2.0  0
701 2.0  0
702 2.0  0
703 2.0  0
704 2.0  0
705 2.0  0
706 2.0  0
707 2.0  0
708 2.0  0
709 2.0  0
710 2.0  0
#
*
#######################################################################
# Additional module parameters (modules will not run if not included)
#######################################################################
WELL LOCATIONS
```

```
# locations in meters from sedsim-grid origin (draws them in sedview)
# river inputs in order of flow volumes
# X  Y   well name
#423445  4226785  MHC
422947   4226870  328
423554   4227060  368
457445   4245785  1
456445   4245785  2
455445   4245785  3
454445   4245785  4
453445   4245785  5
452445   4245785  6
451445   4245785  7
450445   4245785  8
449445   4245785  9
448445   4245785  10
447445   4245785  11
446445   4245785  12
445445   4245785  13
444445   4245785  14
443445   4245785  15
442445   4245785  16
441445   4245785  17
440445   4245785  18
439445   4245785  19
438445   4245785  20
437445   4245785  21
436445   4245785  22
435445   4245785  23
434445   4245785  24
433445   4245785  25
432445   4245785  26
431445   4245785  27
430445   4245785  28
429445   4245785  29
```

```
428445   4245785  30
427445   4245785  31
426445   4245785  32
425445   4245785  33
424445   4245785  34
423445   4245785  35
#423445  4245785  36
#424445  4245785  37
#425445  4245785  38
#426445  4245785  39
#427445  4245785  40
#428445  4245785  41
#429445  4245785  42
#430445  4245785  43
#431445  4245785  44
#432445  4245785  45
#433445  4245785  46
#434445  4245785  47
#435445  4245785  48
#436445  4245785  49
#437445  4245785  50
#438445  4245785  51
#439445  4245785  52
#440445  4245785  53
#441445  4245785  54
#442445  4245785  55
#443445  4245785  56
#444445  4245785  57
#445445  4245785  58
#446445  4245785  59
#447445  4245785  60
#448445  4245785  61
#449445  4245785  62
#450445  4245785  63
#451445  4245785  64
```

```
#452445  4245785  65
#453445  4245785  66
#454445  4245785  67
#455445  4245785  68
#456445  4245785  69
#457445  4245785  70
#
* end of well data
#
#-----------------------------------------------------------
#SLOPE FAILURE
# Parameters for calculating slope failure    (optional)
# Maximum Subaerial and Marine slope before failure can occur   (dz/dx) (dz/dx)
# Minimum and maximum height allowed to fail(m) (bigger heights will be split)
# Concentrations slumped material after release (kg/m^3)
# Concentration of the material where it transitions from a debris flow to a tubidite (kg/m^3)
 0.2   0.1
 0.5   5.0
 100.0
 60.0
#-----------------------------------------------------------
#DEPOSIT
# Sediment deposited prior to this run.              (optional)
# *.spc
#---------------------------------------------------------
COMPACTION
# Enable compaction module;     (optional)
# Depth of post depo burial by sediment (m) and depth of post depo burial by water (m)
500                       250
#---------------------------------------------------------
#ISOSTASY
# Calculate isostatic subsidence        (optional)
#
# Mantle density [kg/m3]   Flexural rigidity [Nm2]  Calling interval [a]
    3500       1.0E23   100000
```

```
#-------------------------------------------------------
#TECTONICS
# Define tectonic movement          (optional)
#
# Tectonic movement file name
# *.tec
#-------------------------------------------------------
#EXPERT AEOLIAN
# Define the sediment sources
# Definition of source
# One line per event, entries are:
# Event start and end time                [year]
# Source location    (x,y)                 [m]
# Sediment height      (H)                 [m]
# Sediment composition (C)                 [%]
#
#  nb  t1  t2    x   y    H  %C  %M  %F    %FF
#50 -301999999 -301990001 743000    2606000
*
# Define:
# - display wind time step,
# - transport parameter aliasing,
# - aeolian parametric sampling interval.
#0.04  1  0.001
# Define a global wind regime for the entire area
#
# Wind measurement height Zu [m]
#10
# Aerodynamic roughness length of the surface zo [m]
#0.01
# Zero displacement height D [m]
#0.03
# Vegetation cover growth function
# Vegetation cover updated time [year]
#0.1
```

```
# number of points defining the curve
#0
# define the curve for the considered vegetation type
# each point defined sedimentation balance and according annual concentration growth
#-1.5 0.0 0.1 0.0 0.5 0.0 1.0 0.0 2.2 0.0
# Critical vegetation density over which sand movement decreases sharply and
# maximum efficiency of suppression parameter
#0.75  2.8
# input of initial vegetation cover (percent of cell area)
#vegetation.dat
# This module allows the input of external wind data. the format for the
# input file is
#    header line
#    x velocities -one for each grid point in standard matrix format
#    header line
#    y velocity -one for each grid point in standard matrix format
# Frequency factor controls circulation calling interval.
# The bigger the factor the longer the interval
#  astrix ends input list
# start_time, end_time, frequency factor, input_file_name
#0.00  4.0   1.0  wind.dat
*
#################################################################
# Optional parameters section. Defaults will be used if not entered
#################################################################
#-------------------------------------------------------
ACCURACY FACTOR
# accuracy determines to what percentage accuracy the solution is solved to.
# importantly a small accuracy does not necessarily lead to longer runtimes
# as the solution stays more stable recommended=0.001  maximum=0.01
0.001
#-----------------------------------------------------------------------
BOUNDARY
#specify the boundary types for the coarse grid. (optional)
# 0 = regular boundary  1= insert a wall to prevent sediment and fluid loss
```

```
# without this section the default is regular boundaries
# North South East West
    0    0     0   0
#-----------------------------------------------------------------------
DENSITIES
# Water densities          (optional)
#  fresh water 1000.0 kg/m3,  sea water with 30000ppm NaCl 1027 kg/m3
# density of fluid entering the system [kg/m3] sea density [kg/m3]
    1015.0       1000.0
#-------------------------------------------------------------
PARAMETRIC SAMPLING INTERVAL
#         (optional)
#
# This should be seen in relation to temporal resolution - ie. think aliasing
# Sampling interval for sea-level and tectonics [y]
    500
#-------------------------------------------------------------
SLOPE ANGLES
# Define maximum slope per grain size     (optional)
#
#     tan(1.0)=0.017; tan(2.0)=0.035
#
# a rough guide to appropriate slopes derived from deltas around the world:
#  slope(deg)=0.4+0.5log(sand/shale ratio)
#
# Example slopes:
# a. based on sand/shale ratio  for ratios 0.2-0.8 -  use Sabesi equation :
#           slope (gradient) = tan(0.4 + 0.52 log(sand/shale ratio))
# b. based on median grain size  -
#      from Dean(1983) quoted in Olsen 1990 p.38 (NTH Diplom)
#                h(x) = Ax^m
# where :
#               A =0.24 + 0.254*log(d50mm)
#               m= 2/3
# Modified by Griffiths (1993) to agree more closely with
```

```
#   Short(1979)'s␣observations␣as␣below.
#␣␣␣␣(Short␣noted␣that␣0.5mm+␣gave␣5-6deg,␣0.25-0.5mm␣gave␣between␣1.5-5.5,
#␣and␣<0.25␣mm␣gave␣less␣than'␣1.5deg)
#␣Therefore␣to␣give␣a␣slope␣in␣degrees␣from␣a␣grain␣size
#␣␣between␣0.1␣and␣50␣mm␣use
#␣␣␣␣␣␣␣␣Slope(deg)␣␣=␣atan(((0.28␣+␣0.23*log(d␣mm))*100^(2/3))/100)
#or
#␣␣␣␣␣␣␣␣Slope(gradient)␣␣=␣((0.28+␣0.23*log(d␣mm))*100^(2/3))/100
#
#␣Max.␣slope␣of␣four␣grain␣sizes␣below␣water␣level␣(dz/dx)
#␣Max.␣slope␣of␣four␣grain␣sizes␣above␣water␣level␣(dz/dx)
#␣Max.␣slope␣of␣four␣reworked␣grain␣sizes␣below␣water␣level␣(dz/dx)
#
#␣␣␣␣Coarse␣␣␣␣␣␣Medium␣␣␣␣␣␣␣␣Fine␣␣␣␣Finest
#␣␣␣␣␣␣25.0␣␣␣␣␣␣␣5.0␣␣␣␣␣␣␣␣␣␣0.2␣␣␣␣␣␣0.04
#
0.04␣␣0.03␣␣0.02␣␣0.01
0.1␣␣0.1␣␣0.003␣␣0.003
0.03␣␣␣0.02␣␣␣0.01␣␣␣0.001
#␣max␣slope␣carb␣grains␣below␣sea␣level␣(dz/dx)␣2␣grains
#␣max␣slope␣carb␣grains␣above␣sea␣level␣(dz/dx)␣2␣grains
3.0␣0.7
0.001␣0.0001
#␣Minimum␣slope␣(dz/dx)
#␣Slope␣module␣calling␣interval␣[years]
0.0001
␣100.0
#-----------------------------------------------------------
SLOPE␣PARAMETERS
#␣Parameters␣for␣calculating␣equilibrium␣slope␣␣␣␣(optional)
#
#␣Number␣of␣diffusion␣cycles␣during␣one␣pass
#␣Maximum␣number␣of␣iterations␣per␣diffusion␣cycle
#␣Diffusion␣residual␣[m]
␣␣␣4␣1000␣0.0001
```

```
#-------------------------------------------------------
SEDIMENT␣TRANSPORT␣PARAMETERS
#␣Limiting␣factors␣for␣sediment␣transport␣␣␣␣␣(optional)
#
#␣Sedimentation␣time␣step␣factor␣(sedimentation␣time␣step␣=
#␣␣␣␣␣flow␣time␣step␣*␣sedimentation␣time␣step␣factor)
#␣Maximum␣depth␣of␣fluid␣elements␣␣␣␣[m]
#␣Minimum␣velocity␣of␣fluid␣elements␣[m/s]
#␣Minimum␣ratio␣of␣sediment␣load␣fluid␣element␣to␣average␣sediment
#␣load␣at␣source␣␣␣␣␣[kg/m3]
#␣Basement␣hardness␣factor
␣␣␣␣1.0e4␣␣␣15.0␣␣␣0.01␣␣␣0.01␣␣␣␣1.0
#-----------------------------------------------------------
MANNING
#␣Manning's coefficients          (optional)
#
# Coefficient for open-channel flow
# Coefficient for hyperpycnal flow
# Coefficient for hypopycnal flow
# Coefficient for debris flow
#default: 0.020   0.010    0.070  0.080
 0.02   0.010    0.070  0.080
#-----------------------------------------------------------
POROSITY TABLE
# Porosity function          (optional)
#  Hawtah Trend Unayzah
#
# Number of entries in effective pressure look-up table
  4
# Effective pressure look-up table  [MPa]
               0.0   45.0   68.0   113.0
# depth in m    0    2000   3000   5000
# Number of entries in fine-to-coarse-ratio look-up table
  12
# Fine-to-coarse-ratio look-up table
```

```
0.0 0.05  0.10  0.15  0.20  0.25  0.30  0.40  0.50  0.65  0.85  1.0
# Porosity look-up table
# must have the size of (pressures*ratios)
# rows: constant fine-to-coarse ratio
# columns: constant effective pressure
0.39  0.28  0.23  0.19
0.37  0.24  0.21  0.18
0.34  0.24  0.20  0.17
0.33  0.23  0.19  0.16
0.31  0.22  0.18  0.15
0.29  0.21  0.17  0.14
0.27  0.21  0.16  0.13
0.27  0.21  0.16  0.13
0.29  0.21  0.15  0.13
0.32  0.22  0.15  0.13
0.35  0.23  0.14  0.11
0.43  0.25  0.15  0.10
*
# Porosity table one row for each carbonate and organic
  .70 .65 .50 .49
  .30 .30 .30 .30
  .60 .50 .40 .30
  .20 .16 .13 .10
# Linear weighting coefficients for 4 grain sizes:
# r=Sum(h*w))/Sum(h)
# r fine-to-coarse ratio
# h thickness of individual grain size
# w linear weighting coefficient of individual grain size
# 8 coefficients:
  0.0   0.0   1.0   1.0
#     *** End of input file ***
```

Part 4

Documentation

Bibliography

Anikiyev, V., Zaytsev, O., Hieu, T., Savil'yeva, I., Starodubtsev, Y., and Shumilin, Y. (1986). Variation in space-time distribution of suspended matter in the coastal zone of the Mekong River. *Oceanology*, 26(6):725–729. 49, 50, 62

Archer, A. W. (1996). Panthalassa: paleotidal resonance and a global paleocean Seiche. *Paleooceanography*, 11(5):625–632. 68

Archer, A. W., Kuecher, G. J., and Kvale, E. P. (1995). The role of tidal-velocity asymmetries in the deposition of silty tidal rhythmites (carboniferous, eastern interior coal basin, u.s.a.). *Journal of Sedimentary Research*, 65(2a):408–416. 68

Atherton, E., Emrich, G. H., Glass, H. D., Potter, P. E., and Swann, D. H. (1960). Differentiation of Caseyville (Pennsylvanian) and Chester (Mississippian) Sediments in the Illinois Basin. 44

Bear, J. (1972). *Dynamics of Fluids in Porous Materials*. American Elsevier, New York. 22

Beckner, J. R. (1996). Cementation Processes and Sand Petrography of the Zia Formation, Albuquerque Basin, New Mexico. Master's thesis, New Mexico Institute of Mining and Technology, Socorro, New Mexico. 2, 4, 7

Berner, R. A. and Morse, J. W. (1974). Dissolution Kinetics of Calcium Carbonate in Sea Water, Part IV. Theory of Calcite Dissolution. *American Journal of Science*, 274:108–134. 5

Bethke, C. M., Lee, M.-K., and Park, J. (2002). *Basin Modeling with Basin2: A Guide to Using the Basin2 Software Package. Release 5.0*. University of Illinois, Urbana, IL, USA. 9, 10

Boggs, S. (2001). *Principles of Sedimentology and Stratigraphy*. Prentice Hall, Upper Saddle River, N. J., 3rd edition. 6

Bramlette, M. N. (1941). The Stability of Minerals in Sandstone. *Journal of Sedimentary Petrology*, 11(1):32–36. 5

Buschbach, T. and Kolata, D. (1991). *Regional setting of Illinois basin*, volume 51, chapter 1, pages 29–55. 44

Cibin, U., Cavazza, W., Fontana, D., Milliken, K. L., and McBride, E. F. (1993). Comparison

of Composition and Texture of Calcite-Cemented Concretions and Host Sandstones, Northern Apennines, Italy. *Journal of Sedimentary Petrology*, 63(5):945–954. 5, 6, 7

Connell, S. D. (2001). Stratigraphy of the Albuquerque Basin, Rio Grande Rift, Central New Mexico: a Progress Report. In Connell, S. D., S. G. L. D. W. L., editor, *Stratigraphy and Tectonic Development of the Albuquerque Basin, Central Rio Grande Rift*, chapter Open-File Report 454B, pages A1–A27. New Mexico Bureau of Mines and Mineral Resources, Socorro, NM. 12

Connell, S. D., Allen, B. D., and Hawley, J. W. (1998). Subsurface Stratigraphy of The Santa Fe Group From Borehole Geophysical Logs, Albuquerque Area, New Mexico. *New Mexico Geology*, 20(1):2–7. 10

Craig, L. C. and Varnes, K. L. (1979). History of the Mississippian System – An Interpretive Summary. Technical Report 1010, USGS. 45

Davis, J. M., Lohmann, R. C., Phillips, F. M., Wilson, J. L., and Love, D. W. (1993). Architecture Of The Sierra Ladrones Formation, Central New Mexico: Depositional Controls on the Permeability Correlation Structure. *Geological Society of America Bulletin*, 105(8):998–1007. 10, 11, 12, 13

Droste, J. and Keller, S. (1995). *Subsurface Stratigraphy and Distribution of Oil Fields of the Buffalo Wallow Group (Mississippian) in Indiana*, volume 63 of *Indiana Geological Survey Bulletin*. Indiana University, Bloomington. 43, 45, 48

Feldman, H. R., Archer, A. W., Kvale, E. P., Cunningham, C. R., Maples, C. G., and West, R. R. (1993). A tidal model of carboniferous konservat-lagerstaetten formation. *Palaios*, 8(5):485–498. 68

Fouke, B. W. (2011). Hot-spring systems geobiology: abiotic and biotic influences on travertine formation at mammoth hot springs, yellowstone national park, usa. *Sedimentology*, 58(1):170–219. 41

Frank, J. R., Carpenter, A. B., and Oglesby, T. W. (1982). Cathodoluminescence and Composition of Calcite Cement in the Taum Sauk Limestone (Upper Cambrian), Southeast Missouri. *Journal of Sedimentary Petrology*, 52(2):631–638. 4

Frykman, P. (1986). Diagenesis of Silurian Bioherms in the Klinteberg Formation, Gotland, Sweden. In Schroeder, J. H. and Purser, B. H., editors, *Reef Diagenesis*, pages 399–423. Springer-Verlag, Berlin, Federal Republic of Germany. 4

Garven, G. and Freeze, R. A. (1984). Theoretical Analysis of the Role of Ground Water Flow in the Genesis of Stratabound Ore Deposits 1: Mathematical and Numerical Model. *American Journal of Science*, 284:1085–1124. 20

Griffiths, C. M. (2001). *Brief Review of Stratigraphic Forward Modeling: Short Course Notes*. Number September. 43

Haq, B. U. and Schutter, S. R. (2008). A Chronology of Paleozoic Sea-Level Changes. *Science (New York, N.Y.)*, 322(5898):64–8. 58

Harris, P. M., Kendall, C. G.-S.-C., and Lerche, I. (1985). Carbonate Cementation a Brief Review. In Schneidermann, N. and Harris, P. M., editors, *Carbonate Cements, Special Publication - Society of Economic Paleontologists and Mineralogists*, volume 36, pages 79–95. SEPM (Society for Sedimentary Geology), Tulsa, OK. 4

Heidlauf, D., Hsui, A., and Klein, G. (1986). Tectonic subsidence analysis of the Illinois Basin. *The Journal of Geology*, 94(6):779–794. 44, 47

Howard, R. H. (1991). *Hydrocarbon Reservoir Distribution in the Illinois Basin*, chapter 21, pages 299–327. AAPG. 45

Hubbert, M. K. (1940). The Theory of Ground-Water Motion, Part 1. *Journal of Geology*, 48(8):785–944. 20

IGSPDMS (2011). Petroleum Database Management System: Indiana Geological Survey Web Site, `http://igs.indiana.edu/pdms/`, date accessed, May 24. 63

Istok, J. (1989). *Groundwater Modeling by the Finite Element Method*. Water Resources Monographs. American Geophysical Union, 2000 Florida Ave., NW, Washington, DC 20009, USA, 1st edition. 31

Javandel, I., Doughty, C., and Tsang, C. F. (1984). *Groundwater Transport: Handbook of Mathematical Models*, volume 10 of *Water Resources Monographs*. American Geophysical Union, 2000 Florida Ave, N. W., Washington, DC 20009, USA. 31

Johnson, M. R. (1989). Paleogeographic Significance of Oriented Calcareous Concretions in the Triassic Katberg Formation, South Africa. *Journal of Sedimentary Petrology*, 59:1008–1010. 7, 17

Kahmann, J. and Driese, S. (2008). Paleopedology and geochemistry of Late Mississippian (Chesterian) Pennington Formation paleosols at Pound Gap, Kentucky, USA: Implications for high-frequency climate variations. *Palaeogeography, Palaeoclimatology, Palaeoecology*, 259:357 – 381. 45

Kandianis, M. T., Fouke, B. W., Johnson, R. W., Veysey, John, I., and Inskeep, W. P. (2008). Microbial biomass: A catalyst for caco3 precipitation in advection-dominated transport regimes. *Geological Society of America Bulletin*, 120(3-4):442–450. 40

Kestin, J., Khalifa, H., and Corriea, R. (1981). Tables of the Dynamics and Kinematic Viscosity of Aqueous NaCl Solutions in the Temperature Range of 20-150 degrees C

and the Pressure Range of 0.1-35 MPa. *Journal of Physical Chemistry Reference Data*, 10:71–87. 21

King, C. V. and Liu, C. L. (1933). The Rate of Solution of Marble in Dilute Acids. *American Chemical Society Journal*, 55:1928–1940. 5

Koltermann, C. and Gorelick, S. M. (1995). The Fractional Packing Model for Hydraulic Conductivity Derived from Sediment Mixtures. *Water Resources Research*, 31(12):3283–3297. 22

Kvale, E. P., Archer, A. W., and Johnson, H. R. (1989). Daily, monthly, and yearly tidal cycles within laminated siltstones of the mansfield formation (pennsylvanian) of indiana. *Geology*, 17(4):365–368. 68

Kvale, E. P., Fraser, G. S., Archer, A. W., Zawistoski, A., Kemp, N., and McGough, P. (1994). Evidence of seasonal precipitation in pennsylvanian sediments of the illinois basin. *Geology*, 22(4):331–334. 68

Kvale, E. P., Johnson, H. W., Sonett, C. P., Archer, A. W., and Zawistoski, A. (1999). Calculating lunar retreat rates using tidal rhythmites. *Journal of Sedimentary Research*, 69(6):1154–1168. 68

Lasaga, A. C. (1984). Chemical Kinetics of Water-Rock Interactions. *JGR. Journal of Geophysical Research. B*, 89(6):4009–4025. 9

Lee, M.-K. (1997). Predicting Diagenetic Effects of Groundwater Flow in Sedimentary Basins; a Modeling Approach with Examples. In Montaneez, I. P., Gregg, J. M., and Shelton, K. L., editors, *Basin-wide Diagenetic Patterns; Integrated Petrologic, Geochemical, and Hydrologic Considerations, SEPM Special Puplication No. 57*, pages 3–14. Society for Sedimentary Geology. 9, 10

Lee, M.-K. and Bethke, C. M. (1994). Groundwater Flow, Late Cementation, and Petroleum Accumulation in the Permian Lyons Sandstone, Denver Basin. *AAPG Bulletin*, 78(2):217–237. 10

Longman, M. W. (1980). Carbonate Diagenetic Textures from Nearsurface Diagenetic Environments. *AAPG Bulletin*, 64(4):461–487. 2, 3, 4

López, D. L. and Smith, L. (1995). Fluid Flow in Fault Zones: Analysis of the Interplay of Convective Circulation and Topographically Driven Groundwater Flow. *Water Resources Research*, 31(6):1489–1503. 39, 72

Machette, M. and McGimsey, R. G. (1983). *Map of Quaternary and Pliocene Faults in the Socorro and Western Part of the Fort Sumner* 1° *x* 2° *Quadrangles, Central New Mexico*. U.S. Geological Survey Miscellaneous Field Studies Map MF-1465-A, 12 p. pamphlet, 1

sheet, scale 1:250,000. 13

Machette, M. N. (1978). Geologic Map of the San Acacia Quadrangle, Socorro County, New Mexico. Open-File Report Map GQ-1415, U.S. Geological Survey. 12, 13, 14

Machette, M. N., Personius, S. F., Kelson, K. I., M.Haller, K., and Dart, R. L. (1998). Map and Data for Quaternary Faults and Folds in New Mexico. Open-File Report 98-521, U.S. Geological Survey. 12, 13

May, M. T., Rexroad, C. B., and Brown, L. M. (2009). *Carboniferous Conodont Biostratigraphy Along the Southeastern Periphery of the Eastern Interior Basin, Kentucky, U. S. A.*, chapter 8, pages 101–113. 43

McAda, D. P. and Barroll, P. (2002). Simulation of Ground-Water Flow in the Middle Rio Grande Basin between Cochiti and San Acacia, New Mexico. Water Resources Investigative Reports 02-4200, United States Geological Survey. 11

Mcbride, E. F., Picard, M. D., and Folk, R. L. (1994). Oriented Concretions, Ionian Coast, Italy: Evidence of Groundwater Flow Direction. *Journal of Sedimentary Research*, A64:535–540. 7

Miller, D. J. and Eriksson, K. A. (1997). Late mississippian prodeltaic rhythmites in the appalachian basin: A hierarchical record of tidal and climatic periodicities. *Journal of Sedimentary Research, Section B: Stratigraphy and Global Studies*, 67(4):653–660. 68

Moore, C. H. J. (1977). Beach Rock Origin, Some Geochemical, Mineralogical and Petrographic Considerations. *Geoscience and Man*, 18:155–163. 4

Morse, J. W. (1983). The Kinetics of Calcium Carbonate Dissolution and Precipitation. In Reeder, R. J., editor, *Carbonates Mineralogy and Chemistry*, volume 11, pages 227–264. 6

Mozley, P. S., Beckner, J., and Whitworth, T. M. (1995). Spatial Distribution of Calcite Cement in the Santa Fe Group, Albuquerque Basin, NM: Implications for Groundwater Resources. *New Mexico Geology*, 17(Special Issue: Albuquerque Basin – Studies in Hydrogeology):88–93. 17, 18

Mozley, P. S. and Davis, J. M. (1996). Relationship between oriented calcite concretions and permeability correlation structure in an alluvial aquifer, Sierra Ladrones Formation, New Mexico. *Journal of Sedimentary Research*, 66(1):11–16. 5, 7, 10, 14, 15, 17, 18

Mozley, P. S. and Goodwin, L. B. (1995). Patterns of Cementation Along a Cenozoic Normal Fault: a Record of Paleoflow Orientations. *Geology*, 23(6):539–542. 7, 14

Norby, R. (1991). *Biostratigraphic Zones in the Illinois Basin*, chapter 13, pages 179–194. AAPG. 43, 67

Parkhurst, D. L., Stollenwerk, K. G., and Colman, J. A. (2003). Reactive-Transport Simulation of Phosphorus in the Sewage Plume at the Massachusetts Military Reservation, Cape Cod, Massachusetts. U.S. Geological Survey Water-Resources Investigations Reports 03-4017, U.S. Geological Survey. 9

Person, M. (2005). Personal Communication, Department of Geological Sciences, Indiana University, Bloomington, Indiana. 28, 39

Person, M., Roy, P., Wright, H., Gutowski, W., Ito, E., Winter, T., Rosenberry, D., and Cohen, D. (2007). Hydrologic response of the crow wing watershed, minnesota, to mid-holocene climate change. *Geological Society of America Bulletin*, 119(3-4):363–376. 28, 39

Plummber, L. N., Parkhurst, D. L., and Wigley, T. M. L. (1979). Critical Review of the Kinetics of Calcite Dissolution and Precipitation. In Jenne, E. A., editor, *Chemical Modeling in Aqueous Systems, ACS Symposium Series 93*, pages 537–573. American Chemical Society, Washington, D. C., United States. 6

Potter, P. (1962). Late Mississippian sandstones of Illinois. *Illinois State Geol. Surv. Circ*, 340:36. 43, 62

Potter, P. E. and Pryor, W. A. (1961). Dispersal Centers of Paleozoic and Later Clastics of the Upper Mississippi Valley and Adjacent Areas. *Geological Society of America Bulletin*, 72(8):1195–1249. 45, 48

Reddy, J. N. (1984). *An Introduction to the Finite Element Method*. McGraw-Hill Book Company, New York. 31

Rexroad, C., Blake, B., and Beuthin, J. (2010). Conodonts from the Mauch Chunk Group (Chesterian), Southern West Virginia, Usa. In *Geological Society of America, North-Central Section, 44th annual meeting and Geological Society of America, South-Central Section, 44th annual meeting, Anonymous,) Abstracts with Programs - Geological Society of America (April 2010), 42(2):71*, volume 42, page 71. 43, 45, 67

Rocha, A. A., Frydman, M., da Fontoura, S. A. B., Rosário, F. F., and Bezerra, M. C. M. (2001). Numerical Modeling of Salt Precipitation During Produced Water Reinjection, SPE Paper # 68336. In *Society of Petroleum Engineers (SPE) Third International Symposium on Oilfield Scale*, page 8, Aberdeen, United Kingdom. Society of Petroleum Engineers (SPE). 9

Root, P. (2010). Personal Communication, Department of Geological Sciences, Indiana University, Bloomington, Indiana. 48

Sanford, W. E. and Konikow, L. F. (1989a). Porosity Development in Coastal Carbonate Aquifers. *Geology*, 17(3):249–252. 3

Sanford, W. E. and Konikow, L. F. (1989b). Simulation of Calcite Dissolution and Porosity Changes in Saltwater Mixing Zones in Coastal Aquifers. *Water Resources Research*, 25(4):655–667. 6

Scheidegger, A. E. (1974). *The Physics of Flow Through Porous Media*. Univ. of Toronto Press, Toronto, Canada, 3rd edition. 22

Schwartz, F. W. and Longstaffe, F. J. (1988). Ground Water and Clastic Diagenesis. In W. Back, S. J. R. and Seaber, P. R., editors, *Hydrogeology*, pages 413–434. Geological Society of America, Boulder, CO, United States. 4

Scotese, C. R. and McKerrow, W. S. (1990). Revised world maps and introduction. *Memoirs of the Geological Society of London*, 12:1–21. 45

Segerlind, L. J. (1984). *Applied Finite Element Analysis*. John Wiley, New York, 2nd edition. 33

Siever, R. (1951). The Mississippian-Pennsylvanian Unconformity in Southern Illinois. *AAPG Bulletin*, 35(3):542–581. 44, 45

Slingerland, R., Harbaugh, J., and Furlong, K. (1994). *Simulating clastic sedimentary basins: Physical fundamentals and computer programs for creating dynamic systems*. PTR Prentice Hall, Englewood Cliffs, New Jersey. 54

Smith, L. B. J. and Read, J. F. (2001). Discrimination of Local and Global Effects on Upper Mississippian Stratigraphy, Illinois Basin, U.S.A. *Journal of Sedimentary Research*, 71(6):985–1002. 45, 46, 47

Sracek, O., Bhattacharya, P., Jacks, G., Gustafsson, J.-P., and von Brömssen, M. (2004). Behavior of Arsenic and Geochemical Modeling of Arsenic Enrichment in Aqueous Environments. *Applied Geochemistry*, 19(2):169–180. 9

Steefel, C. and Lasaga, A. C. (1992). Putting Transport into Water-Rock Interaction Models. *Geology*, 20(8):680–684. 9

Swann, D. H. (1963). Classification of Genevievian and Chesterian (late Mississippian) Rocks of Illinois. Report of Investigations 216. 43, 45, 46, 48, 51, 62

Swann, D. H. (1964). Late Mississippian Rhythmic Sediments of Mississippi Valley. *AAPG Bulletin*, 48(5):637–658. 43, 44, 45, 48, 49, 62, 67

Swann, D. H. and Bell, A. H. (1958). Habitat of oil in the Illinois Basin. In *Weeks, L. G., ed., Habitat of oil–a symposium*, pages 447–472. 45

Swann, D. H. and Willman, H. B. (1961). Megagroups in Illinois. *AAPG Bulletin*, 45(4):471–483. 45

Tetzlaff, D. (1986). Computer simulation model of clastic sedimentary processes (abs.).

AAPG Bulletin, 70(5):655. 56

Tetzlaff, D. (1991). The Combined Use of Sedimentary Process Modeling and Statistical Simulation in Reservoir Characterization. In *SPE Annual Technical Conference and Exhibition*. 54

Tetzlaff, D. M. and Harbaugh, J. W. (1989). *Simulating Clastic Sedimentation*. Computer Methods in the Geosciences. Van Nostrand Reinhold, New York, NY, United States. 51, 52, 53, 54, 55

Theakstone, W. H. (1981). Concretions in Glacial Sediments at Seglvatnet, Norway. *Journal of Sedimentary Petrology*, 51:191–196. 7

Thompson, E. G. (2005). *Introdcution to the Finite Element Method: Theory, Programming, and Applications*. John wiley & Sons, Inc., NJ, USA, 1st edition. 31

Thompson, T. A. (2011). Personal Communication, Indiana Geological Survey, Indiana University, Bloomington, Indiana. 68

Treworgy, J. (1988). The Illinois Basin- a tidally and tectonically influenced ramp during mid-Chesterian time. 45

Treworgy, J. (1991). *Kaskaskia Sequence, Mississippian Valmeyeran and Chesterian Series*, volume 51, chapter 9, pages 125–142. AAPG. 43

Treworgy, J. (2004). Mississippian Rocks in Illinois. GeoNote 1. 43, 45, 46, 47

Tucker, M. E. and Wright, V. P. (1990). *Carbonate Sedimentology*. Blackwell Science, Oxford, United Kingdom. 4

van der Kooij, B., Immenhauser, A., Steuber, T., Rionda, J. R. B., and Tome, O. M. (2010). Controlling factors of volumetrically important marine carbonate cementation in deep slope settings. *Sedimentology*, 57(6):1491–1525. 40

Wang, H. and Anderson, M. P. (1982). *Introduction to Groundwater Modeling: Finite Difference and Finite Element Methods*. Academic Press, Inc., 525 B Street, Suite 1900, San Diego, CA 92101-4495, USA. 31

Wang, Y., Wang, Y., and Merino, E. (1995). Dynamic Weathering Model: Constraints Required by Coupled Dissolution and Pseudomorphic Replacement. *Geochimica et Cosmochimica Acta*, 59(8):1559–1570. 26

Weller, J. M. (1956). Argument for Diastrophic Control of Late Paleozoic Cyclothems. *AAPG Bulletin*, 40(1):17–50. 67

Weller, S. (1913). Stratigraphy of the Chester group in southwestern Illinois. *Transactions of the Illinois State Academy of Science*, pages 118–129. 43

Wilkinson, M. and Dampier, M. D. (1990). The Rate of Growth of Sandstone-Hosted Calcite

Concretions. *Geochimica et Cosmochimica Acta.*, 54(12):3391–3399. 5, 7

Williams, G. E. (1989). Late precambrian tidal rhythmites in south australia and the history of the earth's rotation. *Journal of the Geological Society*, 146(1):97–111. 68

Wolanski, E., Nhan, N., and Spagnol, S. (1998). Sediment dynamics during low flow conditions in the Mekong River Estuary, Vietnam. *Journal of Coastal Research*, 14(2):472–482. 49, 50, 51, 62

Wood, J. R. and Boles, J. R. (1991). Evidence for Episodic Cementation and Diagenetic Recording of Seismic Pumping Events, North Coles Levee, California, U.S.A. *Applied Geochemistry*, 6(5):509–521. 8

Zaihua, L., Hailong, S., Baoying, L., Xiangling, L., Wenbing, Y., and Zeng, C. (2010). Wet-dry seasonal variations of hydrochemistry and carbonate precipitation rates in a travertine-depositing canal at baishuitai, yunnan, sw china; implications for the formation of biannual laminae in travertine and for climatic reconstruction. *Chemical Geology*, 273(3-4):258–266. 40

Vita

Graduate School
Indiana University, Bloomginton

Mohammad R. Khadhrawi

3248 Fateh Street, Bahr 4th District, Qatif, Saudi Arabia

Email: mrkqatif@gmail.com

King Fahd University of Petroleum and Mineral, Dhahran, Saudi Arabia
B. S. Industrial Chemistry, January 1991
M. S. Chemistry, January 1996

Research Paper Title:

Stratigraphic-Forward and Reactive-Transport Modeling of Depositional and Diagenetic Processes in Siliciclastic Sandstones

Major Professor: Dr. L. M. Pratt

Professional Experience:

- 2006–Present: Petroleum Scientist, Geology Technology Team, Saudi Aramco EXPEC Advanced Research Center, Dhahran, Saudi Arabia.
- 2001-2006: Graduate Student, Department of Geological Sciences, Indiana University, Bloomington, Indiana.
- 1995-2001: Lab Scientist, Geochemistry Unit, Saudi Aramco Research & Development Center, Dhahran, Saudi Arabia.
- 1993-1995: Graduate Student, Chemistry Department, King Fahd University of Petroleum & Minerals, Dhahran, Saudi Arabia.
- 1991-1993: Lab Scientist, Geochemistry Unit, Saudi Aramco Research & Development Center, Dhahran, Saudi Arabia.
- 1990-1991: Technical Brand Manager, Product Development Department, Modern Industries Company/Procter & Gamble, Jeddah, Saudi Arabia.

Publications:

(1) Root, P., M. Parke, *M. Khadhrawi*, and L. Pratt, Reservoir Characterization and Facies Architecture of the Chesterian Clore Formation (Upper Mississippian) at Mumford Hills Field, Southwestern Indiana. American Association of Petroleum Geologists Abstracts with Programs, Eastern Section Meeting September, 2011.

(2) Root, P., M. Parke, *M. Khadhrawi*, Characterization of a Chesterian Sandstone Hydrocarbon Reservoir in the Clore Formation, Southwestern Indiana. Crossroads

Conference Abstract, Indiana University Department of Geosciences, 2011.

(3) *Khadhrawi, Mohammad*, D. Cantrell, C. Griffiths,and S. Franks, Quantitative Prediction of Reservoir Quality: A Permo-Carboniferous Reservoir, Saudi Arabia, in Geological Society of America 2010 Annual Meeting Abstracts with Programs: Vol. 42, No. 5, p. 636, November 2010, Denver, Colorado.

(4) Cantrell , Dave L., Cedric M. Griffiths, Stephen G. Franks, and *Mohammad R. Al-Khadhrawi*, Prediction of Unayzah Reservoir Quality Ahead-of-the-Bit, AAPG GEO 2010 Middle East Geoscience Conference & Exhibition, March 7-10, 2010 - Manama, Bahrain.

(5) *Khadhrawi, Mohammad*, Mark A. Person, Enrique Merino, and Peter S. Mozley, Geochemical and hydrologic controls on calcite cementation within the Sierra Ladrones Formation and along the Loma Blanca Fault, Rio Grande Rift, NM, in Geological Society of America, 2004 Annual Meeting Abstracts with Programs: Vol 36, No 5, pp:572-573, November 2004, Denver, Colorado.

(6) Farhat Ali, Mohammad; *M. R. Al-Khadhrawi*; H. Perzanowski; H. I. Halpern Central Saudi Arabian Crude Oils: A Geochemical Investigation, Petroleum Science and Technology, 1532-2459, Volume 20, Issue 5 & 6, 2002, pp. 633-654.

(7) Halpern, Henry I., Mark H. Tobey, William M. Petersen, William J. Carrigan, Peter J. Jones, *Mohammad R. Al-Khadhrawi*, Mohammed A. Al-Amoudi, and Hani O. Al-Ohaily, Geochemical evidence for reservoir compartmentalization in central Arabian Paleozoic reservoirs (in GEO'98, 3rd Middle East geoscience conference and exhibition; The Middle East, catalyst for E&P technology; conference abstracts, Al-Husseini,), GeoArabia (Manama, Bahrain) (March 1998), 3(1):96-97.

(8) Jones, Peter J., Henry I. Halpern, William J. Carrigan, Jay E. Leonard, Marshall W. Titus, *Mohammad R. Al-Khadhrawi*, and Ibrahim A. Al-Ghamdi, Exploration implications of basin modeling studies on known and potential source rocks in the Rub' Al-Khali, Saudi Arabia using BasinFlow (in GEO'98, 3rd Middle East geoscience conference and exhibition; The Middle East, catalyst for E&P technology; conference abstracts, Al-Husseini,), GeoArabia (Manama, Bahrain) (March 1998), 3(1):107.

(9) Halpern H. I., M. H. Tobey, W. M. Petersen, W. J. Carrigan, P. J. Jones, *M. R. Al Khadhrawi (Presenter)*, M. A. Al-Amoudi, H. O. Al-Ohaily, 1998, Geochemical Evidence For Reservoir Compartmentalization In Central Arabian Paleozoic Oils, 3rd Middle East Geosciences Conference & Exhibition (GEO '98), April 20-22, Manama, Bahrain.

(10) Jones P. J., H. I Halpern, W. J. Carrigan, J. E. Leonard, M. W. Titus, *M. R. Al Khadhrawi*, and I. A. Al Ghamdi, 1998, Exploration Implications of Basin Modeling Studies on Known and Potential Source Rocks in Rub' Al-Khali, Saudi Arabia, Using Basin Flow, 3rd Middle East Geosciences Conference & Exhibition (GEO '98), April 20-22, Manama, Bahrain.

(11) *Al-Khadhrawi, M. R.*, A Geochemical Investigation of a Suite of a Central Arabian Oils, M. S. Thesis, January 1996, King Fahd University Of Petroleum and Minerals, Dhahran, Saudi Arabia, p. 227.

(12) Cole, G. A., W. J. Carrigan, E. L. Colling, H. I. Halpern, *M. R. Al Khadhrawi*, and P. J. Jones, 1994, Organic Geochemistry of the Jurassic Petroleum System in Eastern

Saudi Arabia, in Embry, A.F., Beauchamp, B., and Closs, D.J., eds., Pangea, global environments and resources: Canadian Society of Petroleum Geologists Memoir 17, p.413-438.

Professional Associations:

(1) American Association of Petroleum Geologists
(2) American Geophysical Union
(3) Geological Society of America.